LBL-9553

Lawrence Berkeley Laboratory
UNIVERSITY OF CALIFORNIA

Materials & Molecular Research Division

ELECTRONS ON THE SURFACE OF LIQUID HELIUM

David Kay Lambert
(Ph. D. thesis)

May 1979

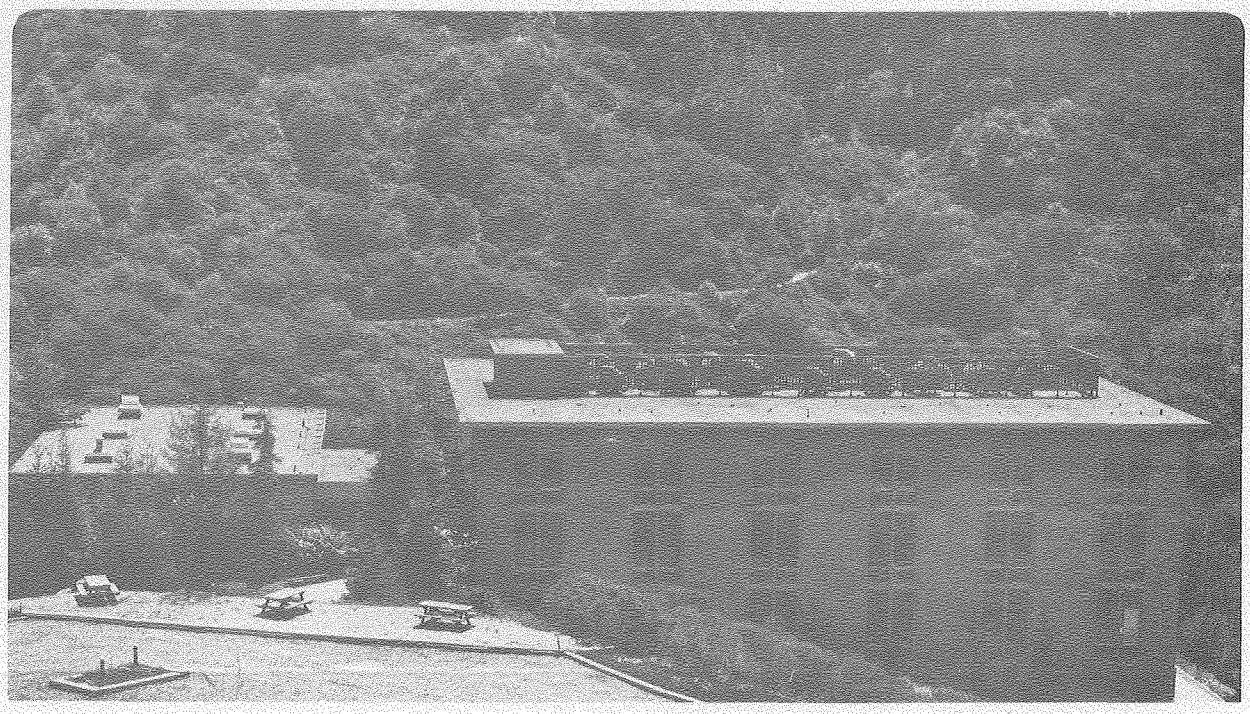

Prepared for the U.S. Department of Energy under Contract W-7405-ENG-48

LBL-9553

ELECTRONS ON THE SURFACE OF LIQUID HELIUM

David Kay Lambert

Materials and Molecular Research Division
Lawrence Berkeley Laboratory and Department of Physics
University of California
Berkeley, California 94720

ABSTRACT

We have used spectroscopic techniques to study transitions of electrons between bound states in the potential well near a helium surface. The charge density distribution of electrons on the surface was independently obtained from electrical measurements. From our measurements we have obtained information both about the interaction of the bound state electrons with the surface of liquid helium and about local disorder in the positions of electrons on the surface.

In the limit of zero surface charge density we have found that the transition frequency from the ground state to excited states as a function of electric field differs by a nearly constant amount from the transition frequency calculated by assuming that the helium surface is an abrupt change in density between the liquid and the gas. This implies that the model of an abrupt surface gives accurate results for the change in average height above the surface as electrons change from one state to another. The nearly constant difference frequency as a function of

electric field can be obtained from first principle calculations of fluid density near a liquid helium surface as well as from our measurements. Much should be learned about the accuracy of the first principle calculations when they are extended to make this comparison.

The presence of nearby electrons in the ground state changes the local electric field acting on an electron in an excited state. The change is proportional to the quantity $\sum_i' |r_i|^{-3}$ where r_i is the distance along the helium surface from the excited electron to the i^{th} other electron. For a given charge density, this quantity will increase as the local disorder increases. We have defined the quantity κ to be the ratio of this measured quantity to the value it would assume if the electrons formed a hexagonal lattice. Using measurements taken with the parameter $\Gamma = \pi^{\frac{1}{2}} n_s^{\frac{1}{2}} e^2/kT$ in the range $9 < \Gamma < 44$ we found the best level fit of $\kappa(\Gamma)$ to be given by $\kappa = 1.174 \pm 0.036$. One may also calculate $\kappa(\Gamma)$ from the radial-distribution function $g(r)$ of the two-dimensional electron gas. Our measured κ is significantly larger than one obtains from the tables of $g(r)$ that have appeared in the literature. To resolve this discrepancy we suggest that the calculations of $g(r)$ be improved and that additional measurements be taken at lower temperatures.

One additional qualitatively new result was obtained. We discovered that the distribution of charge on the helium surface is appreciable only within a "charge pool" that does not in general cover the entire surface and that the distribution of charge in the charge pool can be obtained from electrostatics.

TABLE OF CONTENTS

(If an electron does enter liquid helium it does not remain in a non-localized conduction band state. A "bubble" about 30 Å in diameter forms within which the electron is localized. The energy of an electron in a bubble[8] is believed to be about 0.1 eV above the energy at rest in vacuum.)

The short-range nature of exchange forces suggests that as the surface is approached from the gas there is an effective repulsive potential which is large only within atomic distances from the surface. Because liquid helium has a dielectric constant ε unequal to unity, there is an attractive potential at distances large on the atomic scale caused by the extra electron polarizing the liquid and being attracted by the polarization charge. For an electron of charge e a distance z above the liquid, the resulting potential is:

$$V(z) = -\frac{(\varepsilon - 1)}{(\varepsilon + 1)} \frac{e^2}{4z} = -\frac{\bar{e}^2}{z} \quad . \tag{1.1}$$

Here we have defined $\bar{e} = \frac{e}{2}\left(\frac{(\varepsilon - 1)}{(\varepsilon + 1)}\right)^{\frac{1}{2}}$. Very accurate measurements of ε for bulk ^{4}He have been reported in the literature.[9,10]

In our experiment we needed to have the charge remain on the surface. To confine mobile charge on the surface it is necessary to use an external electric field. At points on the surface where a static distribution of mobile charge is present, the average total electric field along the surface must be zero. Therefore, if the surface charge distribution is static there will be an external electric field component F directed out of the surface acting on the electrons in addition to the image potential. Neglecting for the moment the electric fields of nearby

electrons, the Hamiltonian for an electron near the liquid surface (but far enough away that the effective repulsive interaction may be ignored) is given by:

$$H = \frac{p^2}{2m} - \frac{\bar{e}^2}{z} + eFz \quad . \tag{1.2}$$

We have measured the transition frequencies between the bound states at the surface as a function of applied external electric field. In the limit that the surface charge is small, our measurements provide information about how, within a few Å of the surface, the effective repulsive interaction causes the potential to differ from the potential used in Eq. (1.2). Because of a novel technique we developed that enables us to measure the surface charge density, we are also able to obtain information about the local positional disorder of the surface electrons by measuring the effect of increasing surface charge density on the applied electric field at which resonance occurs. We measure the surface charge density by interpreting AC capacitance measurements made between plates that are separated by the helium surface on which the electrons are located. To be able to interpret the AC capacitance measurements we self-consistently solved the electrostatics of our cell. One interesting qualitative result obtained from this calculation is that free surface charge does not, in general, cover the entire liquid surface. The free charge is contained in a "charge pool," the dimensions of which can be altered by changing experimentally accessible potentials.

We are able to compare our measurement of the local positional disorder with the result of theoretical calculations of the radial-distribution function of the two-dimensional electron gas. This

comparison is meaningful since the wavefunction of an electron in the ground state only extends on the order of 10^2Å above the surface while individual electrons are separated by more than 3×10^3Å. A recent publication[11] has reported the measurement of a phase transition of the surface electrons to a state of long range order and much theoretical interest presently exists as to the nature of disorder in two-dimensional systems.

Theoretical calculations of the local structure of the liquid helium surface are also available. There are several competing techniques for obtaining the density variation near the surface that give conflicting results. It is hoped that our measurement of transition frequency as a function of applied electric field (in the limit that the surface charge is small) will motivate those doing the theoretical calculations to obtain results that can be compared with experiment.

II. EXTERNAL ELECTRON SURFACE STATES

In this chapter we discuss the bound states of electrons near, but outside of, a helium surface (there is another set of states for electron "bubbles" inside liquid helium near the surface[7]). The Hamiltonian for distances large enough away from the surface that the effective repulsive interaction with bulk liquid may be ignored, and neglecting the electric fields of nearby electrons, is given in Eq. (1.2). We begin by assuming that this Hamiltonian is valid to $z = 0$ and represent the surface of the helium with an abrupt rise to infinite potential.

The potential in our model Hamiltonian is given by:

$$V(z) = -\frac{\bar{e}^2}{z} + eFz \qquad \text{for } z > 0 \,,$$

$$V(z) = \infty \qquad \text{for } z < 0 \,. \tag{2.1}$$

Because of the singularity in the potential at $z = 0$ the wavefunction must approach zero linearly in the limit that z approaches zero and will be zero for z less than zero.[12] Schrodinger's equation is solvable only if the electric field $F = 0$. For the case of non-zero F the problem can be approached in several ways. One may use perturbation theory and treat F as a small parameter,[5] however, under the conditions of our experiment this is not valid. One may use the WKB approximation,[13] however, this is not sufficiently accurate[14] except at small F where it becomes exact. One may use a variational technique.[5] One may find the Hamiltonian matrix (in terms of the eigenfunctions when $F = 0$) and diagonalize a sub-block of finite dimensionality numerically. Or finally, one may numerically integrate Schrodinger's equation. We will discuss

both the matrix approach and the numerical integration technique. The numerical integration technique was used to calculate energy eigenvalues for $F \neq 0$.

To obtain the Hamiltonian matrix we solve Schrodinger's equation analytically for $F = 0$ and use these eigenfunctions to calculate matrix elements for $F \neq 0$. For motion in the z direction Schrodinger's equation has the form:

$$\frac{d^2}{dz^2}\,\psi(z) + \left(\frac{A}{z} - B\right)\psi(z) = 0 \qquad (2.2)$$

where $A = 2m\bar{e}^2/\hbar^2$ and $B = -2mE_z/\hbar^2$. We require that $\psi(z) = 0$ at $z = 0$ and that $\int_{z=0}^{\infty} |\psi(z)|^2 dz$ be finite. Making the substitutions $\psi(z) = z\,f(z)\,e^{-\beta^{1/2}z}$, $\omega = \alpha z$, and $\alpha = 2\beta^{1/2}$, the differential equation takes the form:

$$f''(\omega) + (2-\omega)f'(\omega) + \left[\frac{A}{2\beta^{1/2}} - 1\right] f(\omega) = 0 \quad . \qquad (2.3)$$

This equation is satisfied by the generalized Laguerre polynomial[15] $L^1_{n-1}(\omega)$ if $n = A/2\beta^{1/2}$ for $n = 1,2,\ldots$. The energy eigenvalues are then $E_z = -m\bar{e}^4/2\hbar^2n^2$ for $n = 1,2,\ldots$. This is a hydrogenic energy spectrum. For electrons on ^{4}He the Rydberg is about 159 GHz. The normalized wavefunction is given by:

$$\psi_n(z) = \frac{2}{n}\left(\frac{m\bar{e}^2}{n\hbar^2}\right)^{3/2} L^1_{n-1}\left(\frac{2m\bar{e}^2}{n\hbar^2}\,z\right)\cdot z \cdot e^{-m\bar{e}^2 z/\hbar^2 n} \quad . \qquad (2.4)$$

The matrix elements $\langle k|z|\ell\rangle$ are given by:

$$\langle k|z|\ell\rangle = \left(\frac{2m\bar{e}^2}{\hbar^2}\right)^{-1} \cdot \frac{1}{(k\ell)^{5/2}} \sum_{i=0}^{k-1} \sum_{j=0}^{\ell-1} \frac{(-1)^{i+j}\; k!\;\ell!}{(k-(i+1))!\,(\ell-(j+1))!}$$

$$\times \frac{2^{i+j+3}\; k^{j+4}\; \ell^{i+4}\; (i+j+3)!}{(i+1)!\;(j+1)!\;i!\;j!\;(k+\ell)^{i+j+4}} \quad . \qquad (2.5)$$

In particular $\langle n|z|n\rangle = \left(\frac{2m\bar{e}^2}{\hbar^2}\right)^{-1} \cdot 3n^2$. The Hamiltonian matrix for $F \neq 0$, in terms of the eigenfunctions of the problem for $F = 0$, is then

$$H_{k\ell} = -\frac{m\bar{e}^4}{2\hbar^2 k^2}\delta_{k\ell} + e\,F\langle k|z|\ell\rangle . \qquad (2.6)$$

The eigenvalues of this matrix are the energy eigenvalues for $F \neq 0$ and the eigenvectors are the expansion of the eigenfunctions in terms of the complete orthonormal set $\psi_n(z)$.

To use the numerical integration technique to find the energy eigenvalues we used Schrodinger's equation in the form

$$\frac{d^2}{d\omega^2}\psi(\omega) + \left(\frac{1}{\omega} + AE_z - B\omega F\right) = 0 \quad , \qquad (2.7)$$

where $A = \hbar^2/2m\bar{e}^4 = 1.5709375 \times 10^{-3}\ (\mathrm{GHz})^{-1}$, $B = e\hbar^4/4m^2\bar{e}^6 = 1.4447871 \times 10^{-4}\ (\mathrm{volt})^{-1}$, and $\omega = \alpha z$, where $\alpha = 2m\bar{e}^2/\hbar^2$, so $1/\alpha \sim 38\text{Å}$. Since $\psi(\omega)$ is a smooth square integrable function, then for any $\varepsilon > 0$ we may choose an M such that if $\omega > M$ then $|\psi(\omega)| < \varepsilon$. We begin with a range of E_z which contains an eigenvalue and a value M of ω at which $\psi_n(\omega)$ can be assumed to be very small. The value of E_z which corresponds to an eigenvalue will result in a $\psi(\omega)$ which rises linearly from zero for ω near zero and is close to zero for $\omega = M$. We assume that $\psi(\omega)$ increases linearly from zero for ω near zero and numerically integrate[7] the differential equation to find $\psi(M)$. We then vary E_z until $|\psi(M)| < \varepsilon$ to find $E_z(F)$. It is straightforward to check the accuracy of the computation by changing M and ε. To interpolate between eigenvalues computed in this way a smooth polynomial fit to the difference between the computed eigenvalues and the eigenvalues obtained using the WKB

approximation[16] was used. The calculated energy difference between the ground state and the first ten excited states are shown in Fig. 1.

We now extend our discussion from the one-dimensional model Hamiltonian, $\mathcal{H}_0$, discussed above to the unknown physical Hamiltonian, $\mathcal{H}$, valid near the surface, which we assume to be one-dimensional. Let $u_n(z)$ and E_n be the eigenfunctions and eigenvalues of $\mathcal{H}$ and let $v_n(z)$ and E_n' be the eigenfunctions and eigenvalues of $\mathcal{H}_0$. Let $V(z)$ be the potential appearing in $\mathcal{H}$ and let $V'(z)$ be the potential appearing in $\mathcal{H}_0$. Then one can show[17] that:

$$E_n - E_n' = \frac{\left[\int_0^\infty u_n^* \, (V(z) - V'(z)) \, v_n dz - \frac{\hbar^2}{2m} \left.\frac{du_n^*}{dz}\right|_{z=0} v_n(0)\right]}{\int_0^\infty u_n^* \, v_n dz} \quad . \tag{2.8}$$

If we assume that $v_n(z) = u_n(z)$ in this equation we obtain the result of first order non-degenerate perturbation theory:

$$E_n - E_n' \cong \int_0^\infty v_n^* (V(z) - V'(z)) \, v_n \, dz \quad . \tag{2.9}$$

Near the helium surface the difference between the exact potential and the potential used in our model Hamiltonian is probably very large so first order perturbation theory is not expected to be accurate. In the next chapter we discuss several model calculations for the effect of the helium surface which do not agree with Eq. (2.9).

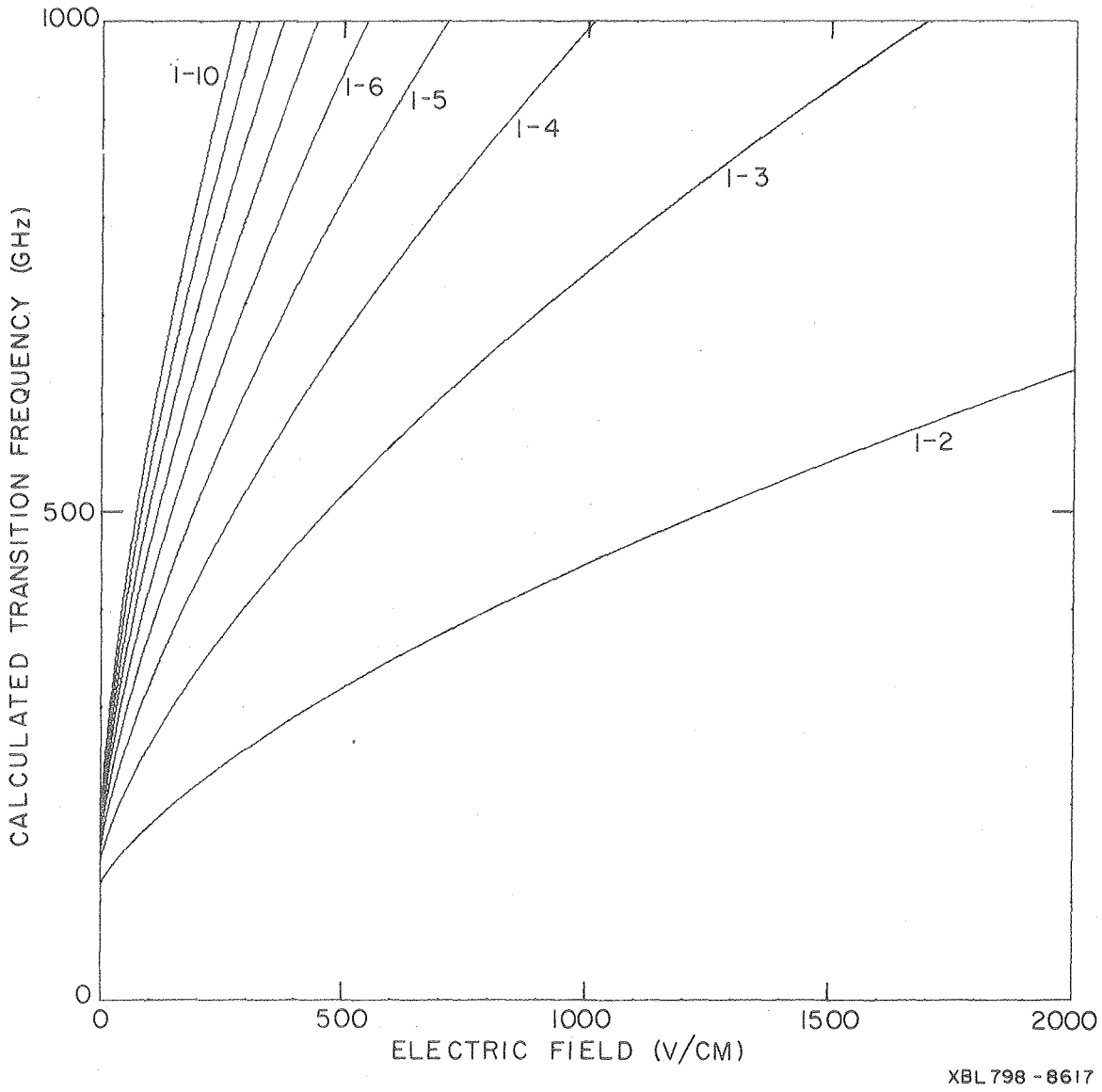

Fig. 1. Transition frequency from the ground state to excited state n as calculated from the model of an abrupt liquid-gas interface.

III. THE SURFACE OF LIQUID HELIUM

In this chapter we review the theoretical and experimental work done by others that has increased our understanding of the liquid helium surface. We begin with first principles calculations of the microscopic structure of the liquid-gas interface. We then discuss previous attempts to extract information about the interface from physical measurements.

By first principles calculations we refer to calculations in which the bulk properties alone are used to calculate the surface properties. These were motivated by a paper by Regge[18] who used Feynman's concept of a macroscopic wavefunction. He wanted the wavefunction to decay exponentially outside the surface and to smoothly join to the translationally invariant behavior inside the liquid. This was found to imply an oscillatory density near the surface which was damped as one went into the liquid. The predicted surface tension was 48% greater than the measured surface tension of ^{4}He at $T = 0$. Soon after, a number of papers appeared attempting to calculate the density distribution near the liquid helium surface using the techniques of quantum many-body theory. A wavefunction is assumed to be of the form:

$$\psi = C \exp\Big(\sum_{i<j} u(r_{ij}) + \sum_{i} t(z_i) \Big) \quad . \tag{3.1}$$

Here $u(r_{ij})$ is the two-particle correlation function and $t(z_i)$ determines how the wavefunction depends on distance from the surface. They differ in the exact form of the two-particle correlation function used. In some cases it is calculated while in others it is taken from x-ray scattering data on bulk ^{4}He. They also differ in the computational

method used (analytic variation using an incomplete function space[19-22] or numerical Monte Carlo methods[23]). In some cases the functional form of the density variation near the surface is constrained[19,20,22] while in other cases it is not.[21,23] One problem common to all of these calculations is that the wavefunction does not include some important degrees of freedom.[24] It neglects surface waves and other forms of long-range hydrodynamic motion. Even though we are interested in the system with all of these modes in their ground state, the zero point motion associated with these degrees of freedom is still important.

In an attempt to avoid this pitfall, density functional theory has been used.[25,26] The total free energy of the system is expressed as a functional of the fluid density and its gradient. The Thomas-Fermi model of the atom is an example of a density functional theory. In the paper[26] by Ebner and Saam the density functional is obtained from the bulk liquid structure factor and a self-consistent technique is used to determine the highest surface wave wavevectors allowed in the theory (the cutoff was set at 0.99 Å^{-1}).

As is also the case when similar techniques are applied to other simple liquids,[27] the two approaches to the problem give quite different results. A comparison of the length over which the density distribution predicted by these theories falls from 90% to 10% of the bulk density has been given by Lekner and Henderson.[28] They find that the predictions range over a factor of three. There is also a qualitative difference between the theoretical predictions. Unless otherwise constrained the calculations based on the microscopic wavefunction find an oscillatory structure on the density profile near the surface. On the other hand,

the density functional approach is found to yield a monotonically varying density profile from the bulk liquid to the vapor. The surface tension calculated from the microscopic wavefunction approach agrees to within 25% with the measured value while the agreement of the density functional calculation of Ebner and Saam[26] is within 2%. The surface tension in the microscopic wavefunction approach is due to the rapid variation of the wavefunction in the z direction while in the density functional approach it is almost exclusively due to the zero point energy of the surface modes. There has been only one first principles calculation reported of the shift in the transition frequency between external surface electron states.[29] The predicted difference between actual transition frequencies and those calculated from the sharp interface model Hamiltonian was about a factor three larger than the measured difference.

In addition to theoretical efforts to find the structure of the ^{4}He surface and from this calculate measurable properties, there have been attempts to start from the measured surface properties and obtain information about the surface structure. The measured surface properties are surface tension,[30-33] the barrier the surface provides to electrons passing in or out of the liquid,[2,34,35] transition frequencies of external surface state electrons,[5] and the reflection of ^{4}He atoms from the surface.[36] A measurement of the ellipticity of light reflected at Brewster's angle is also being attempted.[37]

The first attempt to use ^{4}He surface tension measurements to obtain information about the microscopic liquid-vapor interface was made by Atkins.[38] He found that all of the surface tension at T = 0 could be explained by the zero point motion of the capillary surface waves or "ripplons" and was also able to explain the behavior of surface tension

as a function of temperature at low temperatures. However, he recognized that this agreement could be fortuitous since there were other terms, both positive and negative, contributing to the surface energy.

Atkins work was followed by several other papers which ignored ripplons and tried to interpret the surface tension as a result of the liquid surface density profile.[39,40] Although both used the same quantum mechanical generalization of the classical theory of the liquid-gas interface (where "ripplons" are damped and hence ignored) their results differ by about a factor two for the exponential decay length from the liquid to gas. More recently Lekner and Henderson[41] put forth the point of view that the function $t(z_i)$ in Eq. (3.1) is unnecessary. Starting from this assumption the density is found to change from 90% to 10% of the bulk density over a distance of 3.9 Å.

We next discuss previous work that has been done to interpret measured transition frequencies of external electron surface states. With only two exceptions these have concerned themselves with transition frequencies in the limit of a small external electric field. A model potential is constructed that differs from the image potential near the ^{4}He surface. The model contains one or more adjustable parameters used to obtain agreement with experiment. A model discussed by Cole[3] assumes that the image potential is exact for $Z \geq b$, the potential is constant for $0 < Z \leq b$ and jumps to V_0 for $z < 0$. To be consistent with the data of Grimes et al the parameter b in the model is about 10 Å. To analyze their data Grimes et al[5] used a similar model except that for $0 < z < b$ the potential is taken to be V_0. They found that to be consistent with their data the parameter b in this model is about 1.04 Å.

The class of model used by Grimes et al was later discussed by Sanders and Weinreich[12] and solved exactly by Hipolito and Felicio[42] who found that b was best fit by 1.01Å. In contrast to the results of first order perturbation theory the shift in transition frequencies found by solving this model exactly has a different functional dependence on the parameter b but both predict an energy shift of the n^{th} state proportional to n^{-3}. The exact solution of this model can reproduce the measured data with two distinct values of b, one of which is very small and is rejected as being unphysical. This shows that data taken in the limit as F goes to zero do not necessarily uniquely specify a model potential of given functional form with a single parameter.

Attempts to compare data at non-zero F to model potential results were first carried out by Zipfel and Simons.[43] They used a model in which the potential is V_0 for $z < b - \alpha$, decreases linearly from $b - \alpha$ to b, and is equal to the image potential for $z > b$. They found that b could range from 1Å to 3Å while α ranged from 0Å to 6Å and still for a pair of α and b fit Zipfel's unpublished data. Another model calculation is due to Stern.[44] Rather than working directly with a model for the potential acting on the electron, he constructed a model for the dielectric function near the surface with a smooth change from bulk to vacuum values as the liquid surface was crossed. He found best agreement with Zipfel's data when the effective transition layer thickness was about 5.7Å.

There have been experiments measuring the penetration of energetic electrons from the gas into the liquid[2,34] and tunneling of electrons from bubble states in the liquid to the gas.[35] No information about the

surface thickness has been extracted from these measurements although the tunneling measurements do seem to indicate an excess barrier that is not explained.

Finally, the reflection of ^{4}He atoms from the ^{4}He liquid surface has been measured.[36] Most of the incident atoms are absorbed into the liquid. It is found that the measured reflection depends only on the perpendicular momentum of the atom, is independent of temperature, and that the fraction of the incident beam that is inelastically scattered is less than 10^{-4}. The elastic scattering was also found to be small but measurable. A model of Echenique and Pendry[45] explains the observed smallness of the reflectivity if the liquid helium density at the surface changes from its bulk value to near zero over a distance of at least 5Å.

The conclusion that one draws from previous theoretical and experimental work with respect to the structure of the helium surface is that the situation is unsettled. The liquid gas density profile has most of its change over a distance of 5 ± 3 Å. The zero point motion of "ripplons" is important, but how it affects the local properties of the surface is not completely understood. The density of the liquid may have some oscillatory behavior near the surface, but this could be an artifact of the calculations. Existing measurements are not sufficient to distinguish between competing theories. This is the reason why we made the high accuracy measurements reported here.

IV. THE TWO-DIMENSIONAL ELECTRON FLUID

As discussed in the Introduction, electrons on the surface of liquid helium are a very close approximation to a two-dimensional electron fluid. As such, it provides a way for experimental tests to be applied to the rapidly developing field of phase transitions in two dimensions. It is also an experimentally interesting system in its own right. We begin this chapter by giving an introduction to the theory of the two-dimensional electron fluid. We then discuss some previous experimental results and their interpretation.

Many of the properties of metals, which are a close approximation to a three-dimensional electron gas, can be explained by assuming that the electrons are free particles interacting with each other only through the exclusion principle. We begin by discussing a quantum mechanical system of charge-free electrons in two dimensions. The density of states per unit area (including spin degeneracy) is:

$$N(E)dE = \frac{m}{\pi\hbar^2}\,\theta(E)dE \quad . \tag{4.1}$$

Here $\theta(E) = 1$ if $E > 0$ and $\theta(E) = 0$ if $E < 0$. The probability that a state is occupied is given by the Fermi-Dirac distribution function. The Fermi energy of a two-dimensional electron gas is

$$\varepsilon_F = \frac{\pi\hbar^2}{m}\,\frac{N}{A} \quad . \tag{4.2}$$

For electrons on bulk liquid helium there is an upper limit[46] to the charge density that may be stably placed on the surface. If the density is higher than about 2×10^9 electrons/cm^2 the mutual repulsion

of the electrons causes the surface to become mechanically unstable (in effect it has negative surface tension). Deformations of the surface[47] occur allowing macroscopic "bubblons" of charge to be pulled through the bulk liquid to the source of the electric field. This yields a maximum Fermi energy of about 6×10^{-2}°K. Most experiments[48] have used high enough temperatures and low enough charge densities that quantum corrections to classical statistics are small.

In the classical limit the thermodynamic variable which governs the behavior of the two-dimensional electron gas is the ratio of Coulomb energy per electron to kinetic energy, $\Gamma = \pi^{\frac{1}{2}} n_s^{\frac{1}{2}} e^2/kT$, where n_s is the number density of electrons per unit area of surface. If $\Gamma \ll 1$ then the electrons behave like an ideal gas in two dimensions.[49-53] As Γ increases the ordering of the electrons increases and, if Γ is sufficiently high, the electrons are expected to "crystallize" into a triangular lattice.[54-58] Experimentally, long-range order seems to appear when Γ is about 140.[11,59,60] There is a proof that long-range crystalline order is impossible in the thermodynamic limit[61] because of fluctuations which depend logarithmically on the size of the system. However, long-range order of a macroscopic two-dimensional system is predicted and does seem to be observed experimentally.

Short-range order sets in before long-range order and seems to gradually increase as Γ is increased. In a computer calculation[54] involving 10^4 interacting classical point charges it is found that before long-range order appears the system develops domains of local crystalline structure. As Γ increases the size of the domains increase until the entire system is contained in a single domain. The radial-distribution

function also changes gradually from delta-function-like behavior[54] at large Γ until all structure is lost at small Γ.[52,53]

The first experiment measuring the short-range order of electrons on the surface of liquid helium is reported in this thesis. The experiment was carried out for $9 < \Gamma < 44$.

We next review experiments reported in the literature in which the two-dimensional motion of electrons on the surface of liquid helium have been measured. We begin with cyclotron resonance experiments. When a magnetic field is applied perpendicular to the helium surface the single electron Hamiltonian is still separable. The solution of Landau[62] for free electrons in a magnetic field in three dimensions can be applied to the x-y motion, while our previous discussion applies for motion in the z direction. The density of states for motion parallel to the surface separates into a series of delta functions separated by energy $\Delta E = e\hbar B/mc$. The resonant absorption between different Landau levels is called cyclotron resonance. In the case of electrons on the surface of liquid helium, the frequency of the resonance is found to depend only on the component of B perpendicular to the surface.[6] The resonant frequency has a small shift which depends quadratically on the electric field pressing the electron toward the surface.[63] This is interpreted as a microscopic dimple forming under the electron which contributes to its effective mass. The linewidth of the absorption lines is interpreted to yield the scattering time or mobility of electrons on the surface.

Electromagnetic energy may also be absorbed by surface electrons by exciting standing plasma waves in the surface charge density. Long

wavelength modes are only excited at wavelengths set by the size of the surface. Since the exciting frequency is known, one is able to verify the dispersion relation for a plasma in two dimensions.[64] The linewidths of the resonances provide another way to measure the mobility of surface electrons.

Long-range crystalline order makes possible resonant absorption of electromagnetic energy at another set of frequencies. If the wavelength and frequency of a surface capillary wave match a wavevector in reciprocal space of the electron lattice and the driving frequency, then resonant absorption will occur.[59,60] By observing these resonances as a function of temperature[11] long-range crystalline ordering of the surface electrons has been found to occur at $\Gamma = 137 \pm 15$.

The lineshapes of transitions between the bound states of electrons normal to the surface in the presence of a large magnetic field parallel to the surface[65] has also been interpreted to obtain information about motion of electrons along the surface. A moving electron is acted upon by a Lorentz force perpendicular to the surface which in the rest frame of the electron is equivalent to an extra electric field. The two-dimensional equivalent of the Maxwellian velocity distribution yields a Gaussian lineshape of absorption versus electric field F of the form $A(F) = A_0 \exp[-(F - F_0)^2/2\sigma^2]$ where $\sigma = \left(\frac{kT}{m}\right)^{\frac{1}{2}} \frac{B}{c}$. The observed linewidths are smaller than this equation predicts, an effect which increases in importance as Γ increases. This was interpreted as motional narrowing (the scattering of the electrons into several different velocities before being de-excited in the z direction causes a narrowing of the lineshape just as NMR resonances of nuclei moving in spatially varying fields are

"motionally narrowed"). The amount of motional narrowing is used to extract a velocity autocorrelation time. This interpretation of the data is, however, not universally accepted.[66,67]

Other experiments have attempted to measure the mobility in situations in which large fractions of the surface charge is moved from one place to another. These include time of flight measurements,[68] measurements of the phase difference between current driving one plate and detected in another plate beneath a charged helium surface,[69] and the change in Q of a tuned RF circuit when electrons are put on a liquid helium surface inside of it.[70] These experiments obtained mobilities that are inconsistent with the mobilities deduced from cyclotron and plasmon resonance experiments. The low temperature mobilities obtained from cyclotron and plasmon resonance experiments are many times higher and are in agreement with calculations based on scattering of electrons by ripplons. In the analysis of the measurements made when a large fraction of the surface charge is moved from one place to another, it was not taken into account that electrons need not cover the entire surface as discussed in the next chapter. The possibility of free charge accumulating on the helium film covering the walls of the container was also neglected. It is quite possible that there was no free charge on the helium surface during these experiments.

V. THEORY OF CHARGE DENSITY AND ELECTRIC FIELD MEASUREMENTS

In this chapter it is shown how capacitance measurements, voltage measurements, and a knowledge of the dimensions of the experimental cell are used to calculate the surface charge density and electric field acting on external surface state electrons. In the chapter on data analysis we discuss the dipole electric field from other nearby electrons, how the magnitude of this field is extracted from our measurements, and how it is related to the local disorder in the surface electron lattice.

In Fig. 2 we give the dimensions of the cylindrical cell within which electrons are confined on a helium surface in our experiment. The cell has a radius a and height H. The gap s separates the bottom plate from the grounded cell body. The top plate of diameter D_2 is in a circular hole of radius D_1 in the cell body. The top plate is insulated from the cell body by a 0.084 mm gap and has effective radius $b = (D_1+D_2)/4$. The cell is filled to a depth c with liquid helium. The depth is obtained by measuring AC capacitance between top and bottom plates before and after filling takes place. A positive potential applied to the bottom plate causes an electric field normal to the surface to act on surface electrons. Fringing fields confine the electrons on the surface. Free charge is put on the surface by briefly heating a filament and allowing the thermionically emitted electrons to pass through a small hole in the center of the top plate while a confining positive potential is present on the bottom plate. Free charge on the helium surface screens the top and bottom plates from one another and causes the measured AC capacitance between them to decrease. This AC capacitance change is a function of the positive bias potential applied to the bottom plate. By measuring

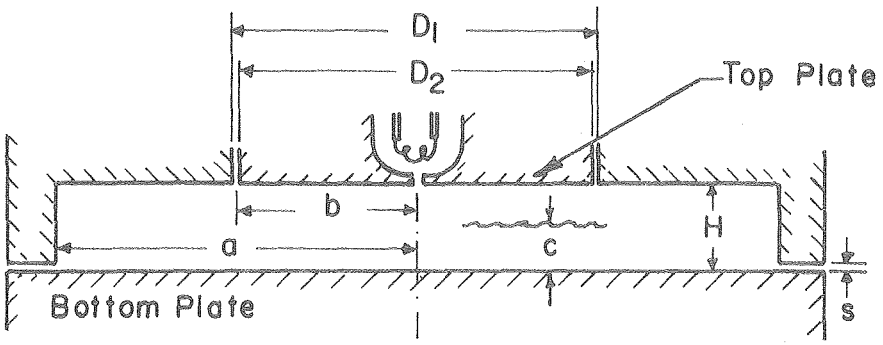

	298 °K	1.2 °K
a	2.47064 ± 0.00005 cm	2.46039 ± 0.00049 cm
$b = \frac{D_1+D_2}{4}$	0.93891 ± 0.00004 cm	0.93501 ± 0.00019 cm
s	0.02540 ± 0.00013 cm	0.02147 ± 0.00032 cm
H:		
from capacitance	0.53335 ± 0.00035 cm	0.52980 ± 0.00042 cm
directly measured	0.53324 ± 0.00031 cm	0.52980 ± 0.00042 cm
combined	0.53329 ± 0.00023 cm	0.52980 ± 0.00030 cm

XBL 798-6719

Fig. 2. Cross-section drawing of the cylindrical cell within which electrons are confined on the helium surface.

the AC capacitance after charge is placed on the surface we are able to calculate the surface charge distribution as a function of radius and bottom plate voltage. Knowing the surface charge distribution we are also able to calculate electric field acting on the external surface state electrons as a function of radial distance and bottom plate voltage.

We begin by discussing how the liquid helium height is calculated from the capacitance measurements. The result is obtained from Gauss' law. However, to justify the approximation involved in using Gauss' law and because we will need the results later, we begin by solving the boundary value problem of a potential V_o applied to the bottom plate in Fig. 2 with the other conducting surfaces at ground potential. A set of functions satisfying Laplace's equation inside the cavity is:

$$\Phi_o = A_o + B_o z$$

$$\Phi_k = [A_k \cos(kz) + B_k \sin(kz)]\, I_o(kr) \quad . \tag{5.1}$$

Here $I_o(x)$ is the zeroth order imaginary Bessel function.[71] From these functions and the techniques of Fourier analysis, we find the following function which satisfies the boundary conditions:

$$V(r,z) = V_o + V_o \cdot \left(\frac{z}{H}\right) + \sum_{n=1}^{\infty} \frac{2V_o}{\left(\frac{s}{H}\right)} \frac{\sin\left(\frac{n\pi s}{H}\right) \sin\left(\frac{n\pi z}{H}\right) I_o\left(\frac{n\pi r}{H}\right)}{(n\pi)^2 I_o\left(\frac{n\pi a}{H}\right)} \quad . \tag{5.2}$$

The electric field inside the cell is:

$$E_r^{ext}(r,z) = -\frac{2V_o}{H} \sum_{n=1}^{\infty} \frac{\sin\left(\frac{n\pi s}{H}\right) \sin\left(\frac{n\pi z}{H}\right) I_1\left(\frac{n\pi r}{H}\right)}{\left(\frac{n\pi s}{H}\right) I_o\left(\frac{n\pi r}{H}\right)} \quad ,$$

$$E_z^{ext}(r,z) = -\frac{V_o}{H} - \frac{2V_o}{s}\sum_{n=1}^{\infty}\frac{\sin\left(\frac{n\pi s}{H}\right)\cos\left(\frac{n\pi z}{H}\right)I_o\left(\frac{n\pi r}{H}\right)}{(n\pi)\ I_o\left(\frac{n\pi a}{H}\right)} . \tag{5.3}$$

Here $I_1(x)$ is the first order imaginary Bessel function. For the dimensions of our cell and $z/H = 0.5$ we have plotted $E_r^{ext}(r,z)$ in Fig. 3. It is found that the lines of flux which pass from the bottom plate to the top plate are almost parallel. The ratio of the capacitance between the top and bottom plates and to that calculated in the absence of fringing fields is for our cell $\xi = 0.998729$ where:

$$\xi = \frac{2}{\left(\frac{b}{H}\right)^2}\int_0^{b/H}\left[1+\sum_{n=1}^{\infty}\frac{2\sin\left(n\pi\frac{s}{H}\right)(-1)^n\ I_o(n\pi x)}{\left(n\pi\frac{s}{H}\right)I_o\left(n\pi\frac{a}{H}\right)}\right]x\ dx . \tag{5.4}$$

Hence the neglect of fringing fields is accurate to order $(\varepsilon-1)\times 10^{-3}$ in predicting the fractional change in the capacitance when the cell is partially filled with liquid helium. We will use the value[9,10] $\varepsilon = 1.057233$ for the dielectric constant of liquid helium in the calculations that follow. Neglecting fringing fields, where C_o is the capacitance of the cell empty of liquid helium and C' is the capacitance when filled to a depth z_o with no charge on the surface, we use Gauss' law to find

$$z_o = \frac{\varepsilon H}{\varepsilon - 1}\left(1 - \frac{C_o}{C'}\right) . \tag{5.5}$$

We next discuss how the surface charge density as a function of radius and bottom plate voltage may be obtained from capacitance measurements. When charge is in equilibrium on a surface of liquid helium the electrochemical potential of the electrons is constant across

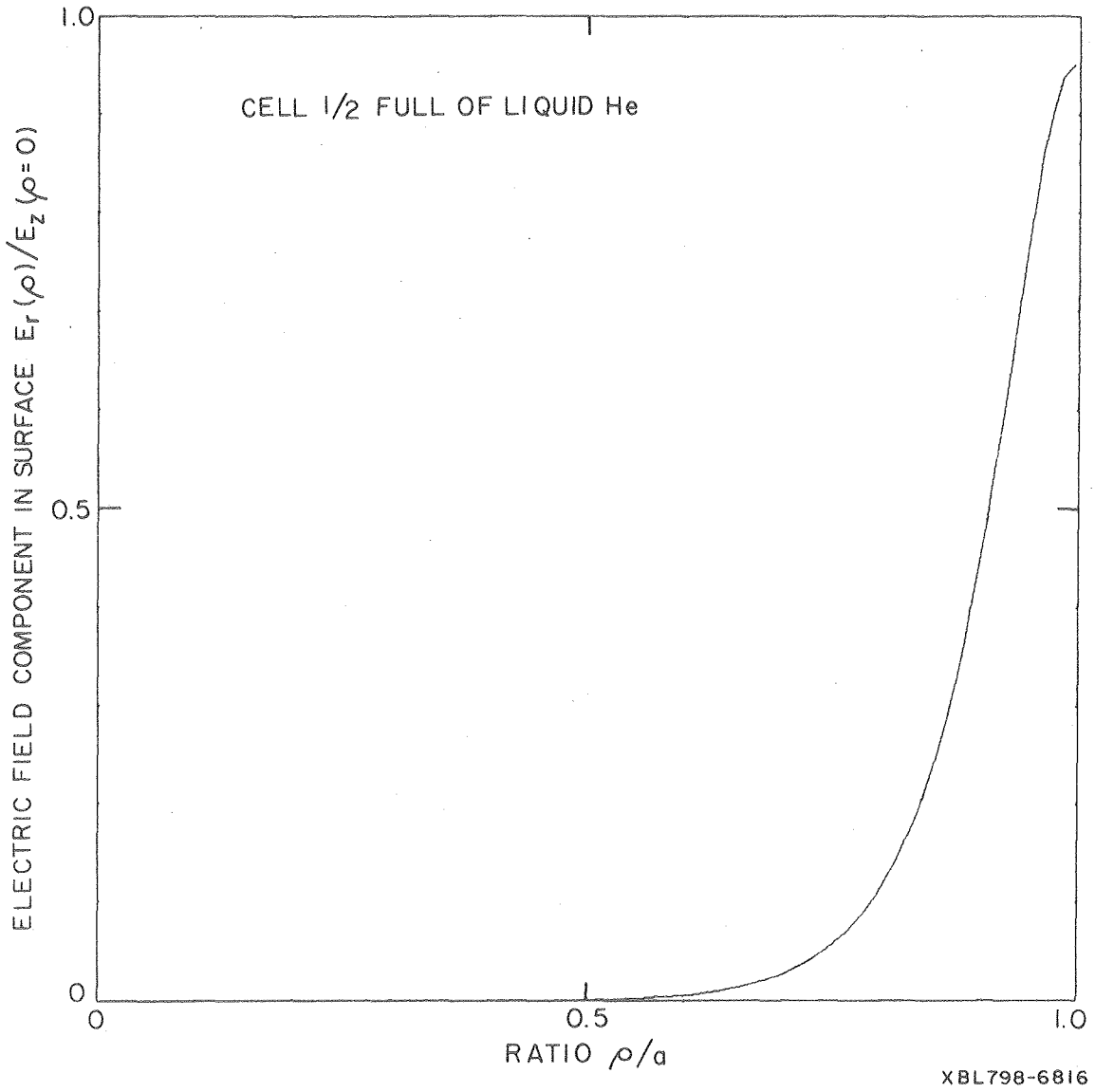

Fig. 3. Plot of the external electric field in the plane of helium surface (which confines charge in the charge pool) as a function of radial distance. The plot is normalized to the electric field along the axis of the cell.

the entire surface. However, the electrical potentials which maintain the electrons on the surface are of the order of volts while the kinetic energy of an electron at 1°K is only 8.6×10^{-5} eV. Hence, with the exception of a slight amount of fuzzing caused by thermal motion of electrons we may use electrostatics to calculate the surface charge distribution. The surface is divided into two regions. One region is a circular charge pool at the center of the cell containing almost all of the charge. The electrical potential across the charge pool is uniform. The other region is an annular ring between the charge pool and the walls of the cell. The annular ring contains no charge and the electric potential is not uniform across it. We solve the problem by first finding the capacitance change and surface charge density distribution as a function of charge pool radius and bottom plate voltage. Since the capacitance change is a monotonic function of charge pool radius these results may be used to obtain the surface charge density distribution as a function of capacitance change.

Given the charge pool radius and the bottom plate potential we wish to find a charge distribution which gives zero radial electric field along the surface within the charge pool. We do this by dividing the charge pool up into concentric rings. The radial field acting on an electron in the i^{th} ring is the sum of the field from external potentials $E_r^{ext}(r,z)$ given in Eq. (5.3), the electric field from each of the other rings, and the electric field from the other charge in the i^{th} ring itself. Requiring that the radial electric field at each ring be zero gives a system of linear equations for charge density at the rings with a unique solution.

We calculate the radial electric field at a given ring of radius ρ due to charge q distributed on another ring of radius r. Using the Green's function of a point charge in cylindrical coordinates[72] we find for $\rho < r$:

$$V(\rho,r) = -\frac{4q}{H}\sum_{n=1}^{\infty}\frac{R_0\left(\frac{n\pi}{H},a,r\right)\,I_0\left(\frac{n\pi\rho}{H}\right)\sin^2\left(\frac{n\pi c}{H}\right)}{I_0\left(\frac{n\pi a}{H}\right)} \quad . \qquad (5.6a)$$

We also find for $\rho < r$:

$$V(\rho,r) = -\frac{4q}{H}\sum_{n=1}^{\infty}\frac{I_0\left(\frac{n\pi r}{H}\right)\,R_0\left(\frac{n\pi}{H},a,\rho\right)\sin^2\left(\frac{n\pi c}{H}\right)}{I_0\left(\frac{n\pi a}{H}\right)} \quad . \qquad (5.6b)$$

Here c is the depth of helium in the cell, and $R_0(k,x,y) = K_0(kx)I_0(ky) - I_0(kx)K_0(ky)$ where $I_0(x)$ and $K_0(x)$ are modified Bessel functions.[71] The charge q on the ring of radius r is given by $q = 2\pi\,(\Delta r)r\sigma(r)$. where Δr is the distance separating the rings. The radial electric field for $\rho < r$ is given by

$$E_\rho^{i<j}(\rho,r) = \frac{8\pi^2(\Delta r)r\sigma(r)}{H^2}\sum_{n=1}^{\infty} nR_0\left(\frac{n\pi}{H},a,r\right)\,I_1\left(\frac{n\pi\rho}{H}\right)\sin^2\left(\frac{n\pi c}{H}\right). \qquad (5.7a)$$

We also find for $\rho > r$:

$$E_\rho^{i>j}(\rho,r) = \frac{8\pi^2(\Delta r)r\sigma(r)}{H^2}\sum_{n=1}^{\infty}\frac{nI_0\left(\frac{n\pi r}{H}\right)}{I_0\left(\frac{n\pi a}{H}\right)}$$

$$\times\left[K_0\left(\frac{n\pi a}{H}\right)\,I_1\left(\frac{n\pi\rho}{H}\right)+I_0\left(\frac{n\pi a}{H}\right)K_1\left(\frac{n\pi\rho}{H}\right)\right]\sin^2\left(\frac{n\pi c}{H}\right). \qquad (5.7b)$$

The electric field acting on an electron in the i^{th} ring from the other

charge in the i^{th} ring must be obtained more carefully. If the charge on the i^{th} ring were on a line the electric field would be infinite.[73] We avoid this difficulty by obtaining the electric field at $\rho = r$ resulting from a surface charge density constant from $r - \Delta r/2$ to $r + \Delta r/2$. This can be done by replacing Δr by dr in Eq. (5.7) and integrating r from $\rho - \Delta r/2$ to $\rho + \Delta r/2$ while keeping ρ fixed. We find

$$E_\rho^{i=j}(\rho) = \frac{8\pi\sigma(\rho)}{H} \sum_{n=1}^{\infty} \frac{\sin^2\left(\frac{n\pi c}{H}\right)}{I_0\left(\frac{n\pi a}{H}\right)} \left\{ -\left(\rho - \frac{\Delta r}{2}\right) I_1\left(\frac{n\pi}{H}\left(\rho - \frac{\Delta r}{2}\right)\right) \right.$$
$$\times \left[K_0\left(\frac{n\pi a}{H}\right) I_1\left(\frac{n\pi\rho}{H}\right) + I_0\left(\frac{n\pi a}{H}\right) K_1\left(\frac{n\pi\rho}{H}\right) \right] + \left(\rho + \frac{\Delta r}{2}\right) I_1\left(\frac{n\pi\rho}{H}\right)$$
$$\left. \times \left[I_1\left(\frac{n\pi}{H}\left(\rho + \frac{\Delta r}{2}\right)\right) K_0\left(\frac{n\pi a}{H}\right) + I_0\left(\frac{n\pi a}{H}\right) K_1\left(\frac{n\pi}{H}\left(\rho + \frac{\Delta r}{2}\right)\right) \right] \right\} \tag{5.8}$$

The charge density as a function of radius is obtained by solving the system of equations:

$$\sum_{j=1}^{i-1} \left(\frac{E_\rho^{i>j}(\rho_i, \rho_j)}{\sigma(r)} \right) \sigma_j + \left(\frac{E_\rho^{i=j}(\rho_i)}{\sigma(\rho)} \right) \sigma_i$$
$$+ \sum_{j=i+1}^{j_{max}} \left(\frac{E_\rho^{i<j}(\rho_i, \rho_j)}{\sigma(r)} \right) \sigma_j + E_r^{ext}(\rho_i, c) = 0 \quad . \tag{5.9}$$

The surface charge density distribution as a function of charge pool radius R may be obtained by solving the above set of equations as j_{max} is decreased one ring at a time. The behavior of $\sigma(\rho)$ for several values of R for a cell of the dimensions used in our experiment and for $c/H = 0.5$ is shown in Fig. 4.

In the case in which $R = a$, so the charge pool covers the entire

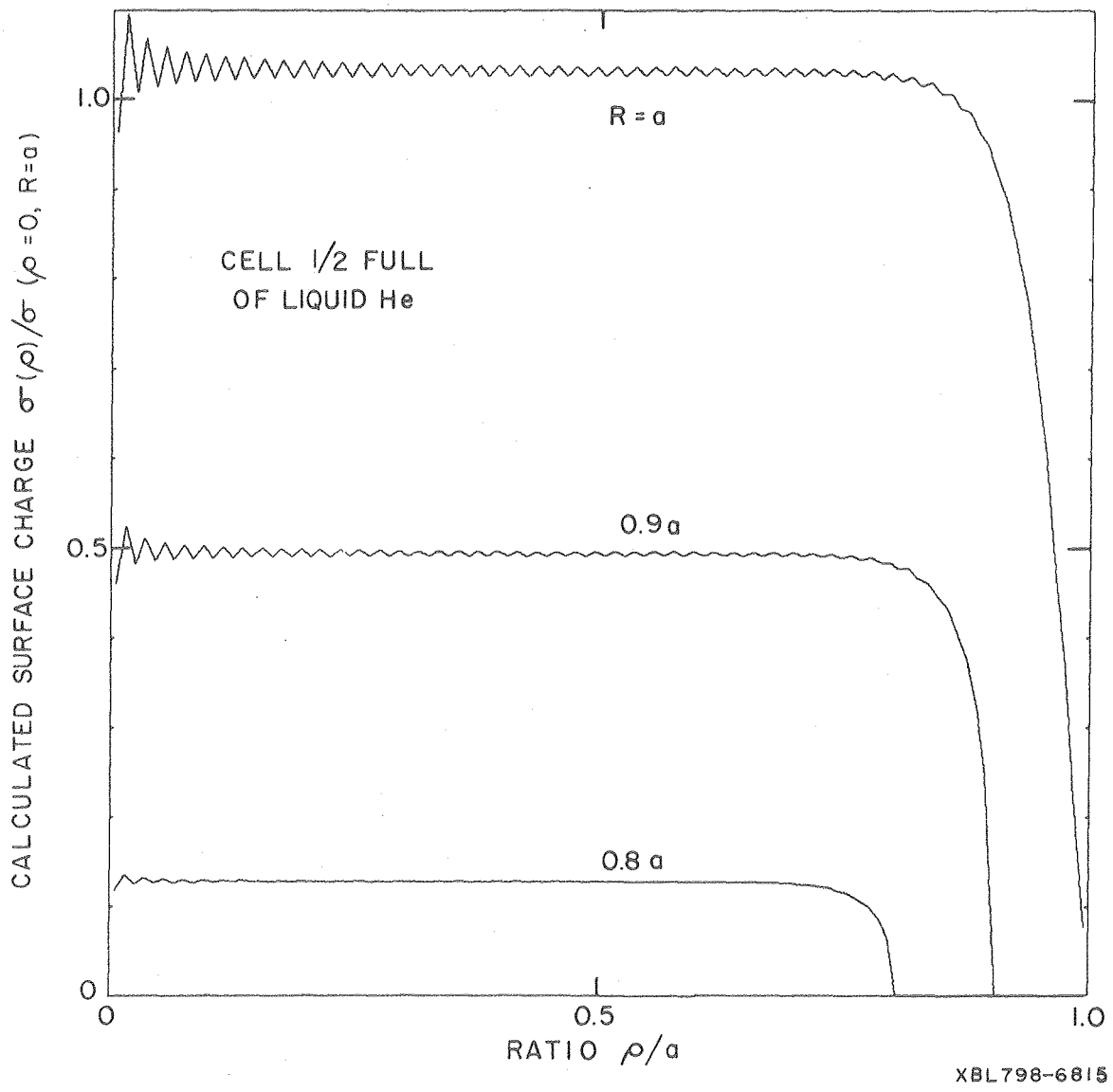

Fig. 4. Plot of the calculated surface charge density for several values of the charge pool radius. The plots are normalized to the surface charge density at the center of the cell when the entire surface is covered with charge. The oscillatory structure at the center of the charge pool is an artifact of the finite element approximation.

surface, the potential must be zero over the entire liquid helium surface. In this case Laplace's equation may be solved explicitly to yield:

$$\sigma(\rho) = -\frac{V_o}{4\pi c}\left[1 + \frac{2}{\left(\frac{s}{c}\right)}\sum_{n=1}^{\infty}\frac{(-1)^n \sin\left(n\pi\,\frac{s}{c}\right) I_o\left(\frac{n\pi\rho}{c}\right)}{(n\pi)\, I_o\left(\frac{n\pi a}{c}\right)}\right] . \qquad (5.10)$$

This provides a useful check of the accuracy of the numerical calculation.

We next discuss the calculation of the change in AC capacitance between the top and bottom plates when there is free charge on the liquid helium surface. In the limit of small AC voltage this is the partial derivative of total charge on one plate with respect to voltage on the other plate with total surface charge on the helium held constant. As discussed in Appendix 1, Green's reciprocation theorem may be used to show that the result is independent of whether we vary the voltage on the top plate V_{top} and measure the change in charge on the bottom plate Q_{bot}, or vice versa, so:

$$\left.\frac{\partial Q_{top}}{\partial V_{bot}}\right|_{Q_{surf}} = \left.\frac{\partial Q_{bot}}{\partial V_{top}}\right|_{Q_{surf}} . \qquad (5.11)$$

The calculation may be done by varying the potential on either the top plate or the bottom plate with a given fixed potential on the bottom plate. We will discuss both approaches to the problem.

If we vary the potential of the top plate from ground potential to ΔV then there is an additional term added to $E_r^{ext}(\rho_i,c)$ in Eq. (5.9) given by:

$$E_r^{top}(\rho,c) = \frac{2b\Delta V}{a^2}\sum_{n=1}^{\infty}\frac{\sinh\left(x_n\,\frac{c}{a}\right) J_1\left(x_n\,\frac{b}{a}\right) J_1\left(x_n\,\frac{\rho}{a}\right)}{\sinh\left(x_n\,\frac{H}{a}\right) J_1^2(x_n)} . \qquad (5.12)$$

Here b is the radius of the top plate, $J_1(x)$ is the ordinary Bessel function of order one, and x_n is the n^{th} zero of the ordinary Bessel function of order zero. For given values of R and c, Eq. (5.9) may then be solved the same as before.

The change in AC capacitance from the AC capacitance measured with no charge on the liquid helium surface is a result of the surface charge moving and changing the induced charge. (If the surface charge were frozen in place there would be no capacitance change, by the principle of superposition.) The total induced charge on the bottom plate from a ring of radius r with total charge q is found to be:

$$q_{bot}(r,c) = 2q \sum_{n=1}^{\infty} \frac{\sin\left(\frac{n\pi c}{H}\right)}{I_0\left(\frac{n\pi a}{H}\right)} \left\{ I_0\left(\frac{n\pi a}{H}\right) I_0\left(\frac{n\pi r}{H}\right) \left[\left(\frac{a}{H}\right) K_1\left(\frac{n\pi a}{H}\right) - \left(\frac{b}{H}\right) K_1\left(\frac{n\pi r}{H}\right) \right] + \left(\frac{a}{H}\right) I_0\left(\frac{n\pi r}{H}\right) K_0\left(\frac{n\pi a}{H}\right) I_1\left(\frac{n\pi a}{H}\right) - \left(\frac{r}{H}\right) I_0\left(\frac{n\pi a}{H}\right) K_0\left(\frac{n\pi r}{H}\right) I_1\left(\frac{n\pi r}{H}\right) \right\} \tag{5.13a}$$

To find the induced charge on the top plate of radius b we must distinguish between the cases $r < b$ and $r > b$. If $r < b$, then:

$$q_{top}(r,c) = \frac{2q}{H} \sum_{n=1}^{\infty} \frac{\sin\frac{n\pi c}{H}\,(-1)^n}{I_0\left(\frac{n\pi a}{H}\right)} \cdot \left\{ s I_0\left(\frac{n\pi r}{H}\right) \times \left[K_0\left(\frac{n\pi a}{H}\right) I_1\left(\frac{n\pi s}{H}\right) + I_0\left(\frac{n\pi a}{H}\right) K_1\left(\frac{n\pi s}{H}\right) \right] - r I_0\left(\frac{n\pi a}{H}\right) \times \left[I_1\left(\frac{n\pi r}{H}\right) K_0\left(\frac{n\pi r}{H}\right) + K_1\left(\frac{n\pi r}{H}\right) I_0\left(\frac{n\pi r}{H}\right) \right] \right\} . \tag{5.13b}$$

If $r > b$, then:

$$q_{top}(r,c) = \frac{2qs}{H} \sum_{n=1}^{\infty} \frac{\sin\left(\frac{n\pi c}{H}\right) (-1)^n \quad I_1\left(\frac{n\pi s}{H}\right)}{I_0\left(\frac{n\pi a}{H}\right)}$$

$$\times \left[K_0\left(\frac{n\pi a}{H}\right) I_0\left(\frac{n\pi r}{H}\right) - I_0\left(\frac{n\pi a}{H}\right) K_0\left(\frac{n\pi b}{H}\right) \right] \quad . \qquad (5.13c)$$

The total induced charge on the top and the bottom plates, Q_{top} and Q_{bot} respectively, is given by:

$$Q_{top} = \sum_{i=1}^{j_{max}} 2\pi\rho_i \, \Delta r \sigma(\rho_i) \left(\frac{q_{top}(\rho_i, c)}{q} \right) \quad ,$$

$$Q_{bot} = \sum_{i=1}^{j_{max}} 2\pi\rho_i \, \Delta r \sigma(\rho_i) \left(\frac{q_{bot}(\rho_i, c)}{q} \right) \quad . \qquad (5.14)$$

We wish to calculate the partial derivatives of these quantities with respect to the appropriate perturbing voltage while constraining the total surface charge to be constant. It is easy to find the derivatives with respect to voltage while constraining the charge pool radius R to be constant, and the derivatives with respect to charge pool radius while constraining the perturbing voltage to be zero. We use the theorem of vector calculus that, given a pair of differentiable functions $F(x,y)$ and $G(x,y)$, where $\partial G/\partial x \neq 0$, then:

$$\left.\frac{\partial F}{\partial y}\right|_G = \frac{\partial F}{\partial y} - \frac{\left(\frac{\partial F}{\partial x}\right)\left(\frac{\partial G}{\partial y}\right)}{\left(\frac{\partial G}{\partial x}\right)} \quad . \qquad (5.15)$$

We find that:

$$\left.\frac{\partial Q_{top}}{\partial V_{bot}}\right|_{Q_{surf}} = \left.\frac{\partial Q_{top}}{\partial V_{bot}}\right|_{R} - \left.\frac{\partial Q_{surf}}{\partial V_{bot}}\right|_{R} \cdot \frac{\left.\frac{\partial Q_{top}}{\partial R}\right|_{V_{bot}}}{\left.\frac{\partial Q_{surf}}{\partial R}\right|_{V_{bot}}} ,$$

$$\left.\frac{\partial Q_{bot}}{\partial V_{top}}\right|_{Q_{surf}} = \left.\frac{\partial Q_{bot}}{\partial V_{top}}\right|_{R} - \left.\frac{\partial Q_{surf}}{\partial V_{top}}\right|_{R} \cdot \frac{\left.\frac{\partial Q_{bot}}{\partial R}\right|_{V_{top}}}{\left.\frac{\partial Q_{surf}}{\partial R}\right|_{V_{top}}} . \quad (5.16)$$

The quantity calculated here is the change in AC capacitance from the presence of free charge on the liquid helium surface. The total AC capacitance is found by adding to this the ordinary linear capacitance which exists in the absence of free surface charge.

In Fig. 5 we have plotted the fractional change in capacitance when free charge is placed on the surface of liquid helium with the bottom plate at a fixed potential V_o versus the ratio V_{sat}/V_o (where V_{sat} is the voltage at which the free charge on the surface would be just sufficient to cover the surface) for the case in which $c/H = 0.5$. In Fig. 6 we compare the measured fractional capacitance change with the result of our calculation. The discontinuity in slope occurs at $V = V_{sat}$ at which point the charge pool exactly covers the helium surface. As the voltage is reduced further, charge moves onto the helium film covering the walls. Only a small fraction of charge that has moved to the walls returns to the surface of the bulk liquid if the bottom plate potential is increased to its former value. This causes hysteresis in curves of AC capacitance versus voltage if the voltage on the bottom plate is reduced below V_{sat}. It is also found that if the voltage on the bottom plate is reduced

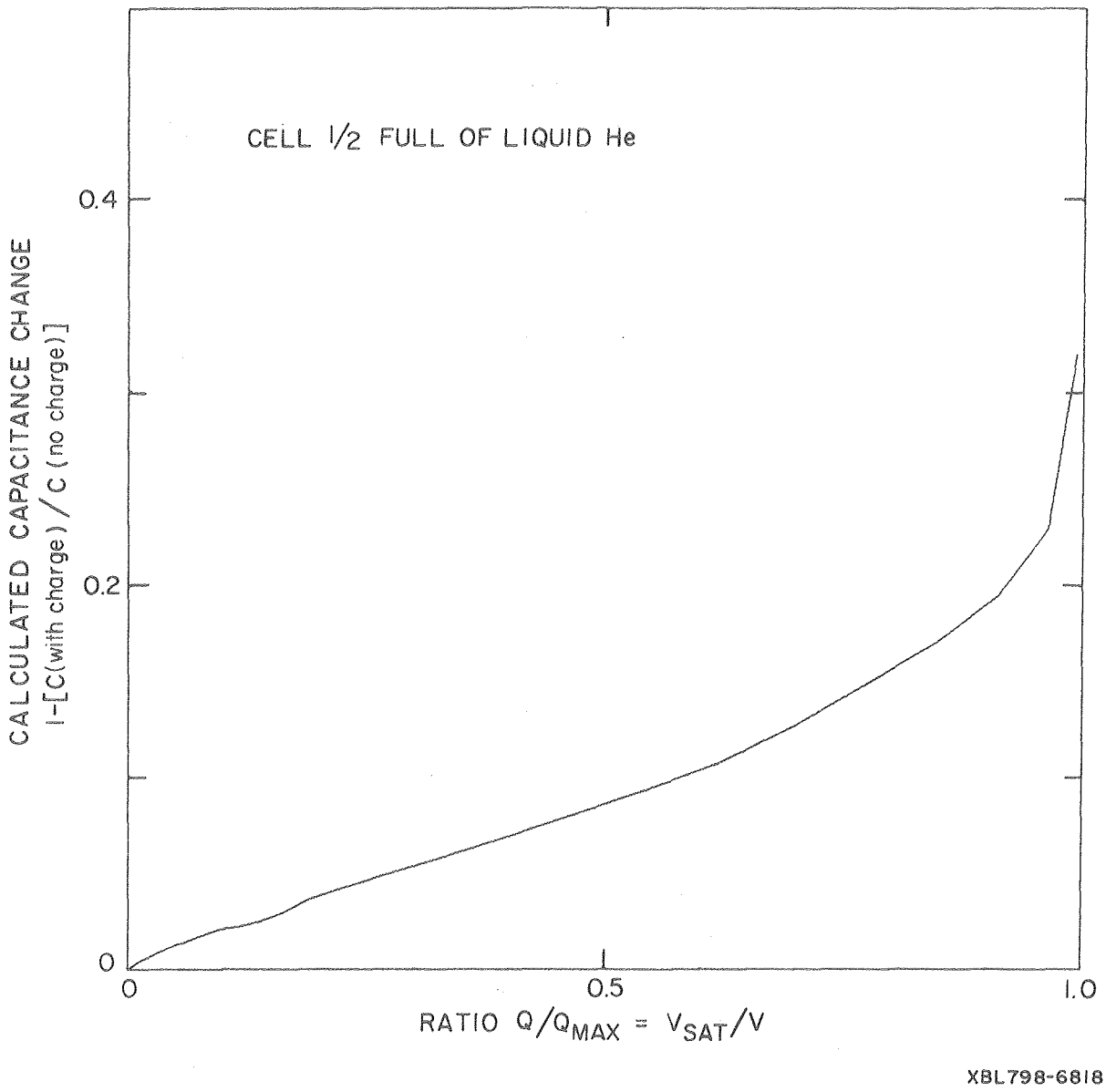

Fig. 5. Calculated capacitance change versus total charge on the helium surface. The maximum amount of charge, Q_{max}, corresponds to covering the entire surface with the charge pool.

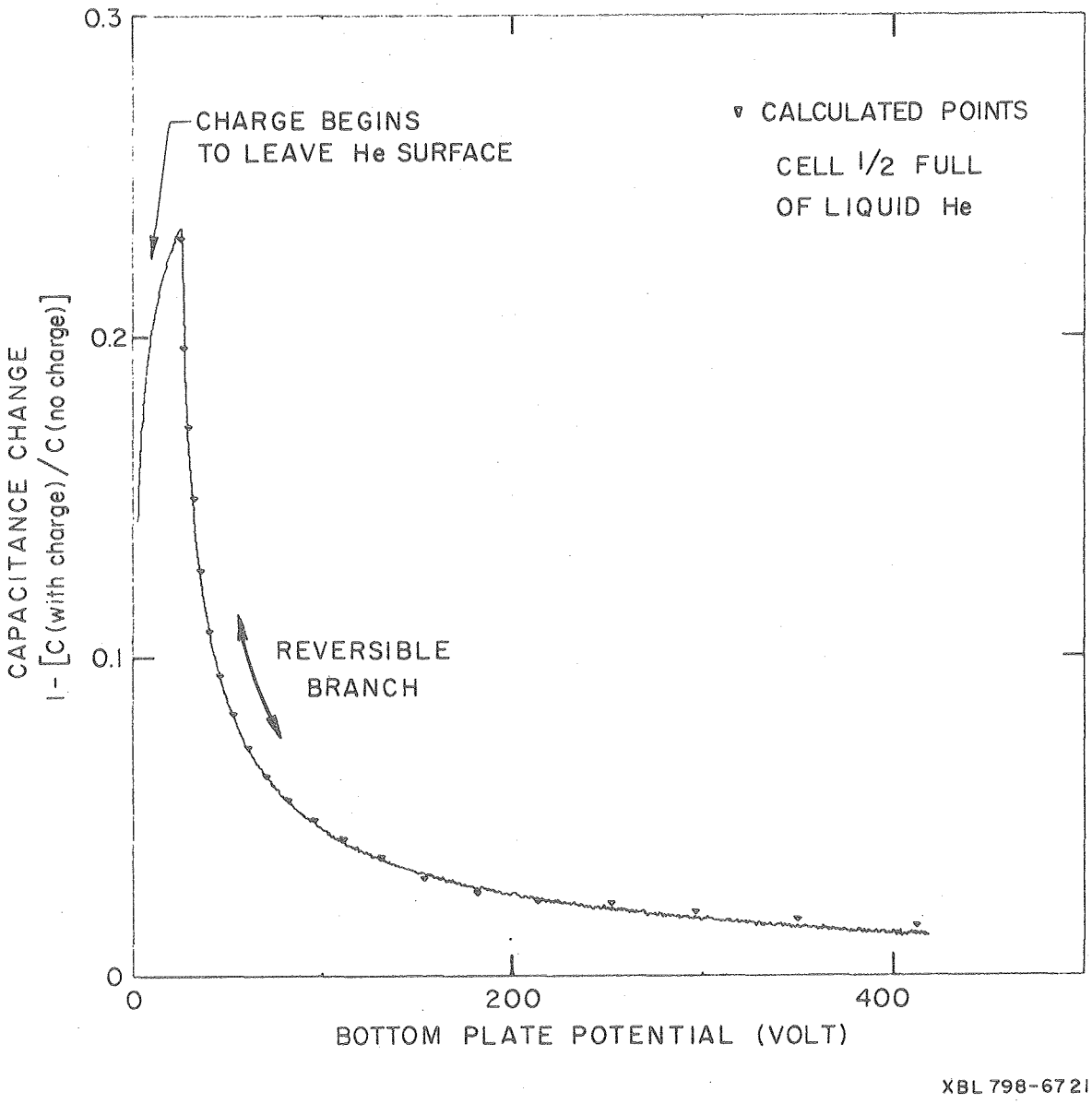

Fig. 6. Comparison between the measured curve of capacitance change versus voltage and the results of our electrostatic calculation. The discontinuity of slope in the measured curve occurs when the charge pool begins to flow off the surface onto the walls.

below V_{sat} that lineshapes of resonance transitions of the bound states discussed in Chapter 2 become distorted. Similar effects were seen by Volodin, Khaikin, and Edel'man[74] when measuring the loss of Q in an RF circuit caused by electrons on the helium film above a metal and above a dielectric. It has been theoretically predicted[8] that electrons on a helium film several hundred Å thick will be "self-trapped" and have greatly reduced mobility.

We next discuss how the local electric field acting on electrons in external surface states is calculated (except for the dipole field from nearby electrons). From Eq. (5.10) we see that near the center of the cell the charge density is almost constant. The lines of flux are therefore very nearly parallel in this region and the local electric field may be found from an argument based on Gauss' law. The local electric field acting upon a surface electron near the center of our cell is the same as the field that would be found in the following situation. We compute the electric field at the center of a small circular hole of radius $r \ll H$ in a sheet of uniform charge density located just above the surface of a dielectric. The dielectric fills an infinite plane parallel capacitor to a depth z. If the bottom plate of the capacitor has potential V and the top plate is maintained at ground potential we find that the local electric field acting on electrons near the center of the charge pool in our cell is to be given by:

$$E = \left[\frac{V}{H} - \frac{4\pi\sigma_F}{1+\varepsilon}\left\{1 - 2\left(\frac{z}{H}\right)\right\}\right] \Big/ \left(1 - \frac{z}{H}\,\frac{(\varepsilon-1)}{\varepsilon}\right) . \qquad (5.17)$$

The z which appears in this equation is the height of liquid

helium at the center of the cell. This is not exactly equal to z_0 calculated from Eq. (5.5) The helium surface is depressed by the electric field acting on the surface charge and is slightly raised because a non-zero electric field causes more liquid to enter the cell. Hydrostatic pressure dominates over surface tension in determining the surface shape for distances large in comparison to the capillary constant which for liquid helium is $(2\alpha/g\rho)^{\frac{1}{2}} \approx 0.073$ cm. Here α is the surface tension discussed earlier, g is the acceleration of gravity, and ρ is the density of liquid helium. Since $R >> 0.073$ cm and since the charge density is almost constant over most of the charge pool we make the approximation that the helium depth under the charge pool changes by a uniform amount. The equilibrium value of z can then be obtained by minimizing the thermodynamic potential[75] at constant bottom plate voltage:

$$\tilde{F} = (z^2 \cdot \pi R^2 + h_2^2 A_2 + h_3^2 A_3) - \frac{(\varepsilon-1)}{8\pi}(zA_1 + h_2 A_2)E^2 - \pi R^2 \sigma_F E + \tilde{F}_0 \,. \tag{5.18}$$

Here A_2 is the area of bulk liquid surface in the cell not covered by the charge pool, A_3 is the area of liquid outside the cell, h_2 and h_3 are the depth of liquid under A_2 and A_3 respectively above the bottom plate of the cell, σ_F is the free surface charge density at the center of the cell, and $\tilde{F}_0$ is the value of $\tilde{F}$ when $E=0$ and $\sigma_F = 0$. The variation is subject to the constraint $z_0(A_1+A_2+A_3) = zA_1 + h_2A_2 + h_3A_3$. We find that:

$$z - z_0 = \frac{E\sigma_F}{\rho g}\left(\frac{A_2 + A_3}{A_2 + A_3 + \pi R^2}\right) + \frac{(\varepsilon-1)\,E^2 A_3}{8\pi\rho g(A_2 + A_3 + \pi R^2)} \,. \tag{5.19}$$

Both of these terms are small under the conditions of our experiment. The first term gives an effect in z/H as large as order 10^{-3} while the second term gives an effect as large as 10^{-4}.

The change in local electric field acting on electrons near the edge of the charge pool may be obtained using Laplace's equation if the holes in the top used to couple light in and out are ignored. However, this calculation was not used in our data analysis which relied on the fact that the center of the cell is a point of symmetry — hence the density of electrons per unit electric field interval will become infinite at the electric field corresponding to the center. In the absence of other sources of broadening this would cause a singularity in the lineshape function.

Our discussion to this point has assumed that the helium surface is flat and parallel to the top and bottom plates. We examine the effect of tilting the cavity axis through an angle $\Delta\theta$ away from being parallel to the helium surface normal. For small $\Delta\theta$ this causes an extra electric field parallel to the helium surface of magnitude $E_z^{ext}\Delta\theta$ where E_z^{ext} is given by Eq. (5.3). The distance the charge pool moves in response to this field is approximately:

$$\Delta x = \frac{RE_z^{ext}(0,c)\Delta\theta}{E_r^{ext}(R,c)} \quad . \tag{5.20}$$

The derivative of charge density with respect to position near the center of the charge pool is given approximately by

$$\frac{d\sigma}{dx} = \frac{E_z^{ext}(0,c)\Delta\theta}{4\pi c} \quad . \tag{5.21}$$

For our preceding analysis to be valid we require that $\Delta x \ll R$, $\Delta x < a-R$,

and $R \frac{d\sigma}{dx} << \sigma$.

Another source of inaccuracy in our calculated electric field arises from the shape of the cell not exactly matching the shape we have used in our analysis. The cell used in our experiment is constructed so that the lack of flatness of the walls, the gap between the top plate and the cell body, and the hole in the center of the top plate all change the electric field at helium surface by less than a few parts in 10^4. The holes to let far infrared light in and out of the cell are unavoidable. However, since they are near the edge of the cavity their influence should decay away as we move to the center of the cavity just as the other edge effects do.

VI. EXPERIMENTAL TECHNIQUES

Our purpose in measuring the far infrared absorption of electrons on liquid helium is to learn about the microscopic behavior of the system. A number of obstacles have been overcome to do this. In the preceding chapter we described how the charge density and local electric field are obtained from capacitance and voltage measurements. Another problem is that of measuring the absorption lines caused by transitions between electron surface states in the presence of noise. The lines are only a few GHz wide and the absorption at line center is only of order 10^{-5} of the light reaching the detector.

A block diagram of the apparatus used to make the optical measurements is shown in Fig. 7. The light source is an optically pumped molecular laser. We measure absorption as a function of electric field. The molecular laser has many possible lasing frequencies between 300 GHz and 10^4 GHz.[76] By selecting the molecular laser gas (CH_3OH), cavity length, and the CO_2 pump laser frequency we cause it to lase at one of these frequencies. We identify the lasing transition by approximate frequency measurement. The exact frequency is then known to within a few MHz (the width of the molecular laser gain curve) from heterodyne measurements reported in the literature.[77] Light from the laser is brought through light pipes to the cell containing the electrons, and a light pipe is also used to carry light from the cell to the detector. The electric field in the cell is the sum of a slow linear ramp and a square wave of frequency ν_m = 60 KHz. The output of the laser is also optically chopped at ν_c = 100 Hz to enable the power reaching the detector to be measured. The output signals from two lock-in amplifiers

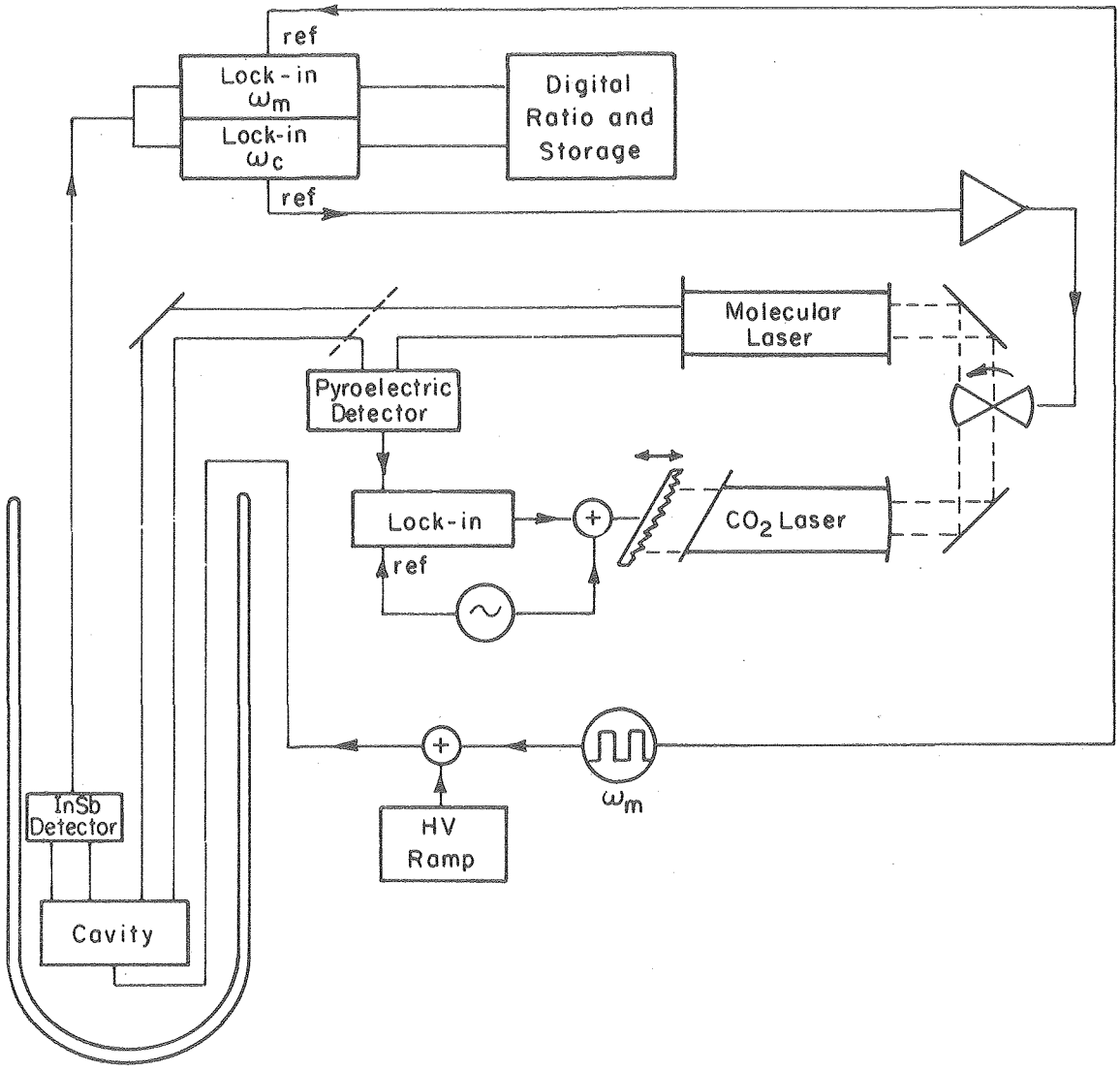

Fig. 7. Block diagram of the apparatus used for optical measurements.

synchronized to ν_m and ν_c and the DC voltage on the bottom plate are recorded about once per second. After repeating with several square wave voltage amplitudes the data are computer-processed to yield optical absorption by the electrons as a function of bottom plate voltage.

We discuss the light source in detail first. The CO_2 pump laser is an Apollo Lasers model 550 modified to allow the cavity length to be set with a piezoelectric transducer. The output power varies with transition used but is typically about 10 W. The lasing transition is monitored with a grating spectrometer (Optical Engineering, Inc., model 16-A) which accepts reflected light when the optical chopper blocks the beam. The output power of the CO_2 laser during alignment is measured with a detector based on the thermoelectric effect.

The molecular laser is of our own design and uses flowing gas. The cavity is 92 cm long and uses machined aluminum mirrors 4.95 cm in diameter. The mirrors have 50 cm focal length which yields stable resonator modes.[79] Light from the CO_2 laser is coupled into the cavity through a NaCl vacuum window and a 1.0 mm diameter hole. Far infrared light is coupled out of the cavity through a 1.6 mm diameter hole and a crystalline quartz vacuum window. The cavity length is varied with a hollow differential screw mechanism. Pump light is coupled into the laser through an axial hole in the screw. The cavity is contained in a fused quartz tube (chosen for low thermal expansion). No mirror adjustments are needed. The molecular laser is found to remain at the peak of the gain curve even after not being used for several months.

The frequency output of the CO_2 pump laser is kept at the peak of the molecular laser gain curve with a feedback loop. A 4.2 μm thickness

mylar beam splitter directs part of the output of the molecular laser to a pyroelectric detector (Molectron Corp., model P4-71). The CO_2 laser cavity length is modulated at ν_ℓ = 30 Hz and the synchronous signal from the detector is measured with a lock-in amplifier. The output from the lock-in amplifier is proportional to the rate of change of molecular laser output with CO_2 laser frequency. It is used as the error signal applied to the piezoelectric transducer which sets the CO_2 laser frequency. The time constant used in the feedback loop is 100 sec. If the feedback loop is not used, thermal drifts in the CO_2 laser will typically quench the molecular laser output in 5 to 15 minutes.

The approximate frequency at which the molecular laser is operating is measured with a Fourier transform Michelson interferometer of the type originally suggested by Martin and Puplett.[79] The theory of this interferometer[80] and a technique to use a two-beam interferometer to measure the optical transfer function as a function of optical and spatial frequency[81] resulted from our work and have been published. Occasionally we have observed several transitions at widely spaced frequencies to lase simulataneously but this has not proved to be a problem when using the laser to measure the absorption lines.

We next discuss the noise limitations of our optical system. For several of the laser lines used the dominant source of noise was fluctuations in the output power of the laser. The noise power spectrum of laser amplitude noise is found to have a 1/f spectral density from about 1 kHz to 20 kHz. For frequencies below 1 kz the noise spectrum has large peaks at harmonics of the line frequency but is otherwise relatively flat. From 20 to 100 kHz the noise decreases by less than

a factor two. The noise spectrum we have observed from our molecular laser agrees with that measured directly from a CO_2 laser similar to our pump laser with a HgCdTe detector.[82] The exact source of the noise is not known but is presumed to originate in the CO_2 laser gas discharge. There is an established theory[83] of noise in a laser oscillator based on spontaneous emission perturbations to the Van der Pol oscillator model. The theory has been experimentally verified for lasers operating very close to threshold[84] where the noise power spectrum is predicted to be a Lorentzian with width inversely proportional to laser output. For our CO_2 laser the theory predicts a linewidth of order 10^{-7} Hz. This is clearly not the source of our observed laser noise. Other previously observed noise sources in laser oscillators are fluctuations in the gas discharge,[85] vibration of end mirrors,[86] fluctuations in light coupled back into the laser,[87] and fluctuation of the distribution of power among several lasing modes while the total power remains relatively constant. It has recently become possible to obtain bandwidths of less than 10 Hz in the methane-stabilized 3.39-micron He-Ne laser[88] by giving careful attention to each of these sources of noise. We have taken several elementary steps to reduce the laser noise, such as carefully shielding and grounding the system, isolating the mechanical vacuum pump from the laser cavity, using a vibration-isolated table to support the laser, and regulating the current in the discharge with a fast feedback loop. The next logical step would be to redesign the discharge tube which is found to oscillate electrically at a pressure-tuned frequency near 50 MHz and harmonics and to be a source of electrical noise spikes that occur at irregular intervals. An optical isolator[89] could also be placed

between the CO_2 laser and the molecular laser to eliminate fluctuations from reflected light. It is observed that the magnitude of the noise from the molecular laser depends upon where on the gain curve the CO_2 laser is pumping. This is probably a result of the molecular laser gain curve converting FM noise of the pump laser to AM noise.

When the optical power detected by the detector drops about one order of magnitude from that of the strongest laser lines, then detector noise becomes the dominant noise source. Our detector is an InSb hot electron bolometer.[90] It has uniform response to optical frequencies below about 15 cm^{-1}, drops by a factor two at 20 cm^{-1}, by a factor six at 30 cm^{-1} and is down to 10^{-2} at 50 cm^{-1}. The response time of the detector is of order 10^{-7} sec (the electron-phonon relaxation time) and the response as a function of frequency should be flat from a few Hz (the thermal relaxation time) to nearly one MHz. At frequencies above about 200 Hz the detector has a 1/f noise power spectra with a coefficient which varies as a function of bias current. At about 50 KHz the detector noise becomes less than noise from the other sources which have a flat frequency noise power spectra of 7 nv/$\sqrt{Hz}$ at higher frequencies. For investigation of absorption using weak laser lines the best way to increase the signal-to-noise ratio would be to increase the fraction of power from the laser absorbed by the detector. At the present time this is of order 10^{-4}. The loss occurring between the output of the molecular laser and the top of the dewar insert is measured to be about a factor 15, which could be eliminated by focusing the light with a concave mirror rather than using the brass light pipe with right-angle bands which is employed at present.

When observing large absorption signals without using the pneumatic vibration-isolation system a modulation of about 10% of the signal was observed from waves on the helium surface. The vibration-isolation system reduces this source of noise by about two orders of magnitude.

We next focus our attention on the dewar insert shown in Fig. 8. The vacuum-tight can containing the experimental cell is submerged in a liquid helium bath. Laser light is brought down the dewar to the cell through a 1.27 cm diameter stainless steel light pipe. Before entering the cavity the light passes through a Fluorogold™ filter which transmits light of frequency less than 50 cm^{-1} but does not transmit room temperature blackbody radiation coming down the light pipe. A Winston reflective light concentrator[91] is used to change the angular distribution of the light coming down the light pipe from being unidirectional to a distribution with intensity proportional to $\cos\theta$ where θ is the off-axis angle. After reflecting a number of times in the cavity, part of the light exits through a hole in the top of the cell. Light leaving the hole is recollimated with another Winston light concentrator, passes up a light pipe through a mylar vacuum window, and is concentrated again onto the InSb detector.

The experimental cell (shown in detail in Fig. 2) is partially filled with liquid helium by condensing pure helium gas into the vacuum can through a small tube while monitoring the capacitance across the cell with a capacitance bridge. The cell was machined from stress-relieved 6061 aluminum alloy, and coated with gold by evaporation.[92] The bottom plate is insulated from the top plate by mylar spacers and is

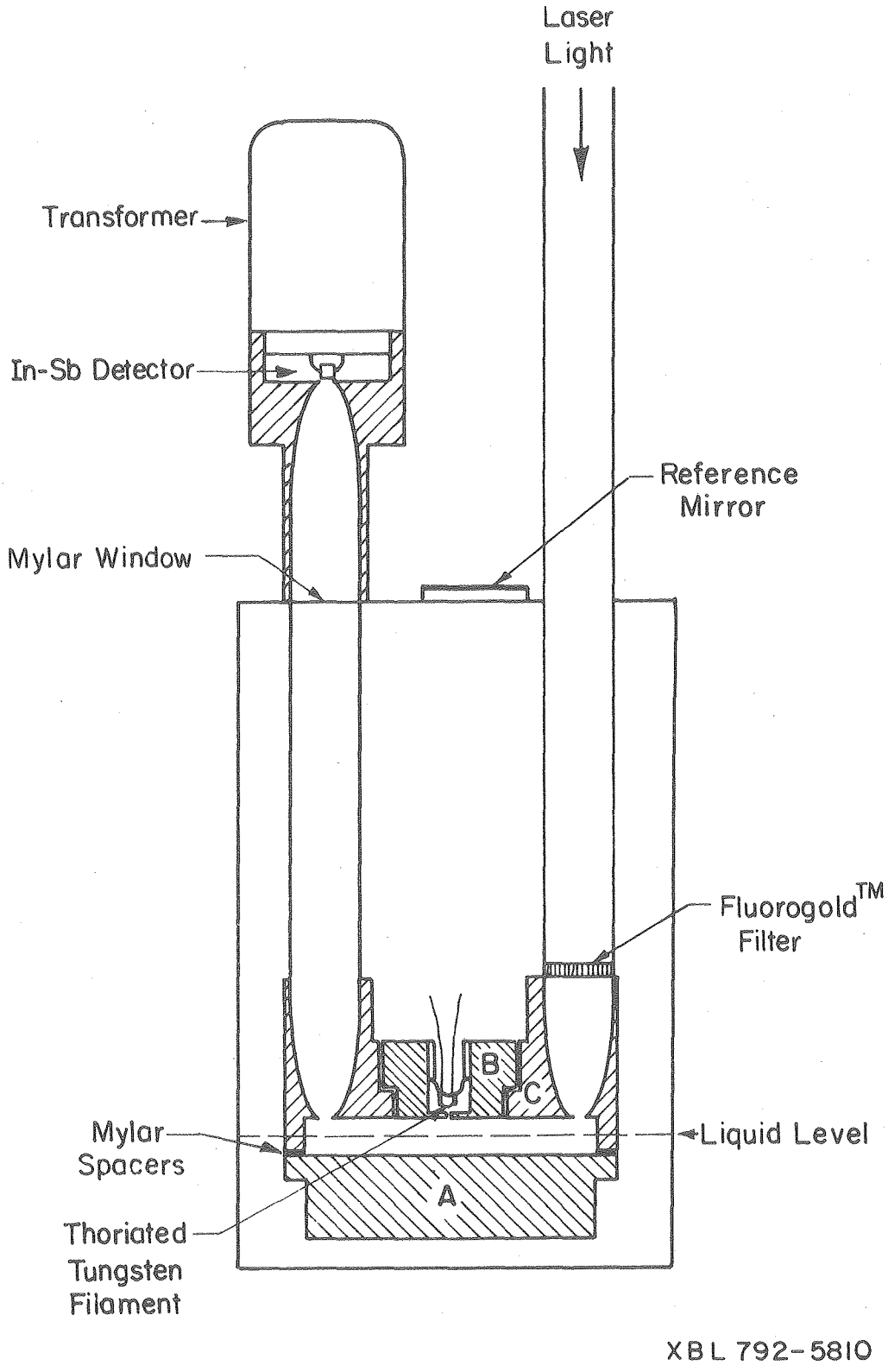

Figure 8. Dewar insert.

attached with nylon screws. The bottom plate is flat to within ±1 μm and the top is flat to within ±2 μm, except near the edges of the two light coupling holes on the top where there is a lip that rises by about 10 μm. The dimensions of the cell at room temperature were measured with a microscope and calibrated lead screw. The total height from the top of the cell to the bottom plate at liquid helium temperature is used in calculating the electric field in the cell and is obtained in two ways. The first is to calculate the thermal contraction using published thermal expansion coefficients[93] of the materials used and including the elastic compression of the mylar spacers as the nylon screws contract. The second is to use the capacitance measured between the top and bottom plates together with the dimensions of the cavity at liquid helium temperature. These results are given in Fig. 2 (pg. 22). The height of the cavity is given by:

$$H[\mathrm{cm}] = \frac{5}{2} \frac{r^2[\mathrm{cm}]\,\xi}{(2.99793)^2\ C[\mathrm{pf}]} \quad . \tag{6.1}$$

Here r is the average of the radius of the top plate and the radius of the circular hole containing it, C is the measured capacitance, and ξ is given in Eq. (5.4).

Electrons are put on the helium surface by thermionic emission from a 13 μm diameter thoriated tungsten filament. The filament is contained in a small chamber in the top plate. Free electrons pass from this chamber into the cell through a circular hole about 0.46 mm in diameter and about 0.2 mm deep. As the filament is heated for the few seconds necessary to put charge on the surface, the surface charge is monitored by measuring the AC capacitance between top and bottom

plates. To prevent charge from reaching the walls as the filament is heated we gradually increase and decrease the filament current but keep it hot enough to emit substantial amounts of charge for only a short time. (If the filament current is suddenly pulsed while charge is on the surface, all the charge is observed to leave the surface.) Large gaps were left between the spacers separating the bottom plate of the cell from the cell body so as to avoid filling the cell by the fountain effect when the filament was heated. The fluid levels inside and outside the cell equilibrate in about one second.

The temperature of the helium bath is obtained by measuring the gas pressure and comparing with published tables to calibrate a carbon resistor as a thermometer. The carbon resistor is used for direct measurements. The temperature is near 1.2°K during all of our runs.

As discussed at the end of the last chapter it is important that parallelism between the helium surface and the surfaces of the cell be maintained if the experimental results are to have a simple interpretation. We have been able to maintain this parallelism to within $\pm 2 \times 10^{-4}$ rad by comparing the direction a He-Ne laser beam is reflected from a reference mirror, attached to the top of the can which surrounds the experimental apparatus, with the direction in which the laser beam is reflected from the surface of a pool of water.

We had hoped to also be able to use the variation of AC capacitance measured across our cell as the cell is tilted, to adjust the cell to be parallel with the helium surface since a minimum in the AC capacitance is expected when parallelism is achieved. The observed minimum is displaced from the axis of parallelism, however, because the cell is

slightly offset from the axis of the can surrounding the apparatus. The observed offset of the capacitance minimum is understood quantitatively (it arises because the average height of the charge pool above the bottom plate changes as the cell is tilted) but it destroys the usefulness of using AC capacitance measurements to adjust for parallelism.

We next discuss how our data are processed to yield the optical signal as a function of voltage on the bottom plate. Referring back to Fig. 7 we see that in the limit that the peak to peak amplitude of the square wave voltage ΔV applied to the bottom plate is small then our data, the modulation signal at ν_m divided by the modulation signal at ν_c, are proportional to the derivative of light intensity transmitted by the cell as a function of bottom plate voltage. However, a small ΔV reduces the modulation signal in comparison to the noise. We give the data reduction technique that allows us to use a large ΔV so the signal will be large in relation to the noise while avoiding the distortion that would occur if we obtained the optical response from the data by simple integration.

To begin, we look at the response of a single data point to a delta function optical response when the bottom plate voltage is V_o. The data point is obtained by integrating the optical response as the voltage applied to the bottom plate is increased from V_o to $V_o + \delta V$. We find the integrated response to be given by:

$$R(V - V_o) = \begin{cases} A & \text{if } -\left(\delta V + \frac{\Delta V}{2}\right) < V - V_o < -\frac{\Delta V}{2} \\ -A & \text{if } \frac{\Delta V}{2} - \delta V < V - V_o < \frac{\Delta V}{2} \\ 0 & \text{otherwise} \end{cases} \qquad (6.2)$$

The measured data points are given by the convolution of $R(V - V_0)$ with the optical transmission of the cavity as a function of the voltage V on the bottom plate, which we call T(V). Then, in the absence of noise, the measured signal is:

$$S(V_0) = \int_{-\infty}^{\infty} R(V - V_0)\, T(V)\, dV \quad . \tag{6.3}$$

Given T(V) over a voltage range I_1 of length ΔV we may recover T(V) over any voltage range I_2 containing I_1 from the values of $S(V_0)$ on I_2 to within a resolution δV by using the relation

$$T(V + \Delta V) = T(V) - 2A\, S\left(V + \frac{\Delta V + \delta V}{2}\right) \quad . \tag{6.4}$$

The effect of noise in the data on T(V) recovered in this way is most easily seen using Fourier transforms. We define:

$$s(u) = \int_{-\infty}^{\infty} S(V)\, e^{-2\pi i u V}\, dV \quad . \tag{6.5}$$

We similarly define r(u) and t(u) from R(V) and T(V) respectively. Since the Fourier transform of the convolution of the two functions is the product of the Fourier transform of each function, then, in the absence of noise, $s(u) = r(u)\,t(u)$. We find that

$$|r(u)| = \frac{A}{\pi u} \left|\sin(\pi \delta V u)\, \sin(\pi \Delta V u)\right| \quad . \tag{6.6}$$

Our process of recovering T(V) from measurements of S(V) is equivalent in u-space to $t(u) = s(u)/r(u)$. In practice, $s(u) = s_0(u) + n(u)$, where n(u) is the result of noise and $s_0(u)$ is the result of a changing

optical signal from electrons on the helium surface. If we represent the recovered optical transmission by $T_R(V)$ and its Fourier transform by $t_R(u)$, then:

$$t_R(u) = \frac{n(u)}{r(u)} + t(u) \quad . \tag{6.7}$$

Since we sample at voltage intervals dV then $s(u)$ will be non-zero only for u in the range $-\pi/dV < u < \pi/dV$. For a given non-zero u the effect of noise may be minimized by choosing $\delta V = u/(2m+1)$ and $\Delta V = u/(2n+1)$ where m and n are integers. However it is impossible to minimize the effect of noise at all frequencies simultaneously. In particular, the effect of noise becomes very large near the zeros of $r(u)$. To minimize the effect of noise we measure $S(V)$ several times using different values of ΔV. For each measurement $S^i(V)$ we compute $T_R^i(V)$ using an algorithm based on Eq. (6.4) and compute $t_R^i(u)$. If we assume that the noise is a stationary random process then the most probable value of $t(u)$ is given by:

$$t(u) = \frac{\sum_i t_R^i(u) \cdot |r^i(u)|}{\sum_i |r^i(u)|} \quad . \tag{6.8}$$

We use this equation to compute $t(u)$ for each u and then Fourier transform back to find $T(V)$. For this procedure to be effective one must choose the values of ΔV used so that the denominator of Eq. (6.8) is small only for u near zero. In practice, we have used $\delta V = 0.224$ volt and ΔV between δV and 5 volt. The $S^i(V)$ for each voltage ramp is the output from the lock-in amplifier synchronized to ν_m divided by the output from the lock-in amplifier synchronized to ν_c (in order to

minimize the errors resulting from changes in the laser output power). Each $T_R^i(V)$ computed using Eq. (6.4) has subtracted from it a linear function (which would arise from a small offset in the zero of the lock-in amplifier at ν_m) so that the first and last computed points as a function of V are zero.

Data collection is done with a ±10V 16-bit AD converter with three multiplexed inputs that is controlled by a PDP 11-23™ minicomputer. In a single integration cycle the computer first digitally integrates the output of the lock-in amplifier synchronized to ν_m for 531 msec. After waiting 100 msec, it integrates the output of the lock-in amplifier synchronized to ν_c for 100 msec. Finally, after waiting another 100 msec it integrates a DC voltage proportional to the voltage applied to the bottom plate for 100 msec. The cycle then starts over. Data are transferred to magnetic tape and processed using a program coded in FORTRAN that runs on the CDC-7600 computer at the LBL computer center. The computed optical signal as a function of bottom plate voltage is plotted, and stored on magnetic tape to await the further processing described in the next chapter.

The linear voltage ramp is generated digitally with a 16-bit DA converter, and is applied to the bottom plate using the circuit shown in Fig. 9. The resistive divider used to measure the ramp voltage is calibrated with a Fluke 343A voltage calibrator, so the absolute accuracy of the measurement of the voltage of the bottom plate is limited only by the resolution and linearity of the AD converter. (During a run the zero of the AD typically drifts by a few bits which limits the absolute accuracy to ±0.05 V.)

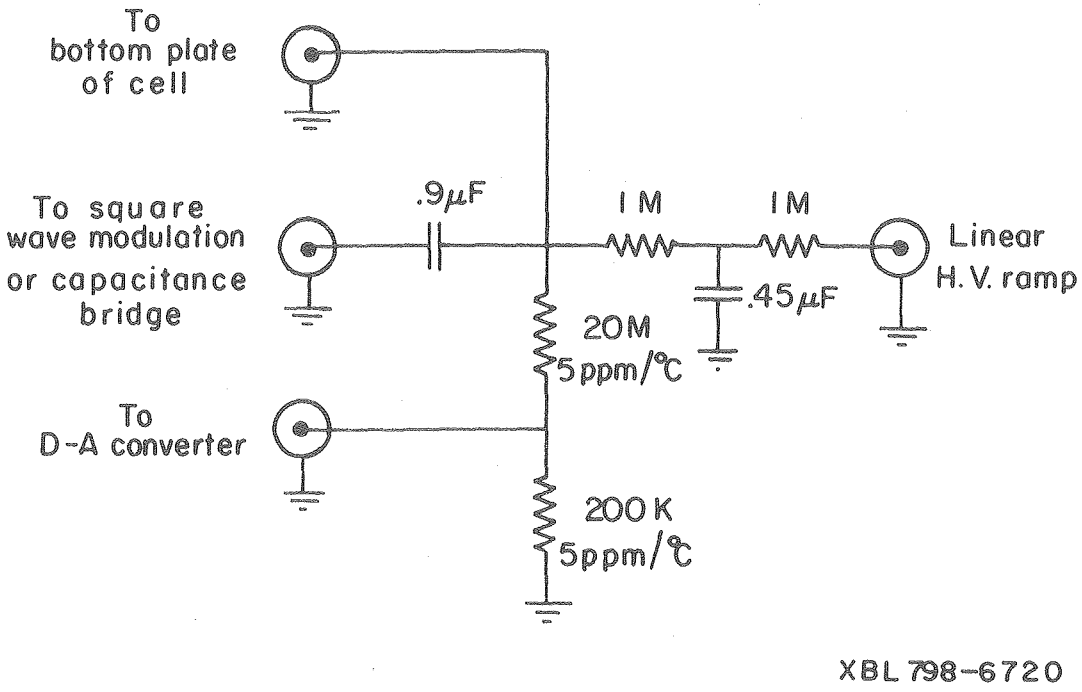

Fig. 9. Circuit used to apply modulation voltage to the bottom plate of the cell.

The height of helium in the cell and the charge density on the helium surface are obtained from measurements made with an AC capacitance bridge using the theory described in the previous chapter. Measurements are made using a General Radio type 1615-A capacitance bridge with PAR 124A lock-in amplifier for oscillator and detector. Measurements are taken at 1 KHz, although it was verified that the measured AC capacitance was independent of oscillator frequency as expected. The liquid height determination is done using 5 V_{rms} to drive the bridge. The surface charge determination is done using 0.5 V_{rms} to drive the bridge. The capacitance measurements used to measure the liquid height are reproducible to a few parts in 10^{-5} pf. Not all the measured capacitance arises from geometric capacitance between the top and bottom of the cell however. When the cell was filled with liquid helium the capacitance increased slightly less than one calculates it should using the most accurate measurement of the dielectric constant of liquid helium reported in the literature.[9] From our measurement we calculate a stray capacitance of 0.00160 pf at liquid helium temperatures. This value of the stray capacitance brings our mechanical measurement of the cell height, corrected for thermal contraction, into better agreement with the capacitance measurement using Eq. (6.1) than the errors involved in the separate measurements predict. At room temperature the stray capacitance measured by grounding the bottom plate and disconnecting the lead attached to it is found to be 0.00020 pf. This also causes the room temperature mechanical measurement of the cell height to agree very well with the cell height obtained from measuring the capacitance. One explanation that may be given for the observed increase of stray

capacitance that occurs when the cell is cooled from liquid helium temperature is that the surface oxide barrier could cause strands of wire in the single braid separating the two leads as they go to the top of the dewar to become electrically isolated when the temperature is lowered.

VII. DATA ANALYSIS

In the previous chapter we discussed the spectroscopic techniques used to observe external electron state transitions from the ground state to various excited states. We obtain two physically distinct quantities from our measurements. The first of these is a measure of the local positional disorder of electrons along the plane of the surface. This is obtained because the electric dipole field of nearby ground state surface electrons changes the external electric field that must be applied to bring a given transition into resonance with a given laser frequency. The shift in applied field is related to the radial-distribution function of the external surface electrons. The second physically distinct quantity is the transition frequency as a function of applied electric field in the limit of zero surface charge density. The difference between the measured transition frequency and the frequency calculated from a model which assumes an abrupt potential change at the surface [Eq. (2.1)], contains information about deviations from the image potential near the surface.

This chapter is divided into a number of sections. In Section A we present the theory of the change in transition energy caused by the electrostatic interaction between a surface electron in an excited state and nearby surface electrons in the ground state. In Section B we discuss the source of a dispersive component observed in our measured lineshapes and explain how it is removed by deconvolution. Section C describes how for each observed resonance we obtain from our data the surface charge density at the center of our cell and the external

electric field acting on the surface electrons at the center of our cell. In Section D we describe how we statistically analyzed our data to obtain a measure of the local positional disorder of the surface electrons and the external electric field that must be applied to cause the observed transition resonances to occur at the laser frequency in the limit as the surface charge density approaches zero. Finally, in Section E we discuss the implications of our measured values.

A. Effect of the Electric Field of Nearby Electrons

In this section we discuss the theory of the change in transition energy caused by the dipole electric field of nearby surface electrons in the ground state. We first consider the case in which the surface electrons are arranged into a perfect hexagonal lattice and then generalize to include the effects of disorder.

The x-y coordinates of a hexagonal lattice of electrons are given by the points:

$$\underset{\sim}{r}_{ij} = a\left[\left(i + \frac{j}{2}\right)\hat{x} + \frac{\sqrt{3}}{2}\, j\hat{y}\right] . \tag{7.1}$$

We consider the case in which all of the electrons are in the ground state except one. The one-electron Hamiltonian for this electron includes a term arising from the electrostatic interaction with the other surface state electrons given by:

$$H' = \sum_{i,j}{}' \frac{e^2}{(r_{ij}^2 + u^2)^{\frac{1}{2}}} - \sum_{i,j}{}' \frac{e^2}{r_{ij}} , \quad \text{where} \quad u = z - \langle z \rangle_1 . \tag{7.2}$$

Here $r_{ij} = |\underset{\sim}{r}_{ij}|$ in Eq. (7.1) and the summation excludes the case where

both i=0 and j=0. We have implicitly assumed that the nearby electrons do not tend to fill the hole an excited electron leaves as it moves away from the surface, which will be a very good approximation if $u \ll a$. We may rewrite Eq. (7.2) in the form:

$$H' = \sum_{i,j}{}' \frac{e^2}{r_{ij}} \left[\frac{1}{(1+x_{ij}^2)^{\frac{1}{2}}} - 1 \right] \quad , \quad \text{where} \quad x_{ij} = \frac{u}{r_{ij}} \quad . \tag{7.3}$$

We are interested in the case in which $x_{ij} \ll 1$. The Taylor expansion of $f(x) = (1+x^2)^{-\frac{1}{2}}$ about the point x_0; neglecting terms of order x_0^3, xx_0^2, x^2x_0, x^3, and higher order terms in x and x_0; is given by:

$$(1+x^2) = 1 - (x_0^2 - \tfrac{1}{2}x^2) \quad . \tag{7.4}$$

Hence

$$H' = -\left(\sum_{i,j}{}' \frac{e^2}{r_{ij}^3} \right) \cdot (u_0^2 - \tfrac{1}{2}u^2) \quad . \tag{7.5}$$

To find the change in transition energy from the ground state to excited state n caused by the nearby external surface state electrons, we use first order perturbation theory. We calculate $\langle 1|H'|1\rangle$ with H' expanded about $z = \langle z\rangle_1$ and also $\langle n|H'|n\rangle$ with H' expanded about $\langle z\rangle_n$. We find:

$$\Delta E_{1-n} = -\left(\sum_{i,j}{}' \frac{e^2}{r_{ij}^3} \right) \left[\left(\langle z\rangle_n - \langle z\rangle_1 \right)^2 - \tfrac{1}{2}\left(\langle z^2\rangle_n - \langle z\rangle_n^2 \right) + \tfrac{1}{2}\left(\langle z^2\rangle_1 - \langle z\rangle_1^2 \right) \right] \quad . \tag{7.6}$$

In obtaining this result we have assumed that $(\langle z\rangle_n - \langle z\rangle_1)/a \ll 1$. For the r_{ij} of a hexagonal lattice the summation appearing in Eq. (7.6) has been done numerically. Using the fact that for the hexagonal lattice the charge density $\sigma = 2e/(\sqrt{3}\, a^2)$, we find that:

$$C(\sigma) = \sum_{i,j}{}' \frac{e^2}{r_{ij}^3} = 8.8927\ |\sigma|^{3/2}\ e^{1/2} \quad . \tag{7.7}$$

The actual arrangement of the surface state electrons is not exactly a hexagonal lattice. Even at zero temperature there will be some disorder due to the zero point motion of the electrons.[94] In the presence of disorder the analysis which led to Eq. (7.6) is still correct but the r_{ij} appearing in the coefficient must be interpreted as the distance from the excited electron to each of the other electrons. Because the other electrons are moving, then $C(\sigma)$ is a fluctuating quantity. To obtain the thermal average of $C(\sigma)$ we use the radial-distribution function $g(r)$ where $g(r)$ is the probability per unit area of finding a second electron a distance r away from a given electron. We find that:

$$\langle C(\sigma)\rangle = \int_{r=0}^{\infty} \frac{e^2}{r^3}\ g(r) \cdot 2\pi r dr \quad . \tag{7.8}$$

If we let $\kappa = \langle C(\sigma)\rangle / C_0(\sigma)$ where $C_0(\sigma)$ is the value obtained for a hexagonal lattice with the same charge density σ from Eq. (7.7), then we find

$$\kappa = 0.70656 \left(\frac{e}{|\sigma|}\right)^{3/2} \int_0^{\infty} \frac{g(r)}{r^2}\ dr \quad . \tag{7.9}$$

The dimensionless quantity κ is the measure of local positional disorder we obtain from our data. Because in the classical limit the only thermodynamic variable which governs the behavior of the two-dimensional electron gas is the ratio of Coulomb energy per electron to kinetic energy, $\Gamma = \pi^{1/2} n_s^{1/2} e^2/kT$, then κ is a function only of Γ. In general,

$\kappa \geq 1$ and $\kappa(\Gamma)$ is monotonically decreasing with Γ.

Several recent publications[52,95] have appeared giving tabulated values of $g(r)$ for various values of Γ. We used these to compute values of $\kappa(\Gamma)$ which we will compare with experiment. We also computed a consistency parameter W from the tabulated values of $g(r)$ given by:

$$W = 2\int_0^\infty (1 - g(r'))r'dr' \quad , \quad \text{where} \quad r' = (n_s \pi)^{\frac{1}{2}} r \quad . \qquad (7.10)$$

Physically W is the number of particles removed before looking at the positions of the other particles to find $g(r)$ and so $W = 1$. Inaccuracies in the tabulated values of $g(r)$ will cause W, as calculated from Eq. (7.10), to differ from unity. The computed results for $\kappa(\Gamma)$ and W are given in Table 1. The results with $W > 1$ come from Ref. 95 while those with $W < 1$ come from Ref. 52. The computed results are in agreement with the general result that $\kappa \geq 1$, but the error in $\kappa(\Gamma)$ that results from using the tabulated values of $g(r)$ is unknown.

TABLE 1.

Γ	$\kappa(\Gamma)$	W
5	1.323	0.779
7	1.248	0.388
15.81	1.137	0.407
22.36	1.104	0.532
36	1.066	1.047
50	1.059	0.769
90	1.032	1.300

Our final result for the change in transition energy from the ground state to excited state n caused by a distribution of surface

electrons in thermal equilibrium is:

$$\Delta E_{1-n} = -C_o(\sigma)\ \kappa(\Gamma)\ D(F) \quad ,$$

where

$$D(F) = (\langle z\rangle_n - \langle z\rangle_1)^2 - \tfrac{1}{2}[(\langle z^2\rangle_n - \langle z_n\rangle^2) - (\langle z^2\rangle_1 - \langle z\rangle_1^2)] \quad . \tag{7.11}$$

To understand this result we consider the change in transition energy caused by changing the external electric field F by an amount ΔF. Using first order perturbation theory we find that:

$$\Delta E_{1-n} = e\Delta F\ (\langle z\rangle_n - \langle z\rangle_1) \quad . \tag{7.12}$$

The expectation value of the dipole electric field acting on an electron in the state n from the other external surface state electrons is given by:

$$\langle \mathcal{E}_z \rangle_n = -\frac{C(\sigma)}{e}\ (\langle z\rangle_n - \langle z\rangle_1) \quad . \tag{7.13}$$

Hence Eq. (7.11) may be interpreted as the transition energy shift from Eq. (7.12) caused by the average microscopic electric field from Eq. (7.13) plus a small correction to account for the variation of electric field with z.

We wish to use the observed quantity E_{1-n} to obtain $\kappa(\Gamma)$ from Eq. (7.11). To do so it is necessary that D(F) be well known. From Eq. (7.12) we obtain

$$\frac{d}{dF}\ (E_{1-n}) = e(\langle z\rangle_n - \langle z\rangle_1) \quad . \tag{7.14}$$

As we will show, our experimental results indicate that in the limit of zero surface charge density, E_{1-n} differs from the value of E_{1-n} obtained from the abrupt interface model discussed in Chapter 2 by an

amount that is almost independent of F. Hence it is a very good approximation to obtain $A = (\langle z\rangle_n - \langle z\rangle_1)^2$ from the results of our calculation discussed in Chapter 2. The remainder of D(F) can be expressed as $B = \frac{1}{2}[\langle(z-\langle z\rangle_1)^2\rangle_1 - \langle(z-\langle z\rangle_n)^2\rangle_n]$. In Fig. 10 we plot the ratio B/A as a function of F, as calculated from the abrupt interface model of Chapter 2. Although B may be somewhat different for the physical system the error is probably small, and since B/A is also small, our calculated values of D(F) are probably accurate to at least 1%.

Because our measurements are taken at constant E_{1-n} rather than at constant applied external electric field it is more convenient to analyze our data in terms of the change in applied field necessary to maintain a constant E_{1-n} as σ is changed, rather than the change in E_{1-n} at a constant applied field. From Eqs. (7.11) and (7.12) the change in applied external electric field necessary to compensate for the dipole electric field of the nearby ground-state external surface electrons is:

$$\Delta F_R = 8.8927 \frac{|\sigma|^{3/2}\kappa(\Gamma)}{e^{1/2}}\left[(\langle z\rangle_n - \langle z\rangle_1) - \frac{(\langle z^2\rangle_n - \langle z\rangle_n^2) - (\langle z^2\rangle_1 - \langle z\rangle_1^2)}{2(\langle z\rangle_n - \langle z\rangle_1)}\right]. \tag{7.15}$$

The final term of Eq. (7.15) is plotted in Fig. 11 as a function of the applied external electric field F.

B. Analysis of Lineshapes

Our data analysis depends fundamentally upon our being able to determine the external electric field F_R applied to the surface electrons, which brings a given transition into resonance with a given laser

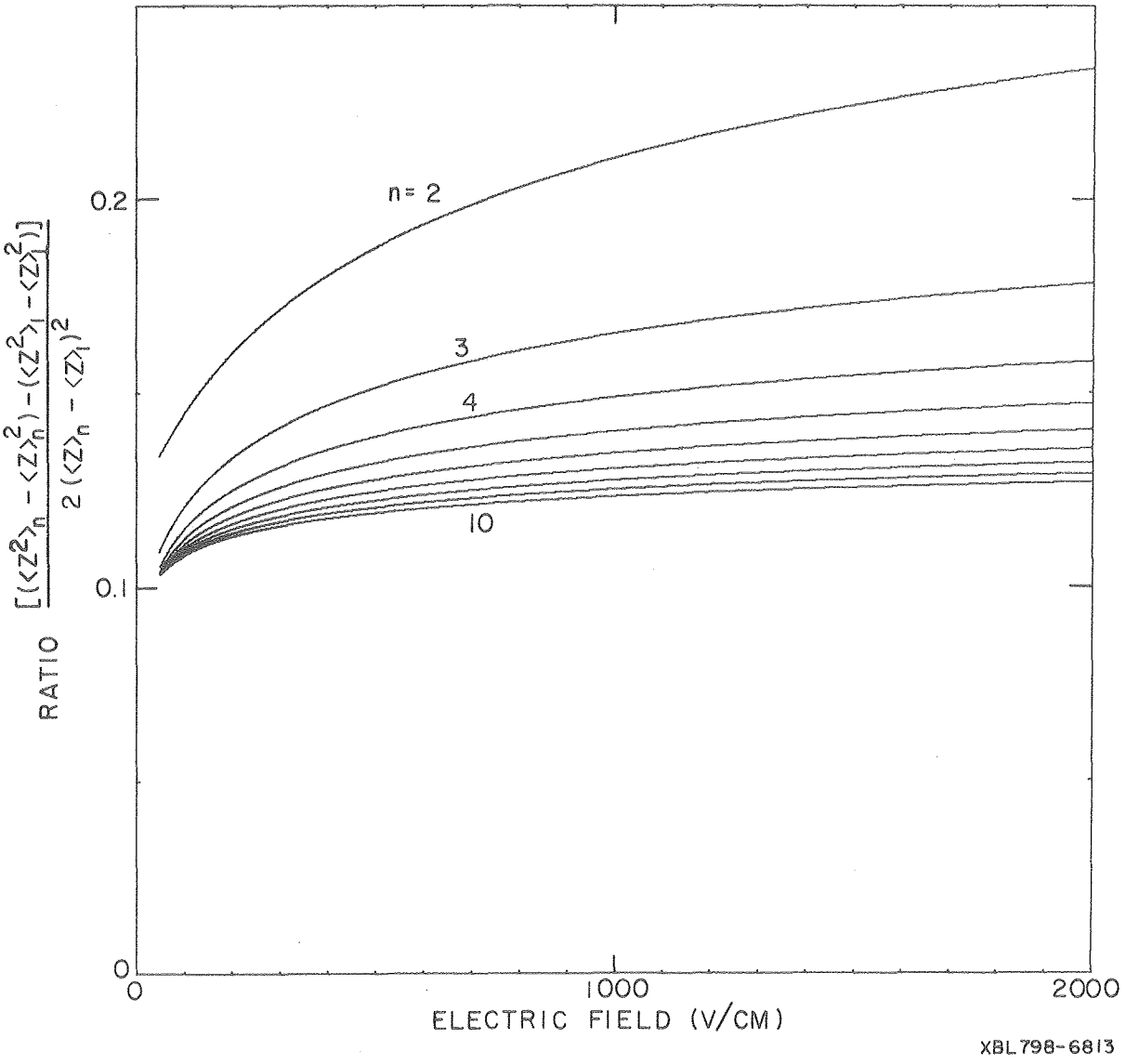

Fig. 10. Fractional influence of the wavefunction not being localized on the energy shift caused by the dipole electric field.

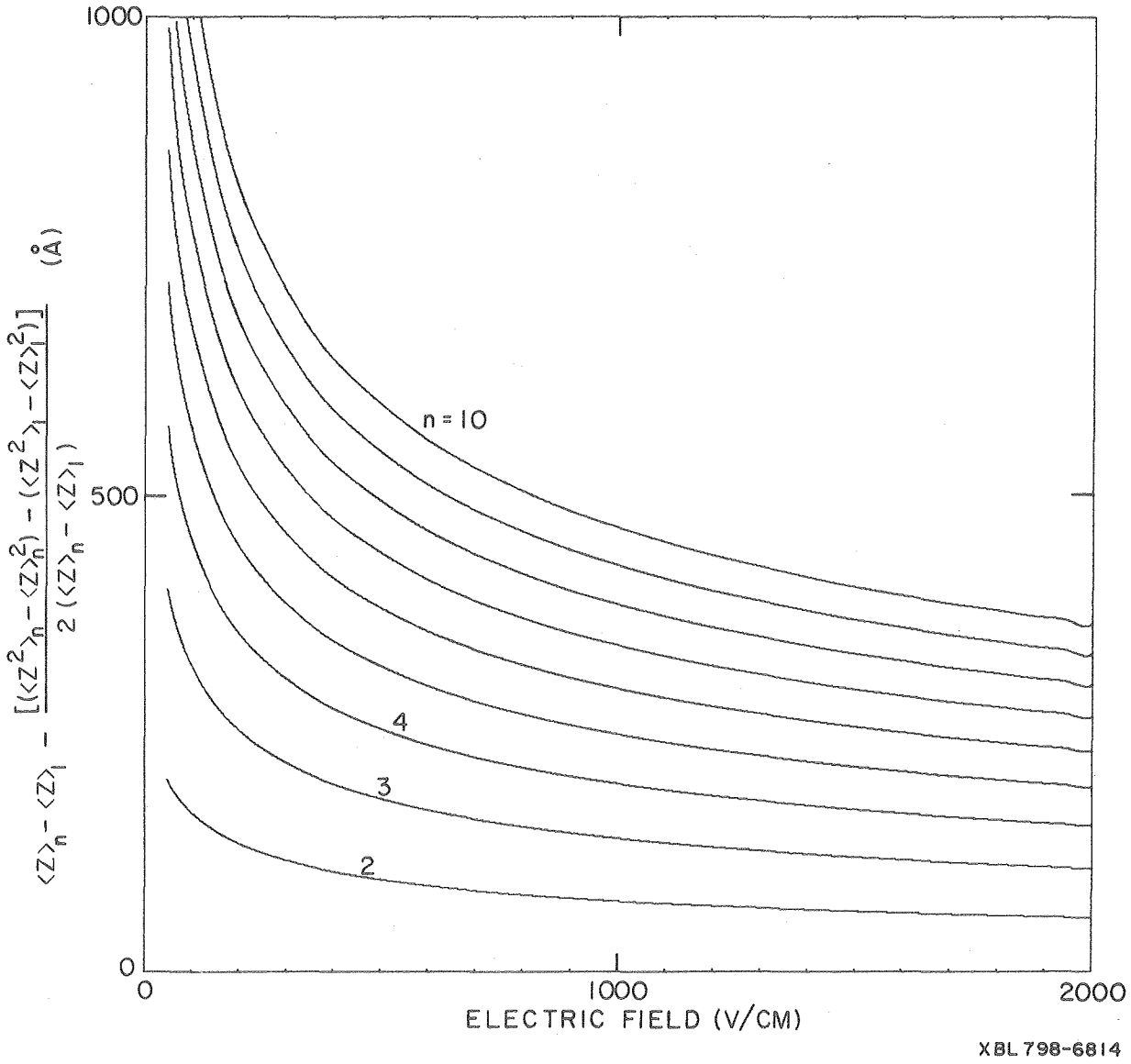

Fig. 11. The distance calculated from the wavefunction that enters into the calculation of the energy shift caused by the dipole electric field.

frequency. We begin by discussing how F_R is obtained from our data. We then discuss how F_R is used to obtain the physical quantities of interest.

We obtain F_R from measurements of optical response versus the voltage applied to the bottom plate of the cell (henceforth called the cell voltage). In Appendix 2 we give plots of the data contributing to our final results. Molecular laser frequencies of 428.628 GHz, 525.4275 GHz, 639.185 GHz, and 764.6426 GHz were used to observe 19 distinct combinations of frequency and final state.

To determine F_R we need to understand the functional form of optical response as a function of cell voltage. One source of line broadening is the inhomogeneous broadening caused by the spatial variation of electric field on the helium surface. As discussed previously, if this were the only source of broadening and if the liquid surface were parallel to the top and bottom of the cell, then from symmetry there would be a singularity in the optical response as a function of cell voltage as the electrons at the center of the cell are brought into resonance. By itself this is not a limitation. Knowing the cell voltage at the singularity and the surface charge density at the center of the cell we could use Eq. (5.17) to calculate F_R for electrons near the axis of the cell.

Unfortunately, there is another source of line broadening (caused by the interaction of helium gas atoms with the external surface state electrons) which removes the singularity from the lineshape. Because of the way the experiment is done we are sensitive to the dispersive part of the homogeneous broadening as well as the absorptive part. We discuss

the cause of the dispersive contribution to optical response and how it is deconvolved from our data.

The microscopic theory of absorption near the resonant frequency of transitions between external electron surface states has been given by Ando.[67] In the range of temperatures in which our experiment is carried out he finds the absorption lineshape to be Lorentzian with FWHM γ proportional to the helium gas atom concentration. The proportionality factor increases by a small fractional amount as the external electric field normal to the surface increases. For our purposes, the external surface state electrons have the same optical response as a collection of harmonic oscillators oriented in the z direction with resonant frequency ω_o set by the local electric field. Given the oscillator strength f of the transition and γ, we look at the response of n_s such oscillators per unit area to an electromagnetic plane wave of amplitude E_0 polarized with electric field in the plane of incidence and incident at an angle θ with respect to the surface. The surface electrons radiate a wave both in the direction of the incident light and in the reflected direction of amplitude:

$$E' = E_0 \frac{2\pi \sin^2\theta \, e^2 n_s \, f[-\omega^2\gamma + i\omega(\omega_o^2 + \omega^2)]}{\cos\theta \, mc[(\omega_o^2 - \omega^2) + \omega^2\gamma^2]} \quad . \qquad (7.16)$$

The c which appears in this equation is the speed of light. The wave emitted in the forward direction cancels the power lost by the electronic absorption and causes a slight phase shift. The reason that a dispersive component can be observed in the optical response is that the light emitted in the reflected direction, which will interfere at the detector with the beam which passes through the surface, has a

definite phase relation at the detector with respect to light that passed through the surface. Similar dispersive contributions to line-shapes are observed in NMR.[96]

A detailed explanation for the observed dispersive component can be given by treating Eq. (7.16) as a perturbation acting on the optical field in the cell. Since it is small we need only consider the first order term. Let $\underset{\sim}{E}_1(\underset{\sim}{r},t)$ be the optical field in the limit that E' is zero. We Fourier analyze $\underset{\sim}{E}_1(\underset{\sim}{r},t)$ into propagating plane waves near the helium surface. We use Eq. (7.16) to compute the perturbation field in the forward and reflected direction from each Fourier component. We keep these two contributions separate and Fourier transform back to real space. Let $\underset{\sim}{E}_2(\underset{\sim}{r},t)$ be the first order term from $\underset{\sim}{E}_1(\underset{\sim}{r},t)$ in the forward direction and let $\underset{\sim}{E}_3(\underset{\sim}{r},t)$ be the first order term from $\underset{\sim}{E}_1(\underset{\sim}{r},t)$ in the reflected direction. Since the source of $\underset{\sim}{E}_2(\underset{\sim}{r},t)$ is the mirror image of the source of $\underset{\sim}{E}_3(\underset{\sim}{r},t)$ and since most of the wave amplitude is reflected from the top and bottom of the cell to return through the surface, then the amplitudes $|\underset{\sim}{E}_2|$ and $|\underset{\sim}{E}_3|$ will be nearly equal when averaged over a volume in the cell with dimension large relative to a wavelength. Since $\underset{\sim}{E}_2(\underset{\sim}{r},t)$ comes from waves emitted with the same direction and phase as those in $\underset{\sim}{E}_1(\underset{\sim}{r},t)$ (but with a different angular weight), then averaged over a large volume $\langle \underset{\sim}{E}_1(\underset{\sim}{r}) \cdot \underset{\sim}{E}_2(\underset{\sim}{r}) \rangle$ will be non-zero to account for the loss of energy density by absorption. The light from the molecular laser is spatially and temporally coherent. Therefore, $\underset{\sim}{E}_1$ and $\underset{\sim}{E}_3$ have a definite phase relation at each point in the cell which is a function of position but independent of time. If the relative phase is not zero or π then $\langle \underset{\sim}{E}_1(t) \cdot \underset{\sim}{E}_3(t) \rangle$ will contain a term

proportional to the imaginary part of Eq. (7.16) that is typically a large fraction of the absorptive part from $\langle \underset{\sim}{E}_1(t) \cdot \underset{\sim}{E}_2(t) \rangle$. The InSb detector we used is about 1 mm × 1 mm × 2 mm; it is not large enough to spatially average the interference between $\underset{\sim}{E}_1$ and $\underset{\sim}{E}_3$. Therefore we expect to observe a dispersive component in the homogeneous lineshape.

In analyzing our data we have assumed that the homogeneous lineshape as a function of cell voltage that is convolved with the line broadening caused by a spatially varying electric field is of the form:

$$D(V) = A\left[\frac{\alpha_1 + B(V-\alpha_2)}{(V-\alpha_2)^2 + \alpha_1^2}\right] . \qquad (7.17)$$

In situations in which the electric field normal to the surface is expected to vary only a small amount for points in the charge pool, this provides a good fit to our data. Here α_1 is related to γ through the rate of change of resonant frequency with respect to cell voltage, α_2 is the cell voltage at which resonance occurs, A is proportional to the strength of the transition, and B is the fraction of the imaginary part of Eq. (7.16) that contributes to the optical response. As one would expect from our analysis it is found that B can be either positive or negative and B tends to be smaller as the frequency increases. The largest magnitude of |B| observed was 0.747 using the 428 GHz CH_3OH laser transition.

For each set of surface electron transitions observed with a single laser frequency in a given run we choose a transition with good signal-to-noise ratio and small distortion from spatially inhomogeneous electric field and use a least squares fitting routine to find α_1, α_2, A

and B in Eq. (7.17). From our knowledge of change in transition frequency with respect to electric field we then obtain α_1 for the other transitions.

Having determined the functional form of the asymmetric homogeneous lineshape we next proceed to remove the dispersive contribution from the experimentally determined lineshape. Let $T_R(V)$ be the measured optical response as a function of cell voltage, let $A(V)$ be the inhomogeneous lineshape, and let $G(x) = (\alpha_1 + Bx)/(x^2 + \alpha_1^2)$. Let $t_R(u)$, $a(u)$ and $g(u)$ be the Fourier transforms of $T_R(V)$, $A(V)$ and $G(V)$ respectively, as defined in Eq. (6.5). The lineshape function is the convolution of $A(V)$ and $G(V)$ so $t_R(u) = a(u)\,g(u) + n(u)$, where $n(u)$ is the Fourier transform of the noise. We deconvolve our data using a fast Fourier transform algorithm that can be written symbolically:

$$A_S(V) = \mathcal{F}^{-1}\left[\frac{t_R(u)}{g(u)}\, h_s(u)\right] \quad . \tag{7.18}$$

Here $\mathcal{F}^{-1}$ symbolizes the operation of taking the inverse Fourier transform, and $h_s(u)$ is the Fourier transform of $H(x) = (s\cdot\alpha_1)/[x^2 + (s\cdot\alpha_1)^2]$. If $s = 2$ it corresponds to convolving $T_R(V)$ with $G(V)$, which can be shown to be the optimum procedure to detect that there really is an absorption line of the form $G(V)$ in white noise.[97] If $s = 1$ it corresponds to removing the asymmetry from the homogeneous lineshape but leaving the linewidth unchanged. As s decreases to zero the noise from $n(u)$ at large u begins to dominate $A_s(V)$.

We calculate $A_s(V)$ for $s = 2, 1$, and 0.25. In going from large to small s the resonance starts as a broad smooth curve, sharpens up at the peak, and is finally drowned in noise. For most transitions we used $s = 1$ to find the cell voltage V_R at which the deconvolved optical response

is a maximum. In a few cases of low signal-to-noise ratio we used $s = 2$. And in one case of exceptionally good signal-to-noise ratio we used $s = 0.25$. The best way to increase the resolution would be to lower the temperature of the cell and thereby reduce the helium gas atom density.

C. Calculation of Charge Density and Electric Field

We use V_R as an estimate of the cell voltage that would cause a singularity in the optical response in the absence of homogeneous broadening. From V_R we wish to calculate the external electric field F_R acting on surface electrons near the axis of the cell. To do so we must first obtain the depth z of liquid helium in the cell and the free surface charge density at the center of the cell σ_F. We begin by calculating the depth z_o of helium in the cell at zero cell voltage and before charge is placed on the surface from Eq. (5.5). (The capacitance used in this equation has subtracted from it the small stray capacitance discussed earlier.) Since $|z - z_o|/H \ll 1$, where H is the cell height, we may assume the liquid depth to be z_o while calculating σ_F. To obtain σ_F we need some preliminary results. From Eq. (5.16) and Eq. (5.4) we obtain the function $f_1(R) = (C_b - C_a)/C_b$ of fractional capacitance screening from the free surface charge as a function of charge pool radius R. From Eq. (5.9) and (5.10) we obtain the function $f_2(R) = Q/Q_{max}$ where Q is the total free surface charge when the charge pool radius is R and Q_{max} is the total free surface charge that would be present if the cell voltage were held fixed and just enough free surface charge were added to the charge pool so that $R = a$. It should be noted that $f_2(R)$ is independent of cell voltage. As can be seen from Fig. 4 (pg 29), near the center of

the cell, the solution to Eq. (5.9) begins to oscillate. This is a consequence of the finite element approximation we have used. We average the computed charge density over ring 3 to ring 8 of the 100 rings used in our numerical calculation and renormalize using the solution to Eq. (5.9) in conjunction with the solution to Eq. (5.10), when $R = a$, to obtain $f_3(R) = \sigma_F(r=0,R)/\sigma_F(r=0,R=a)$. Each of the functions f_1, f_2 and f_3 are monotonically increasing functions of R. Hence there exists unique inverse functions f_1^{-1} and f_2^{-1}. We measure $f_1(R) = \Delta C/C$ when the cell voltage is V_o. When the cell voltage is changed from V_o to V_R the total free surface charge Q remains fixed while Q_{max} is changed by the factor V_R/V_o. Hence f_2 changes by a factor V_o/V_R. Then at cell voltage V_R:

$$\sigma(r=0) = \sigma(r=0,\ V=V_R,\ R=a) \cdot f_3\left(f_2^{-1}\left(\frac{V_R}{V_o} f_2\left(f_1^{-1}\left(\frac{\Delta C}{C}\right)\right)\right)\right) \quad . \quad (7.19)$$

We obtain $\sigma(r=0,\ V=V_R,\ R=a)$ from Eq. (5.10). Knowing $\sigma(r=0)$ and z_o we obtain z/H from Eq. (5.19). We then use Eq. (5.17) to compute F_R, the external electric field applied to the surface electrons that brings the observed transition into resonance with the known laser frequency.

Before discussing how we have used the measured values of F_R we should mention the sources of systematic error involved in the measurement. One of these is the uncertainty in our knowledge of the cell height H given in Fig. 2. Another possible source of systematic error is the difference between the cell voltage at which the deconvolved optical response function is a peak and the cell voltage that would correspond to a singularity in the optical response in the absence of homogeneous broadening. If Q/Q_{max} is small and the helium surface is parallel to the top and bottom of the cell this is not expected to be important since the

applied electric field is then almost constant over the entire charge pool. (We computed this variation, ignoring the distortion of the electric field caused by light-coupling holes in the cell, and found it to be less than 1 part in 10^4 for the conditions of some of our measurements.) In any case, this source of systematic error could be eliminated by decreasing the temperature of the cell. Some possible sources of systematic error that were investigated and found to be small relative to the random error are the change in dielectric constant of liquid helium with temperature and the uncertainty in our measurement of the stray capacitance. One source of concern is the possibility that there could be some free charge on the helium film covering the walls of our cell. We have observed that if free charge is intentionally allowed to reach the cell walls that the lineshapes are distorted and the AC capacitance measured between the top and bottom plates at a fixed cell voltage is time-dependent. The precautions we used to minimize the likelihood of free charge on the helium film are described in the last chapter. When they are taken we observed nothing that indicated that there was free charge on the helium film. If free charge is accidentally allowed to reach the walls during a run, either by reducing the cell voltage until the charge pool begins to flow off the surface or by a large mechanical disturbance to the dewar, then all subsequent data are ignored.

There may also be some systematic error in the value of $\sigma(r=0)$ that we obtain from Eq. (7.19). If there were it could contribute to the value of the disorder parameter $\kappa(\Gamma)$ we obtain from our measurements. Because we measure the total charge on the helium surface with V/V_{sat} slightly greater than unity (see Fig. 5 and 6, pgs. 34,35), where the

capacitance changes rapidly as a function of charge, we do not expect errors in the capacitance measurements themselves to be significant. Of more concern is the possibility that the helium surface could be distorted in some way as the cell voltage is increased. There is no good way to be certain that something of this nature does not occur from our measurements. There is, however, good evidence that it is not important since the AC capacitance change we calculate is in agreement with the measured capacitance change as shown in Fig. 6.

D. Statistical Analysis

We next discuss how our data, which includes random error, is used to obtain $\kappa(\Gamma)$ and the applied electric field F_i which brings the i^{th} observed combination of laser frequency and ground to final state transition into resonance in the limit that σ approaches zero. The measured values of C_o, C', C_b, C_a, and V_o for each of the runs used in our data analysis are given in Table 2. In Table 3 we give the values of V_R, z/H, and the charge density $\sigma(r=0)$ which we used to compute F_R, as well as F_R and the estimated standard deviation of our measurement of F_R. The standard deviation is constrained to be no smaller than the change in electric field during the integration to obtain a single data point. Subject to this constraint we estimate the standard deviation from the s dependence of the V at which A_s computed from Eq. (7.18) is a maximum, and from the observed increase in scatter among the measured F_R as the linewidth increases.

For the purposes of discussion, we label the j^{th} value of F_R measured with the combination of laser frequency and final state that we

TABLE 2.

Run	Date	C_o [pf]	C' [pf]	C_b [pf]	C_a [pf]	V_o [volt]
1	20-Jan-79	0.45902	0.47220	0.47177	0.44724	34.38
2	23-Jan-79	0.45896	0.47209	0.47147	0.45922	34.38
3	27-Jan-79	0.45901	0.47293	0.47185	0.43655	34.38
4	26-May-79	0.45958	0.47229	0.47229	0.41006	81.03
5	26-Jun-79	0.45937	0.47230	0.47220	0.43080	41.92
6	3-Jul-79	0.45971	0.47251	0.47281	0.39361	122.03

TABLE 3.

Date	Laser freq. [GHz]	Transition	V_R [volt]	z/H	$\sigma(r=0)$ [esu/cm^2]	F_R [V/cm]	Δ_{ij} [a] [V/cm]	Δf_{ij} [v/cm]	Γ
20-JAN-79	525.428	1- 3	259.61	.5171	-.0164	503.07	.76	.46	14.4
20-JAN-79	525.428	1- 4	153.18	.5172	-.0151	296.48	.42	.70	13.8
20-JAN-79	525.428	1- 5	107.45	.5173	-.0143	207.73	.79	.91	13.4
20-JAN-79	525.428	1- 6	82.23	.5173	-.0137	158.79	.38	1.12	13.2
20-JAN-79	525.428	1- 7	67.06	.5173	-.0133	129.36	.38	1.33	13.0
20-JAN-79	525.428	1- 8	56.35	.5173	-.0129	108.58	.38	1.52	12.8
20-JAN-79	525.428	1- 9	48.54	.5173	-.0126	93.43	.38	1.70	12.7
20-JAN-79	525.428	1-10	42.74	.5173	-.0124	82.19	.38	1.86	12.5
20-JAN-79	525.428	1- 2	688.78	.5168	-.0194	1336.27	.67	.22	15.7
20-JAN-79	428.628	1- 2	462.09	.5170	-.0181	896.15	.65	.23	15.1
20-JAN-79	428.628	1- 3	170.30	.5172	-.0153	329.71	.78	.49	13.9
20-JAN-79	428.628	1- 4	99.57	.5173	-.0141	192.43	.75	.74	13.4
20-JAN-79	428.628	1- 5	69.57	.5173	-.0134	134.23	.57	.97	13.0
23-JAN-79	525.428	1- 3	259.47	.5154	-.0093	503.27	.76	.20	10.8
23-JAN-79	525.428	1- 4	153.21	.5154	-.0085	296.99	.42	.29	10.4
23-JAN-79	525.428	1- 5	106.49	.5155	-.0080	206.31	.79	.38	10.1
23-JAN-79	525.428	1- 6	81.96	.5155	-.0077	158.69	.38	.47	9.9
23-JAN-79	525.428	1- 7	65.90	.5155	-.0074	127.53	.38	.56	9.7
23-JAN-79	525.428	1- 8	55.42	.5155	-.0072	107.19	.38	.63	9.6
23-JAN-79	525.428	1- 9	48.06	.5155	-.0070	92.91	.38	.71	9.5
23-JAN-79	525.426	1- 2	688.95	.5153	-.0110	1337.08	1.01	.09	11.8
27-JAN-79	639.185	1- 2	990.30	.5444	-.0278	1921.30	4.28	.32	18.8
27-JAN-79	639.185	1- 3	380.64	.5451	-.0236	736.29	.57	.69	17.3
27-JAN-79	639.185	1- 4	226.63	.5453	-.0217	437.07	.76	1.04	16.6
27-JAN-79	525.428	1- 3	260.30	.5453	-.0222	502.47	1.01	.73	16.8
27-JAN-79	525.428	1- 4	154.50	.5454	-.0204	296.99	.63	1.10	16.1
27-JAN-79	525.428	1- 5	108.80	.5455	-.0194	208.29	.79	1.44	15.7
27-JAN-79	525.428	1- 6	83.72	.5455	-.0186	159.64	.38	1.78	15.4
27-JAN-79	525.428	1- 7	68.25	.5455	-.0180	129.65	.38	2.10	15.1
27-JAN-79	525.428	1- 2	690.00	.5447	-.0261	1337.55	.67	.34	18.2
26-MAY-79	764.643	1- 3	532.76	.4966	-.0851	1034.46	1.01	4.19	32.9
26-MAY-79	764.643	1- 4	317.71	.4976	-.0788	616.99	2.61	6.36	31.6
26-MAY-79	525.428	1- 2	688.12	.4958	-.0886	1336.06	1.35	2.12	33.5
26-MAY-79	525.428	1- 3	261.45	.4979	-.0766	507.77	.76	4.67	31.2
26-MAY-79	525.428	1- 4	156.70	.4983	-.0710	304.42	.42	7.05	30.0
26-MAY-79	525.428	1- 5	112.60	.4985	-.0676	218.81	.79	9.25	29.3
26-JUN-79	525.428	1- 3	261.36	.5070	-.0322	506.39	1.06	1.27	20.2
26-JUN-79	525.428	1- 2	689.20	.5062	-.0376	1336.64	1.36	.59	21.9
3-JUL-79	639.185	1- 2	986.90	.4948	-.1504	1917.01	1.49	4.07	43.7
3-JUL-79	639.185	1- 3	385.54	.4998	-.1308	748.06	1.57	9.01	40.7
3-JUL-79	639.185	1- 4	232.59	.5009	-.1214	450.86	1.57	13.64	39.2
3-JUL-79	639.185	1- 5	166.42	.5013	-.1153	322.32	4.28	17.95	38.2
3-JUL-79	525.428	1- 2	691.90	.4973	-.1425	1343.54	2.36	4.32	42.5
3-JUL-79	525.428	1- 3	265.95	.5006	-.1237	515.67	2.26	9.53	39.6
3-JUL-79	525.428	1- 4	159.50	.5013	-.1145	308.88	1.86	14.36	38.1

[a] Note that Δ_{ij} does not include the uncertainty in our measured value of the cell height H. The systematic error in the measured value of F_R that results is 5.7×10^{-4} F_R.

previously labeled by the index i as F_{ij}. We label the standard deviation of this measurement as Δ_{ij}, and from the charge density $\sigma(r=0)$ which we calculated in obtaining F_{ij} we use Eq. (7.15) to calculate $\Delta F_R/\kappa(\Gamma)$ which we label as ΔF_{ij}. Because the errors in this quantity are presumed to be small they will be neglected in our statistical analysis. The computed values of ΔF_{ij} are also given in Table 3. We define e_{ij} from the equation:

$$F_{ij} = F_i + \kappa(\Gamma)\,\Delta F_{ij} + e_{ij} \quad . \tag{7.20}$$

We assume that e_{ij} is a normally distributed random variable with zero mean and standard deviation Δ_{ij}. We wish to minimize the effect of the e_{ij} in estimating values of $\kappa(\Gamma)$, $F_1, \ldots, F_n$ from our data. We also wish to have estimates of the uncertainty in the estimated value of each of these quantities. We do so using the principle of maximum likelihood.[98] Accordingly, we wish to find the values of $\kappa, F_1, \ldots, F_n$ which minimize the sum

$$M(\kappa, F_1, \ldots, F_n) = \sum_{i,j} \frac{(F_{ij} - F_i - \kappa\Delta F_{ij})^2}{2\Delta_{ij}^2} \quad . \tag{7.21}$$

We begin by making the approximation that κ is independent of Γ. Setting the partial derivatives with respect to each of the parameters equal to zero we obtain the following system of linear equations:

$$\begin{aligned} -A + \sum_i B_i F_i + \kappa C &= 0 \quad , \\ -D_i + G_i F_i + \kappa B_i &= 0 \quad . \end{aligned} \tag{7.22}$$

Here

$$A = \sum_{i,j} \frac{\Delta F_{ij} F_{ij}}{\Delta_{ij}^2} ,$$

$$B_i = \sum_{j} \frac{\Delta F_{ij}}{\Delta_{ij}^2} ,$$

$$C = \sum_{i,j} \frac{\Delta F_{ij}^2}{\Delta_{ij}^2} ,$$

$$D_i = \sum_{j} \frac{F_{ij}}{\Delta_{ij}^2} ,$$

and

$$G_i = \sum_{j} \frac{1}{\Delta_{ij}^2} .$$

We find the solution to be given by:

$$\kappa = \frac{A - \sum_i \frac{B_i D_i}{G_i}}{C - \sum_i \frac{B_i}{G_i}} \qquad (7.23)$$

$$F = \frac{(D_i - B_i Q)}{G_i} .$$

In making the approximation that κ is independent of Γ we are finding the best fit horizontal straight line to the curve of $\kappa(\Gamma)$ weighted over our measurements. The standard deviations associated with $\kappa, F_1, \ldots, F_n$

are found from the relations:

$$\frac{1}{\sigma_\kappa^2} = \frac{d^2M}{d\kappa^2} \quad , \qquad \frac{1}{\sigma_{F_i}^2} = \frac{d^2M}{dF_i^2} \quad . \tag{7.24}$$

We find that $\sigma_\kappa = C^{-\frac{1}{2}}$ and $\sigma_{F_i} = G_i^{-\frac{1}{2}}$.

The result of this calculation from our data is $\kappa = 1.174 \pm 0.036$. The values of F_i and σ_{F_i} we have observed for the combinations of laser frequency and final state are given in Table 4. Also given in Table 4 are the transition frequency calculated from the model of an abrupt surface (with potential given by Eq. (2.1), where $F = F_i$), the amount by which the laser frequency is greater than the calculated frequency, and the uncertainty in the calculated frequency that arises from σ_{F_i}. In Fig. 12 we have plotted the laser frequency as a function of F_i. On the scale of this plot it is not possible to see either the difference between laser frequency and the frequency calculated from the model of an abrupt surface or the error bars associated with F_i. In Fig. 13 we have plotted the difference frequency and its associated error bar as a function of F_i. We have included two points from Ref. 5 that were obtained by extrapolating measurements taken at low electric field with a microwave source to the limit as the electric field is reduced to zero. The fact that the curve of difference frequency versus external electric field has very little slope relative to the curve of transition frequency versus electric field indicates that the model of an abrupt surface is very accurate in calculating $\langle z \rangle_n - \langle z \rangle_1$, as discussed previously.

In Fig. 14 we have plotted $F_{ij} - F_i$ as a function of ΔF_{ij}. The observed consistency between the straight line passing through the origin

TABLE 4.

Transition	Laser freq. [GHz]	F_i [V/cm]	σ_{F_i} [V/cm]	Model freq. [GHz]	Dif. freq. [GHz]	Std.dev. of dif.freq. [GHz]
1- 2	428.63	895.89	.66	422.28	6.35	.16
1- 3	428.63	329.13	.80	422.29	6.34	.48
1- 4	428.63	191.57	.78	422.39	6.24	.78
1- 5	428.63	133.09	.61	422.58	6.04	.86
1- 2	525.43	1336.39	.39	518.83	6.60	.08
1- 3	525.43	502.81	.37	518.65	6.78	.19
1- 4	525.43	296.04	.22	518.80	6.63	.19
1- 5	525.43	206.76	.40	518.77	6.66	.48
1- 6	525.43	157.72	.22	518.41	7.02	.35
1- 7	525.43	127.28	.22	518.53	6.90	.43
1- 8	525.43	106.62	.27	518.83	6.59	.62
1- 9	525.43	91.76	.27	519.36	6.07	.72
1-10	525.43	80.00	.46	518.26	7.17	1.41
1- 2	639.19	1913.18	1.41	629.51	9.67	.25
1- 3	639.19	735.71	.54	631.03	8.15	.24
1- 4	639.19	435.65	.68	630.70	8.49	.51
1- 5	639.19	301.24	5.03	626.09	13.09	5.37
1- 3	764.64	1029.55	1.18	756.15	8.49	.48
1- 4	764.64	609.53	2.88	753.67	10.97	1.92

Note that σ_{F_i}, from which the last column is calculated, does not include the systematic error of $5.66 \times 10^{-4} F_i$ that arises from the uncertainty in our measured value of H.

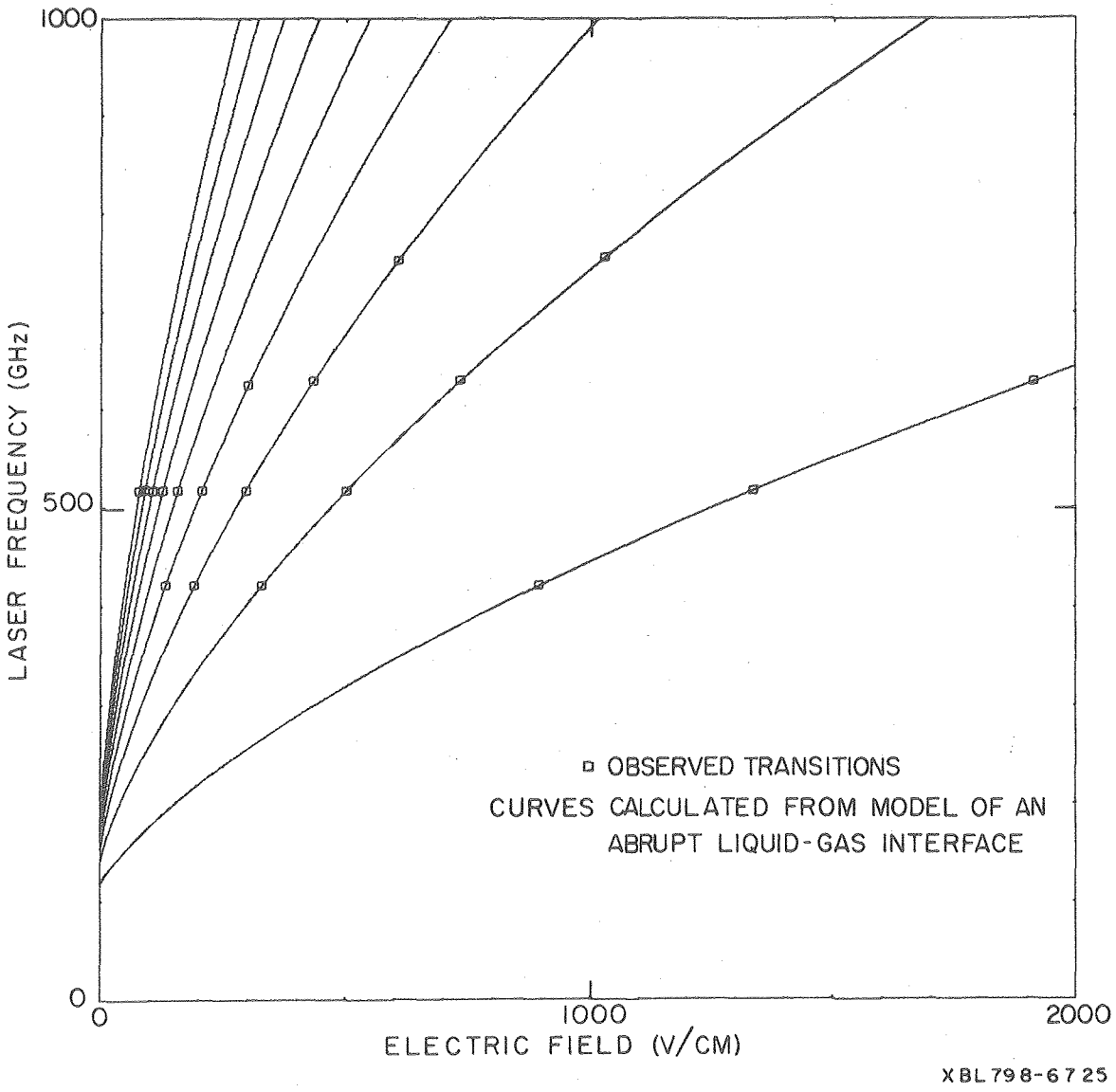

Fig. 12. Plot of the laser frequency versus electric field at which transitions are observed. The curves are the same as in Fig. 1.

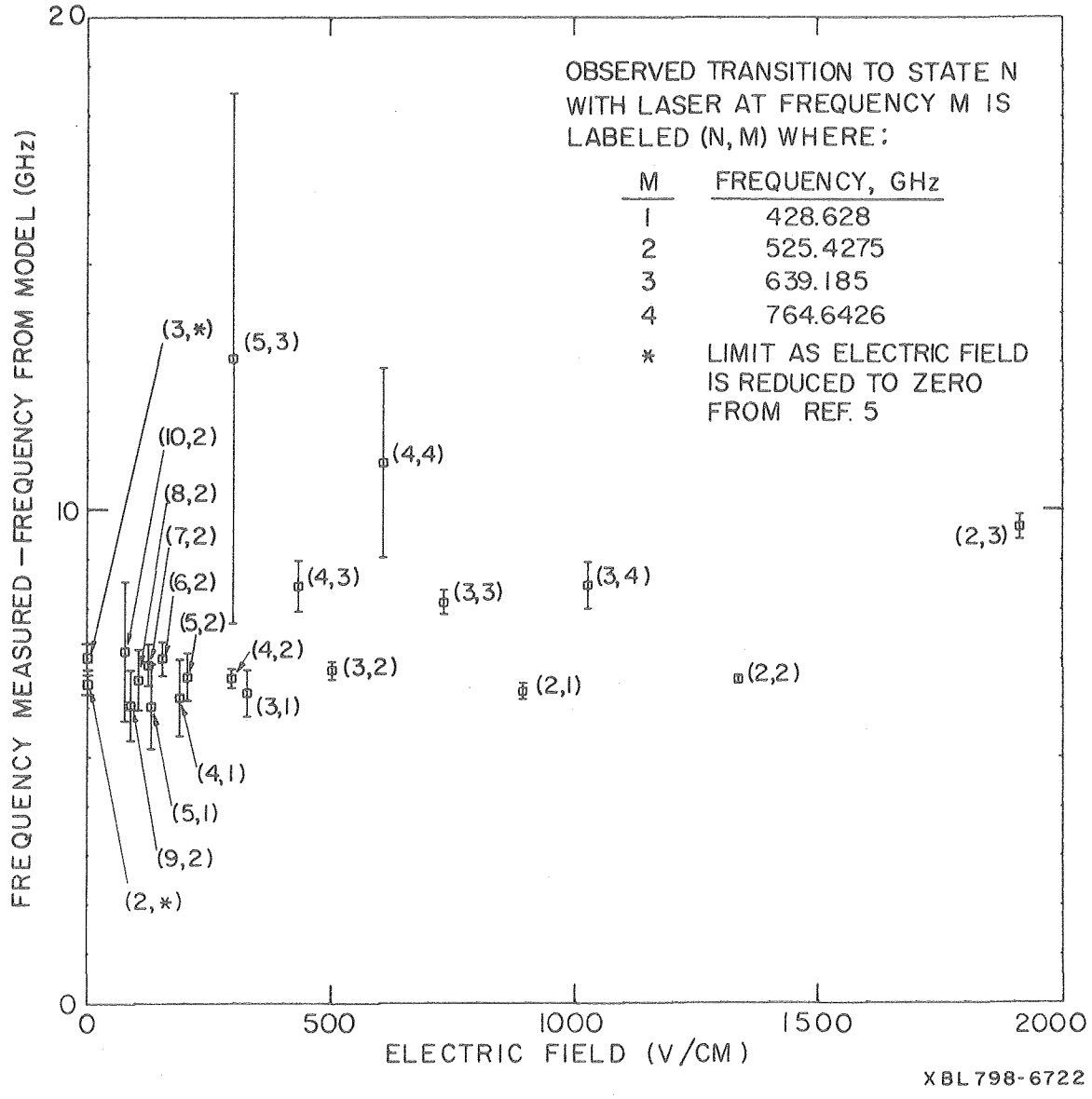

Fig. 13. Plot of the laser frequency minus the frequency calculated from the model of an abrupt liquid-gas interface, plotted as a function of external electric field.

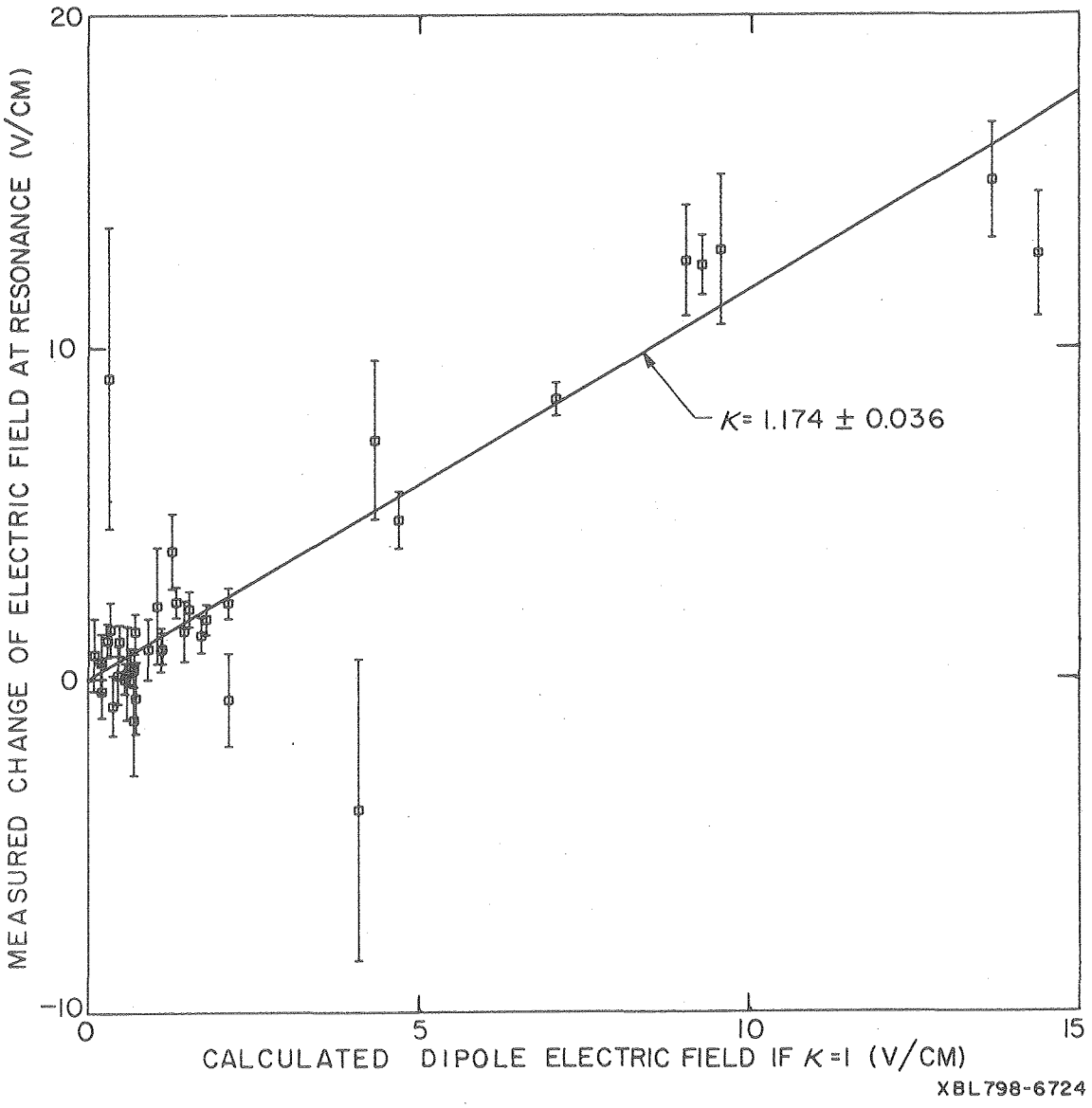

Fig. 14. Plot of measured change of electric field at resonance $F_{ij} - F_i$ versus the change calculated for a hexagonal lattice with the same charge density as the measured charge density.

with slope κ and the plotted points indicates that the model given in Eq. (7.20) does indeed fit the data.

In an attempt to obtain more information about $\kappa(\Gamma)$ than just the best level fit when averaged over our data, and to give an idea of the contribution of the individual values of Γ to the final result, we estimated the $\kappa(\Gamma)$ and the resulting error bar from each F_R for which there were other measurements involving the same transition and for which $\Delta_{ij} < \frac{1}{2}\Delta F_{ij}$. We did so by calculating F_i and σ_{F_i} without using the data from the measurement we are attempting to use to find $\kappa(\Gamma)$. We then use F_{ij} and ΔF_{ij} to compute κ from Eq. (7.19). We compute σ_κ as the propagated error σ_{F_i} and Δ_{ij}. These results are plotted in Fig. 15. A level straight line is not inconsistent with our data, although we know from physical considerations that $\kappa(\Gamma)$ must be a monotonically decreasing function that asymptotically approaches $\kappa = 1$ at large Γ.

E. Implications of Measured Quantities

In comparing our measured quantities with the theoretical predictions discussed earlier the most striking thing is their close agreement. The results shown in Fig. 13 of frequency difference with respect to the model of an abrupt surface indicate that at low electric field there is no measurable variation of the frequency difference while at large electric fields an upward slope becomes evident. The gradual interface model of F. Stern[99] predicts almost similar results. The parameters of his model were fitted to the low field results of Grimes et al. which are consistent with our measurements. The agreement will undoubtedly improve when our measured values are also used in the fitting process. Another use for

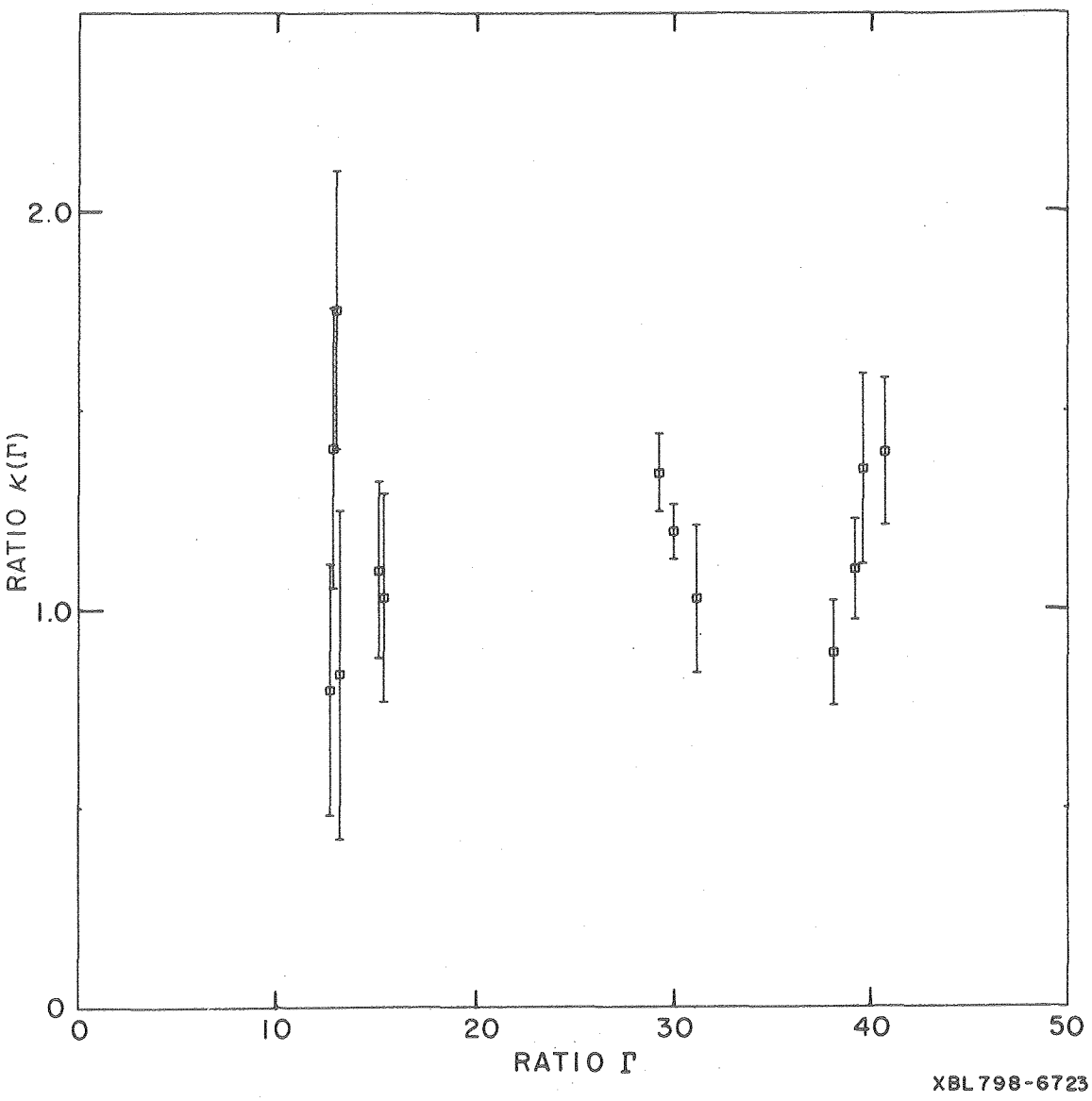

Fig. 15. Plot of the ratio $\kappa(\Gamma)$ as determined from individual measurements versus Γ.

our measurements of transition frequency as a function of electric field is to check the first principles calculations of density variation near a free liquid helium surface. Such a comparison may help to resolve the existing controversy as to whether or not the local density oscillates near the helium surface.

In comparing our measured value of $\kappa(\Gamma)$ with the results given in Table 1, that are obtained by integrating tabulated values of the radial-distribution function $g(r)$, we see that our measured value is larger by a statistically significant amount. We do not know the accuracy of the tables of $g(r)$ from which the calculated values of $\kappa(\Gamma)$ were derived. The variation of the consistency parameter W from the exact value of $W = 1$ indicates that they may be unreliable. Two physical effects which would make our measured value of κ larger than the calculated value are the reconstruction of nearby electrons as the excited state electron moves away from the surface and the zero point motion of the electrons. We expect both of these effects to be small. There could, however, be an additional source of disorder which is not small, such as waves on the helium surface. If we systematically measured the charge density to be less than its true value the same effect would arise. A good way to check our results would be to repeat the experiment at a temperature low enough so that helium gas atom scattering does not dominate the lineshape and look at the effect of changing the temperature as well as the charge density. (Because our linewidths were proportional to helium gas atom density, which increases exponentially with temperature, we took all of our data at the lowest temperature we could reach in our cryostat – about 1.2°K.)

To our knowledge this is the first experimental check of the computed radial-distribution function of a two-dimensional system of free particles interacting with a 1/r potential. The theory will undoubtedly be refined now that there are experimental results with which it can be compared. Also, it appears that a significant improvement in the accuracy of the measurement can be obtained by repeating the experiment at a lower temperature. It would be very interesting to experimentally resolve the Γ dependence of $\kappa(\Gamma)$. The theory and experimental techniques reported in this thesis should allow one to make such a measurement.

VIII. CONCLUSION

In conclusion, we have obtained from our data both the quantity κ, defined as the ratio of $\sum_i' |r_i|^{-3}$ to the same quantity evaluated for a hexagonal lattice with the same charge density, and the electric field dependence of the transition energy from the ground state to various excited states. Our measured value for the best level fit to the function $\kappa(\Gamma)$, using data with Γ between 9 and 44, is $\kappa = 1.174 \pm 0.036$. This is significantly larger than the values of $\kappa(\Gamma)$ calculated from published tables of the radial-distribution function of the classical electron gas with Γ in this interval. It is not clear whether this discrepancy is a result of inaccuracies in the published tables, a possible systematic error in our measurement, or increased disorder from some physical source not included in the calculations such as waves on the helium surface.

The transition energy that we measure at a given applied external field F is found to differ from the transition energy calculated from the model of an abrupt liquid-gas interface by an amount that depends very little on F. This implies that the change in average distance from the helium surface that occurs as electrons change from one state to another can be calculated very accurately from the model. Our data is also consistent with a more elaborate model calculation of F. Stern. A number of first principle theoretical calculations exist which give incompatible results for variation of density at the surface of liquid helium. We expect some of the controversy surrounding these calculations to be resolved when they are extended to compare with our measured values.

Our measurement of the disorder parameter κ was made possible because we were able to measure the surface charge density. We did this

using a novel technique that involved measuring the change in AC capacitance between plates separated by the helium surface that occurs when charge is put on the surface. We found that we were able to calculate the change in AC capacitance for a given total surface charge without using the detailed thermodynamics of a two-dimensional electron gas. A self-consistent electrostatic calculation gives very accurate results. One surprising result of this calculation is that almost all of the surface charge is confined to a "charge pool" which will, in general, only cover part of the helium surface.

The technique we have used to measure κ can give greatly improved accuracy if the temperature is lowered significantly below the 1.2°K used in our measurements. We expect that when this is done it will be possible to study the variation of κ as a function of Γ. This could lead to significant new results in the theory of two-dimensional disordered systems.

ACKNOWLEDGMENTS

I would like to thank Professor Paul Richards, my thesis adviser, for his constant support and encouragment during the course of this work. His desire for excellence and physical insight were an education in themselves. I would like to thank Professors L. M. Falicov, J. D. Jackson, and S. P. Davis for their availability in discussing various aspects of my research. I am indebted to Dr. C. C. Grimes who provided the thoriated tungsten filament material. Helpful conversations are also acknowledged with Frank Stern, who provided unpublished detailed results from his model calculation, and with John Lekner. Finally, I would like to express my gratitude for the financial support I received in the form of a Regents Fellowship and an IBM pre-doctoral fellowship.

This work was performed under the auspices of the U.S. Department of Energy under Contract No. W-7405-ENG-48.

REFERENCES

1. W.T.Sommer, Thesis, Stanford University (1964).
2. W.T.Sommer, Phys. Rev. Lett. 12, 271 (1964).
3. M.W.Cole, Phys. Rev. B2, 4239 (1970); M.W.Cole and M.H.Cohen, Phys. Rev. Lett. 23, 1238 (1969).
4. V.B.Shikin, Zh. Eksp. Teor. Fiz. 58, 1748 (1970) [Sov. Phys.-JETP 31, 936 (1970)].
5. C.C.Grimes, T.R.Brown, M.L.Burns, and C.L.Zipfel, Phys. Rev. B13, 140 (1976).
6. T.R.Brown and C.C.Grimes, Phys. Rev. Lett. 29, 1233 (1972).
7. M.W.Cole, Rev. Mod. Phys. 46, 451 (1974).
8. L.M.Sander, Phys. Rev. B11, 4350 (1975).
9. R.F.Harris-Lowe and K.A.Smee, Phys. Rev. A2, 158 (1970).
10. C.Van Degrift, Thesis, University of California, Irvine (1974).
11. C.C.Grimes and G.Adams, Phys. Rev. Lett. 42, 795 (1979).
12. T.M.Sanders,Jr. and G.Weinreich, Phys. Rev. B13, 4810 (1976).
13. R.F.O'Connell, Phys. Lett. 60A, 481 (1977).
14. Transition frequencies obtained using the WKB method differ from the exact result by an amount of the order of 1% for the electric fields of interest.
15. Handbook of Mathematical Functions, edited by M.Abramowitz and I.A.Stegun (National Bureau of Standards, U.S.GPO, Washington, D.C., 1964), p.773.
16. Eigenvalues from the WKB approximation can be obtained about a factor 10^3 times faster.

17. E.Prugovecki, Quantum Mechanics in Hilbert Space (Academic Press, New York, 1971), p.48.

18. T.Regge, J. Low Temp. Phys. 9, 123 (1972).

19. R.M.Bowley, J. Phys. C3, 2012 (1970).

20. Y.M.Shih and C.W.Woo, Phys. Rev. Lett. 30, 479 (1973); L.A.Wojick, Y.M.Shih and C.W.Woo, J. Low Temp. Phys. 23, 345 (1976).

21. F.D.Mackie and C.W.Woo, Phys. Rev. B18, 529 (1978).

22. C.C.Chang and M.H.Cohen, Phys. Rev. A8, 1930 (1973).

23. K.S.Liu, H.M.Kalos and G.V.Chester, Phys. Rev. B12, 1715 (1975).

24. P.A.Whitlock, D.M.Ceperly, G.V.Chester and M.H.Kalos, Phys. Rev. B19, 5598 (1979).

25. T.C.Padmore and M.W.Cole, Phys. Rev. A9, 802 (1974).

26. C.Ebner and W.F.Saam, Phys. Rev. B12, 923 (1975).

27. C.A.Croxton, Introduction to Liquid State Physics (John Wiley, New York, 1975), pp.170-190.

28. J.Lekner and J.R.Henderson, Physica 94A, 545 (1978).

29. M.H.Huang, Y.M.Shih, C.W.Woo, J. Low Temp. Phys. 14, 413 (1974).

30. J.F.Allen and A.D.Misener, Proc. Cambridge Phil. Soc. 34, 299 (1938).

31. K.R.Atkins and Y.Narahara, Phys. Rev. 138, A437 (1965).

32. J.H.Magerlein and T.M.Sanders,Jr., Phys. Rev. Lett. 36, 256 (1976).

33. J.R.Eckardt, D.O.Edwards, S.Y.Shen and F.M.Gasparini, Phys. Rev. B16, 1944 (1977).

34. M.A.Woolf and G.W.Rayfield, Phys. Rev. Lett. 15, 235 (1965).

35. G.Careri, U.Fasoli and F.S.Gaeta, Nuovo Cimento 15, 774 (1960); L.Brush, B.Maraviglia and F.Moss, Phys. Rev. Lett. 17, 682 (1966).

36. D.O.Edwards, J.R.Eckardt and F.M.Gasparini, Phys. Rev. A9, 2070 (1974).

37. J.Lekner, private communication.

38. K.R.Atkins, Can. J. Phys. 31, 1165 (1953).

39. R.Brout and M.Nauenberg, Phys. Rev. 112, 1451 (1958).

40. D.P.Fits, Physica (Utrecht) 42, 205 (1969).

41. J.Lekner and J.R.Henderson, J. Low Temp. Phys. 31, 763 (1978).

42. O.Hipolito and J.R.Felicio, unpublished.

43. C.C.Grimes, private communication.

44. F.Stern, Phys. Rev. B17, 5009 (1978).

45. P.M.Echenique and J.B.Pendry, Phys. Rev. Lett. 37, 561 (1976).

46. L.P.Gor'kov and D.M.Chernikova, Pis'ma Zh. Eksp. Teor. Fiz. 18, 119 (1973) [JETP Lett. 18, 68 (1973); Dokl. Akad. Nauk. SSSR 228, 829 (1976) [Sov. Phys. Dokl. 21, 328 (1976)].

47. M.S.Khaikin, J. de Physique 39, C6-1295 (1978).

48. The only exception reported to date is: V.S.Edelman, Pis'ma Zh. Eksp. Teor. Fiz. 24, 510 (1976).

49. A.L.Fetter, Phys. Rev. B10, 3739 (1974).

50. J.Chalupa, Phys. Rev. B12, 4 (1975).

51. H.Totsuji, J. Phys. Soc. Japan 39, 253 (1975);
H.Totsuji, J. Phys. Soc. Japan 40, 857 (1976).

52. H.Totsuji, Phys. Rev. A17, 39 (1978).

53. F.Lado, Phys. Rev. B17, 2827 (1978).

54. R.W.Hockney and T.R.Brown, J. Phys. C8, 1813 (1975).

55. P.M.Platzman and H.Fukuyama, Phys. Rev. B10, 3150 (1974).

56. D.J.Thouless, J. Phys. C11, L189 (1978).

57. C.C.Grimes, J. de Physique 39, C6-1352 (1978).

58. L.A.Bonsall and A.A.Maradudin, Phys. Rev. B15, 795 (1979).

59. D.S.Fisher, B.I.Halperin and P.M.Platzman, Phys. Rev. Lett. 42, 798 (1979).

60. A.Tremblay and V.Ambegaokar, Phys. Rev. B, to be published.

61. N.D.Merman, Phys. Rev. 158, 383 (1967); actually the proof does not strictly apply to a Coulomb interaction. See Ref. 95 for a discussion.

62. L.D.Landau and E.M.Lifshitz, Quantum Mechanics (Pergamon Press, New York, 1965), pp.421-427.

63. V.S.Edelman, Pis'ma Zh. Eksp. Teor. Fiz. 24, 510 (1976).

64. C.C.Grimes and G.Adams, Phys. Rev. Lett. 36, 145 (1976).

65. C.L.Zipfel, T.R.Brown and C.C.Grimes, Phys. Rev. Lett. 37, 1760 (1976).

66. P.M.Platzman and B.I.Halperin, Phys. Rev. B18, 226 (1978).

67. T.Ando, J. Phys. Soc. Japan 44, 756 (1978).

68. F.Bridges and J.F.McGill, Phys. Rev. B15, 1324 (1977).

69. W.T.Sommer and D.J.Tanner, Phys. Rev. Lett. 27, 1345 (1971).

70. A.S.Rybalko, Yu. Z. Kovdrya, and B.N.Esel'son, Pis'ma Zh. Eksp. Teor. Fiz. 22, 569 (1975) [JETP Lett. 22, 280 (1976)].

71. Ref. 15, pp.374-378.

72. W.R.Smythe, Static and Dynamic Electricity, 3rd edition (McGraw-Hill, New York, 1968), p.201.

73. The electric field of a circle of charge in free space with a gap removed of angle ε has electric field at the center of the gap proportional to $\ell n(\tan(\varepsilon/4))$. As ε approaches zero the field diverges logarithmically.

74. A.P.Volodin, M.S.Khaikin and V.S.Edel'man, Pis'ma Zh. Eksp. Teor. Fiz. 23, 524 (1976) [JETP Lett. 23, 479 (1976)].

75. L.D.Landau and E.M.Lifshitz, Electrodynamics of Continuous Media (Addison-Wesley, Reading, 1960), p.51.

76. M.Rosenbluh, R.J.Temkin and K.J.Button, Appl. Opt. 15, 2635 (1976).

77. F.R.Petersen, K.M.Evenson, D.A.Jennings, J.S.Wells, K.Goto and J.J.Jiminez, IEEE J. of Quant. Elec. QE-11, 838 (1975).

78. A.Yariv, Quantum Electronics, 2nd edition (John Wiley, New York, 1975), pp.130-135.

79. D.H.Martin and E.Pupplett, Infrared Phys. 10, 105 (1969).

80. D.K.Lambert and P.L.Ricahrds, Appl. Opt. 17, 1595 (1978).

81. D.K.Lambert and P.L.Richards, J. Opt. Soc. Am. 68, 1124 (1978).

82. D.S.Douma and T.R.Geballe, IEEE J. of Quant. Elec. QE-14, 391 (1978).

83. Ref. 78, pp.307-318.

84. E.D.Hinkley and C.Freed, Phys. Rev. Lett. 23, 277 (1969).

85. V.M.Gelikonov and Yu.I.Zaitsev, Sov. J. Quant. Elec. 7, 1353 (1978).

86. T.S.Jaseja, A.Javan and C.H.Townes, Phys. Rev. Lett. 10, 165 (1963).

87. O.Hirota and Y.Suematsu, IEEE J. of Quant. Elec. QE-15, 142 (1979).

88. S.N.Bagaev, L.S.Vasilenko, V.G.Gol'dort, A.K.Dmitriev and A.S.Dychkov, Sov. J. Quant. Elec. 7, 665 (1977).

89. V.J.Corcan, Infrared Phys. 18, 635 (1978).

90. J.C.Mather, Thesis, University of California, Berkeley (Lawrence Berkeley Laboratory Report LBL-2258, 1974).

91. W.T.Welford and R.Winston, The Optics of Nonimaging Concentrators (Academic Press, New York, 1978), p.48.

92. C.C.Grimes, private communication, found that gold plating the surfaces of his cell reduced the effects he attributed to charge accumulating on the walls.

93. F.R.Schwartzberg, R.G.Herzog, S.H.Osgood and M.Knight, Cryogenic Materials Data Handbook (AFML-TDR-64-280, 1970).

94. R.Mehrota and A.J.Dahm, Phys. Rev. Lett. 43, 467 (1979).

95. R.C.Gann, S.Chakravarty and G.V.Chester, Phys. Rev. B20, 326 (1979).

96. A.Abragam, The Principles of Nuclear Magnetism (Oxford, London, 1961), p.76.

97. L.A.Wainstein and V.D.Zubakov, Extraction of Signals from Noise (Dover, New York, 1962), p.86.

98. B.R.Martin, Statistics for Physicists (Academic Press, New York, 1971), pp.72-84.

99. F.Stern, private communication.

APPENDIX 1

We give the proof of Eq. (5.11) in the text. We use Green's reciprocation theorem. Consider three situations: A, B and C. In all three cases the sides of the cell are at ground potential and there is a total charge Q_o in the charge pool on the helium surface. However, in situation B the top plate potential is increased by ΔV from the ground potential present in situation A. In situation C the top plate is at ground potential but the potential of the bottom plate is increased by ΔV from the potential V_o present in situation A. The radius of the charge pool is R_A, R_B and R_C for situations A, B and C. The charge on the top plate Q_T, the charge on the sides Q_S, the charge on the bottom plate Q_B, the potential as a function of position on the helium surface $V_P(\rho)$, and the charge density in the charge pool σ_P in the three situations are denoted as in the following table:

Situation	Q_T	Q_S	Q_B	$V_P(\rho)$	$\sigma_P(\rho)$
A	T_1	S_1	X_1	$V_A(\rho)$	$\sigma_A(\rho)$
B	T_2	S_2	$X_1 + \Delta Q_B$	$V_B(\rho)$	$\sigma_B(\rho)$
C	$T_1 + \Delta Q_T$	S_3	X_2	$V_C(\rho)$	$\sigma_C(\rho)$

Using Green's reciprocation theorem we obtain the following equation:

$$\Delta Q_B \Delta V - \Delta V \Delta Q_T = \int_{\rho=0}^{R_B} 2\pi\rho\ \sigma_B(\rho)\big(V_A(\rho) - V_C(\rho)\big)\,d\rho + \int_{\rho=0}^{R_A} 2\pi\rho\ \sigma_A(\rho)\big(V_C(\rho) - V_B(\rho)\big)\,d\rho + \int_{\rho=0}^{R_C} 2\pi\rho\ \sigma_C(\rho)\big(V_B(\rho) - V_A(\rho)\big)\,d\rho \quad . \tag{A1}$$

We now order the R_A, R_B and R_C so that $R_1 \leqslant R_2 \leqslant R_3$. Then

$$\Delta Q_B \Delta V - \Delta V \Delta Q_T = \varepsilon_{ABC}\left[\int_{R_1}^{R_2} 2\pi\rho\big(\sigma_2(\rho) - \sigma_3(\rho)\big)\ \Delta V_1(\rho)\ d\rho + \int_{R_2}^{R_3} 2\pi\rho\ \sigma_3(\rho)\left(\Delta V_2(\rho) - \Delta V_1(\rho)\right)d\rho\right]. \tag{A2}$$

Here ε_{ABC} is 1 if (ABC) is an even permutation, and is -1 if it is an odd permutation. Both of the integrals on the right-hand side of Eq. (A2) are of the third order of smallness in ΔV since $\sigma_i(\rho)$ goes continuously to zero as ρ approaches R_i. The left-hand side is only of second order smallness in ΔV. Hence:

$$\lim_{\Delta V \to 0} \frac{\Delta Q_B}{\Delta V} = \frac{\Delta Q_T}{\Delta V} \quad . \tag{A3}$$

This completes the proof.

APPENDIX 2

We give plots of optical response as a function of cell voltage. The numbers from which these plots were obtained are stored in named GSS files on the LBL Computer Center tape #35217. The files were created by unformatted writes of the form:

```
WRITE(N)(K,(Y(I1),I1=1,4098),
   (X(I2),I2=1,4098),(XL(I3),I3=1,3),
   (YL(I4),I4=1,3),(TITLE(I5),I5=1,6))
```

The first K values of X are voltages and the first K values of Y are the associated values of the optical response. Alpha-numeric information in "A" format is stored in XL, YL, and TITLE.

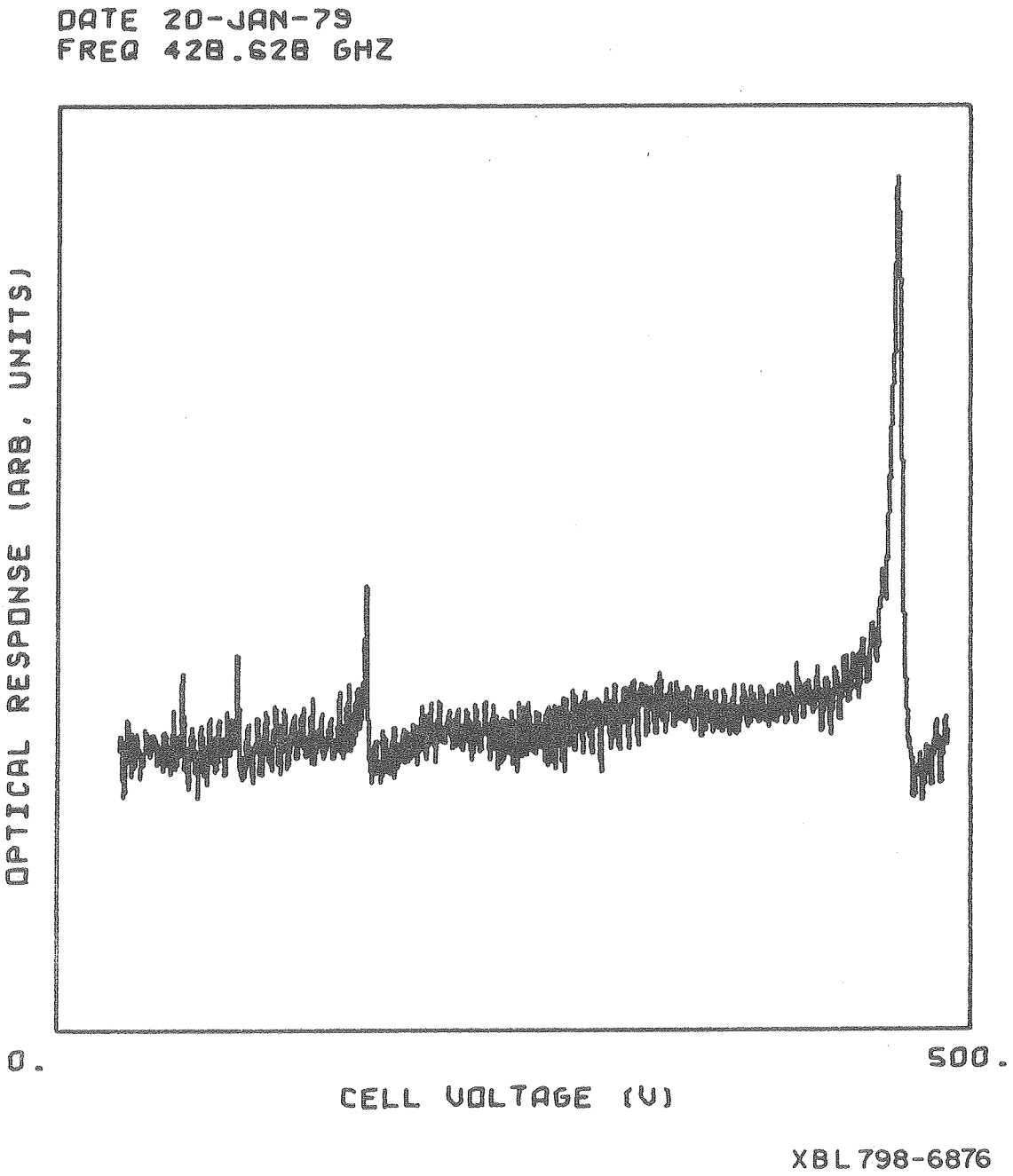

Fig. 16

GSS file SAWIT/E120/R8

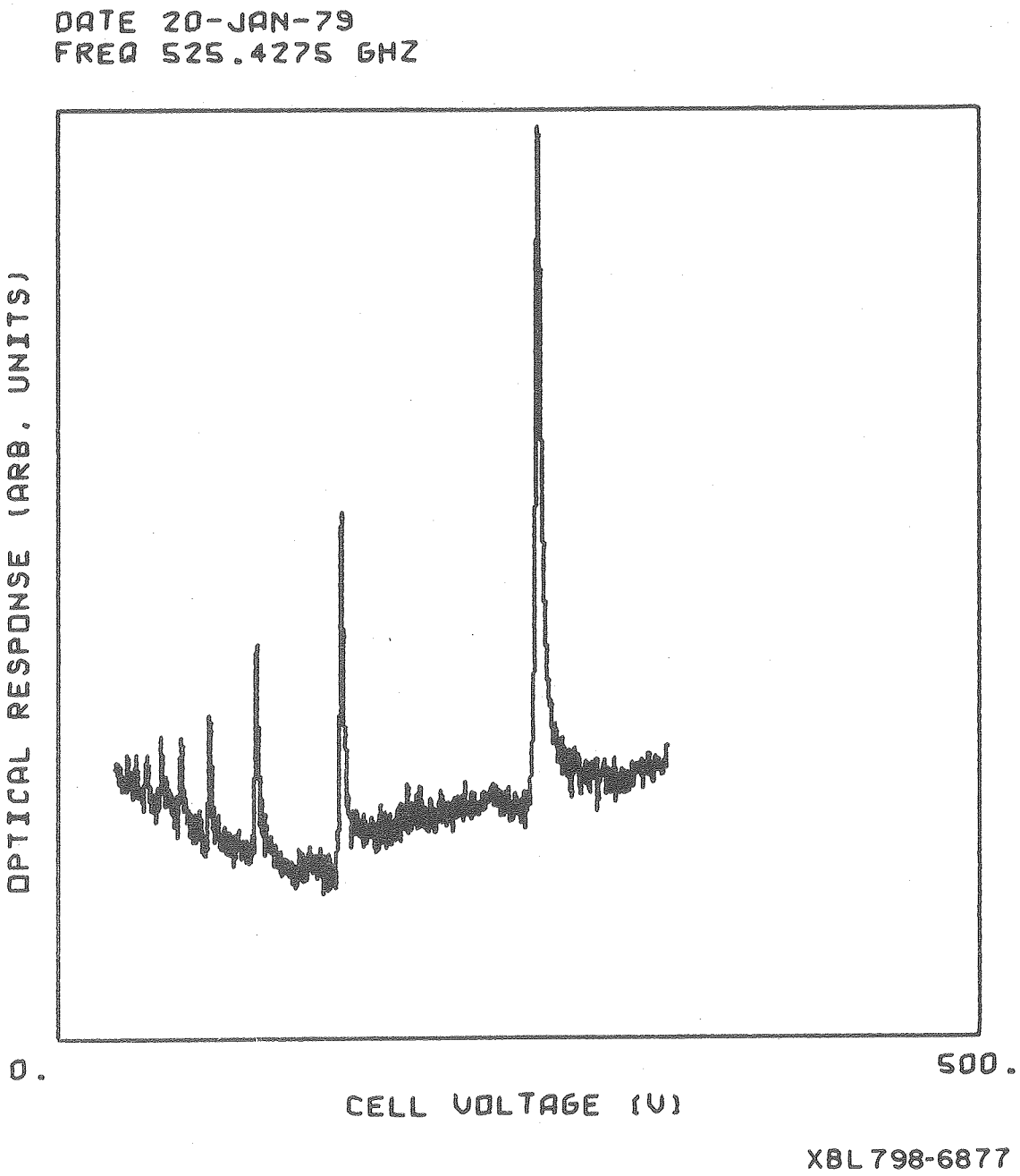

Fig. 17

GSS file SAWIT/E120/R1

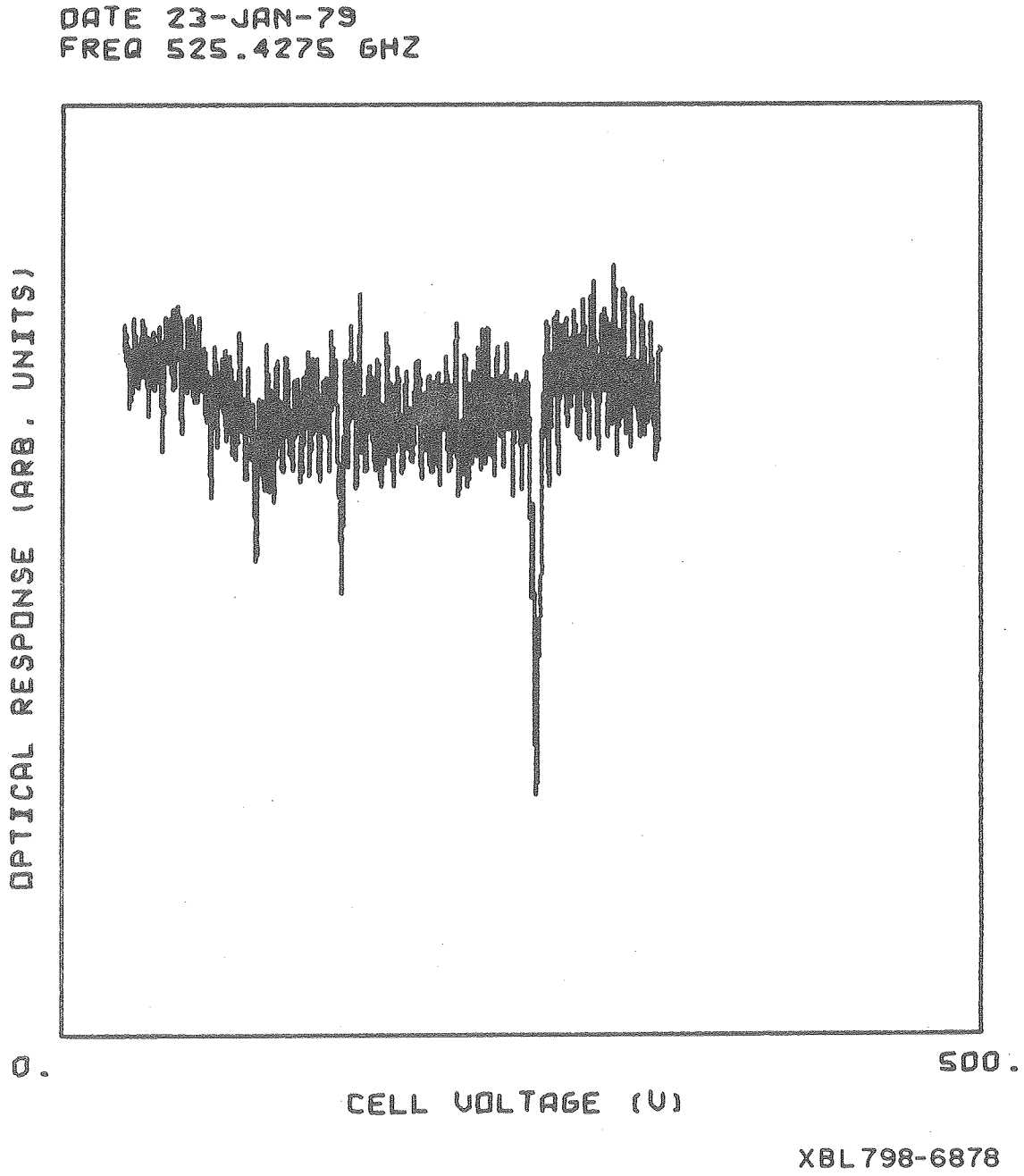

Fig. 18

GSS file SAWIT/E123/R1

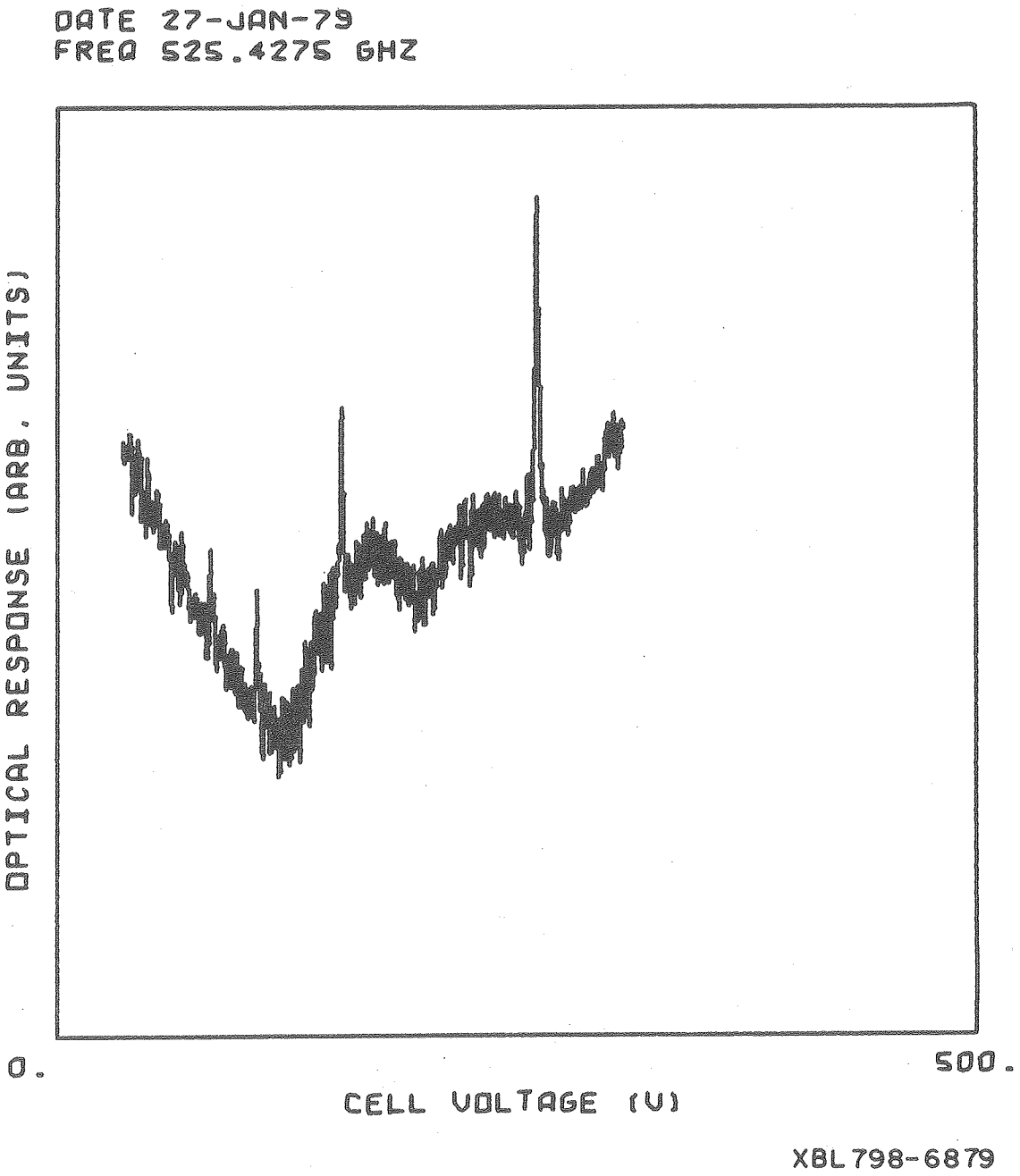

Fig. 19

GSS file SAWIT/E127/R11

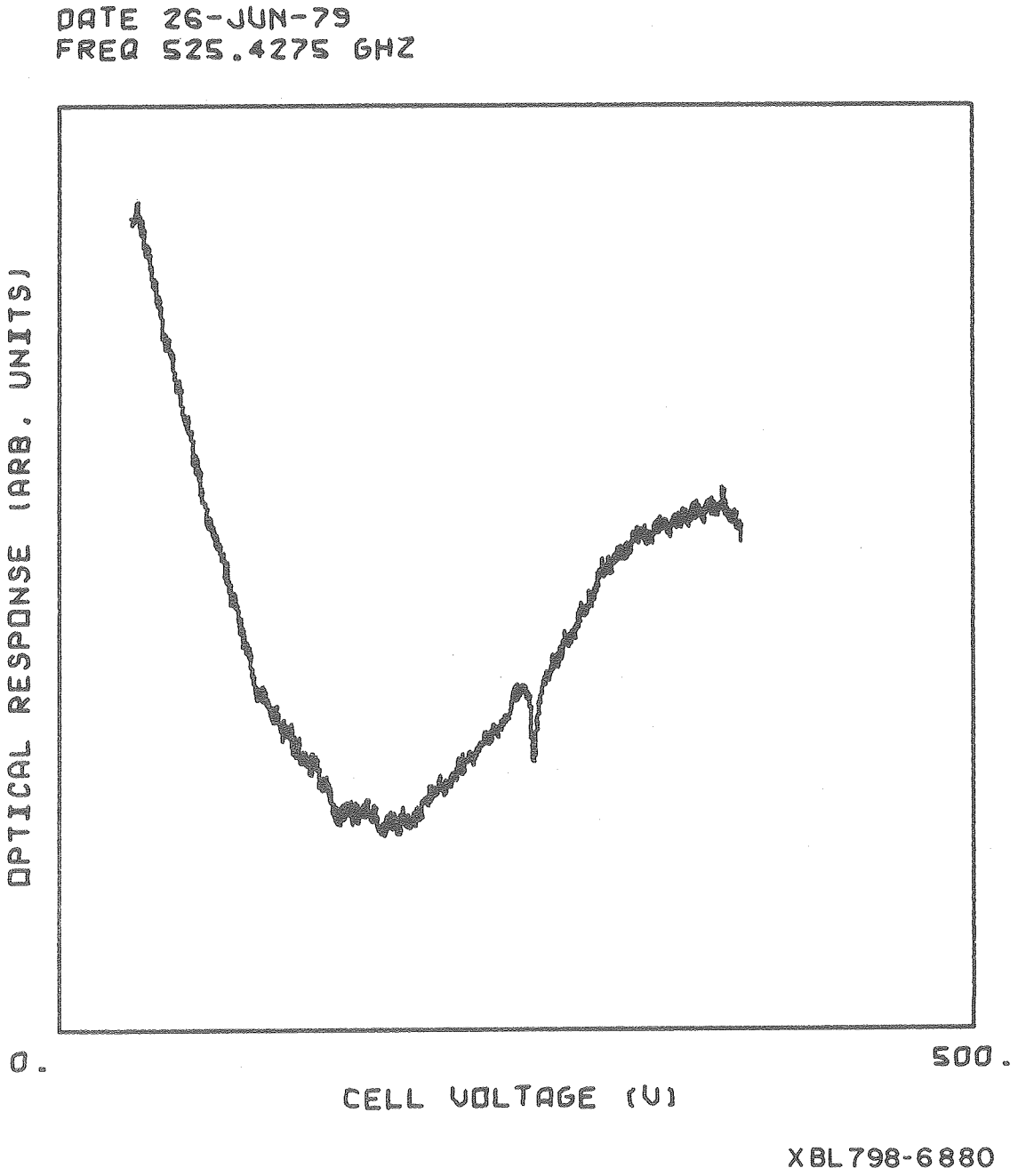

Fig. 20

GSS file SAWIT/E626/R6

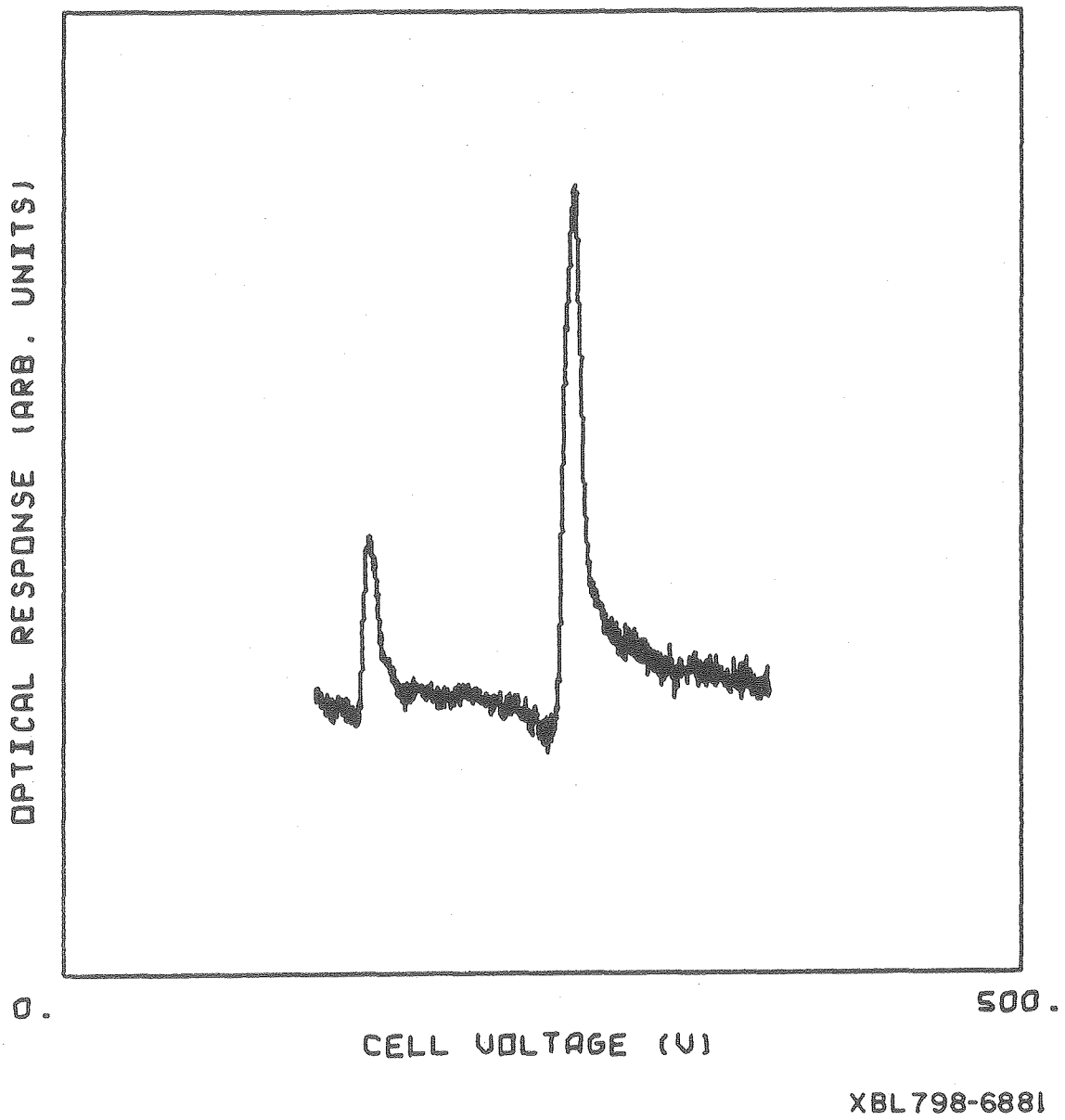

Fig. 21

GSS file SAWIT/E703/R10

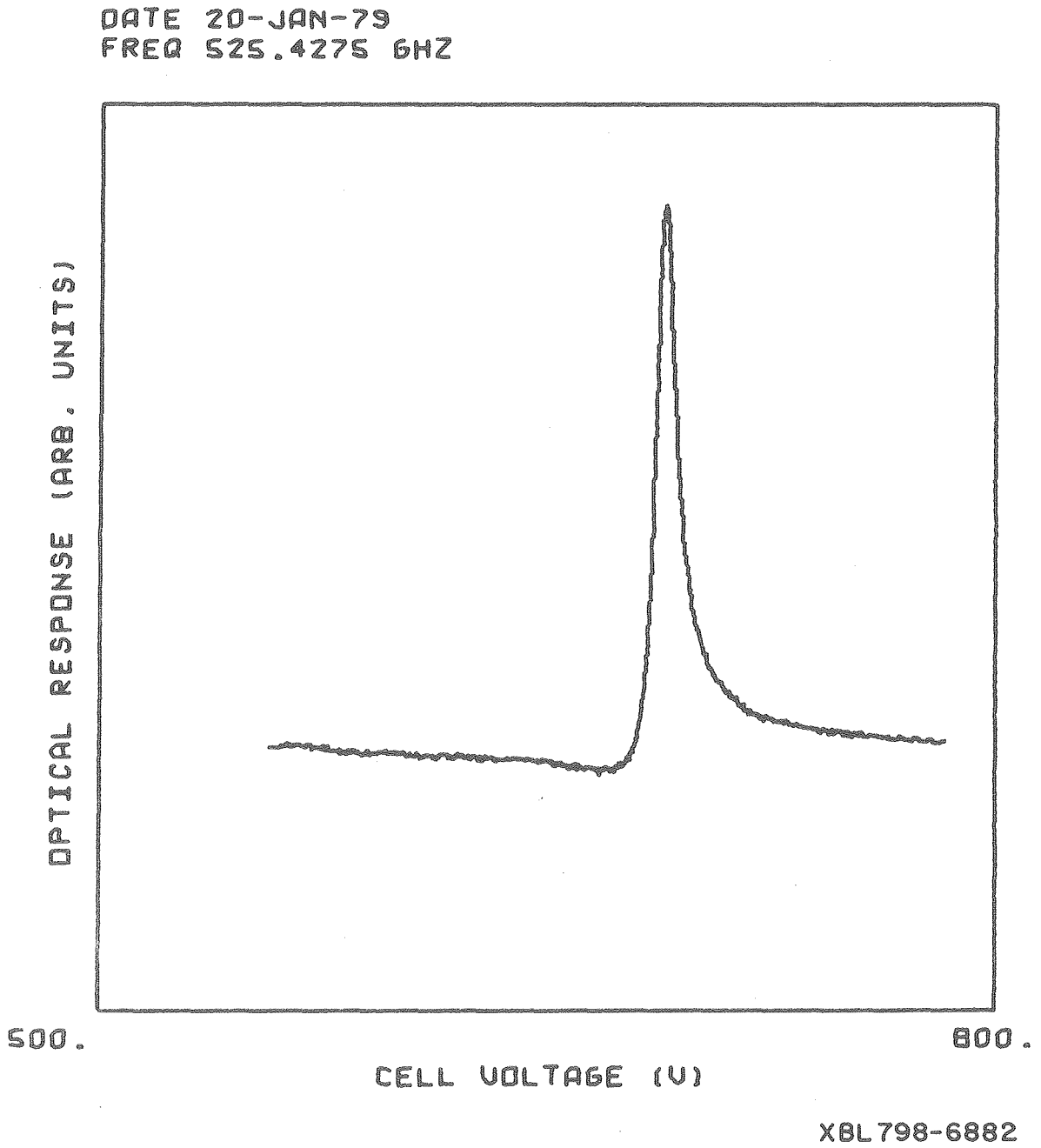

Fig. 22

GSS file SAWIT/E120/R2

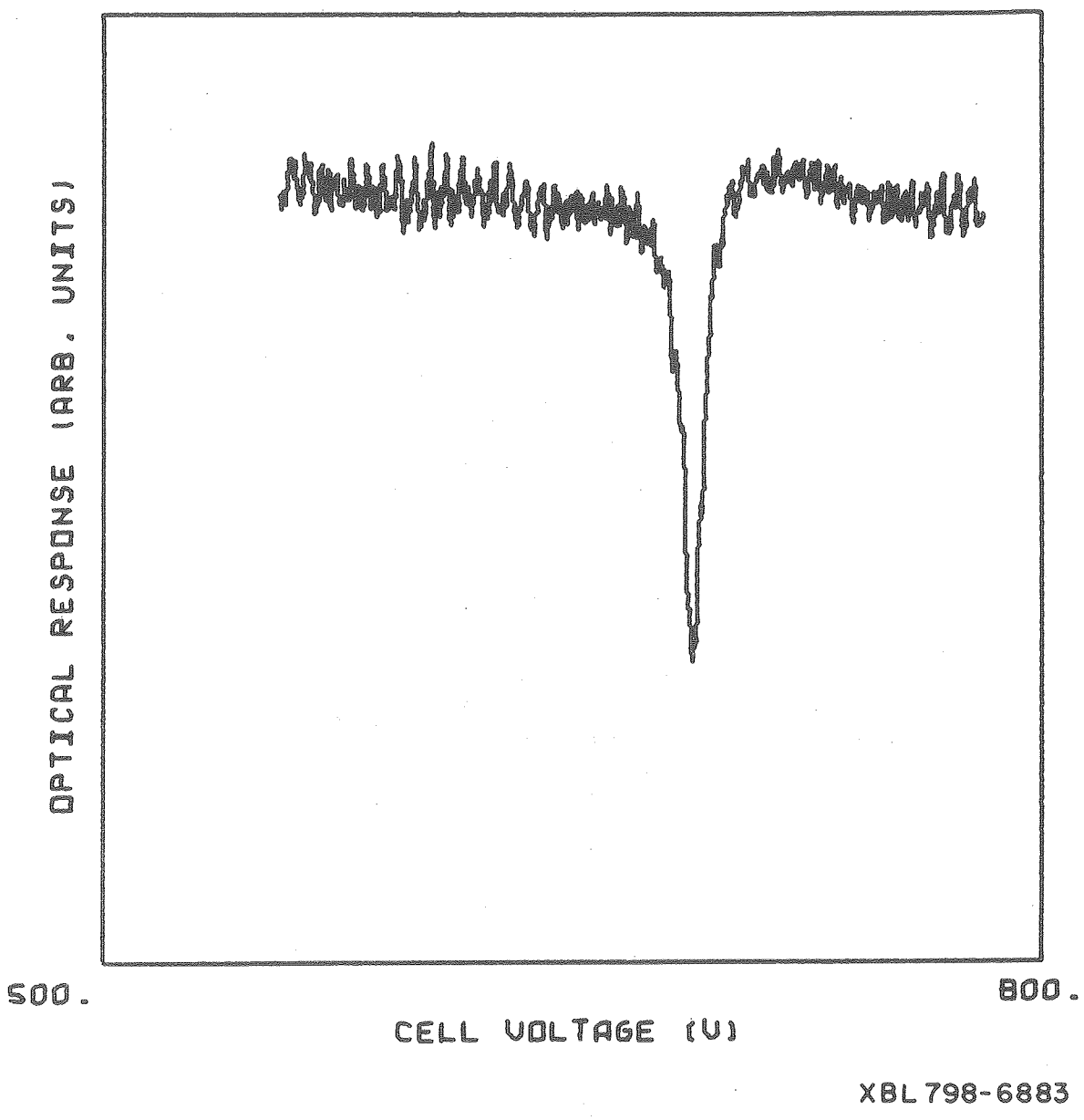

Fig. 23

GSS file SAWIT/E123/R2

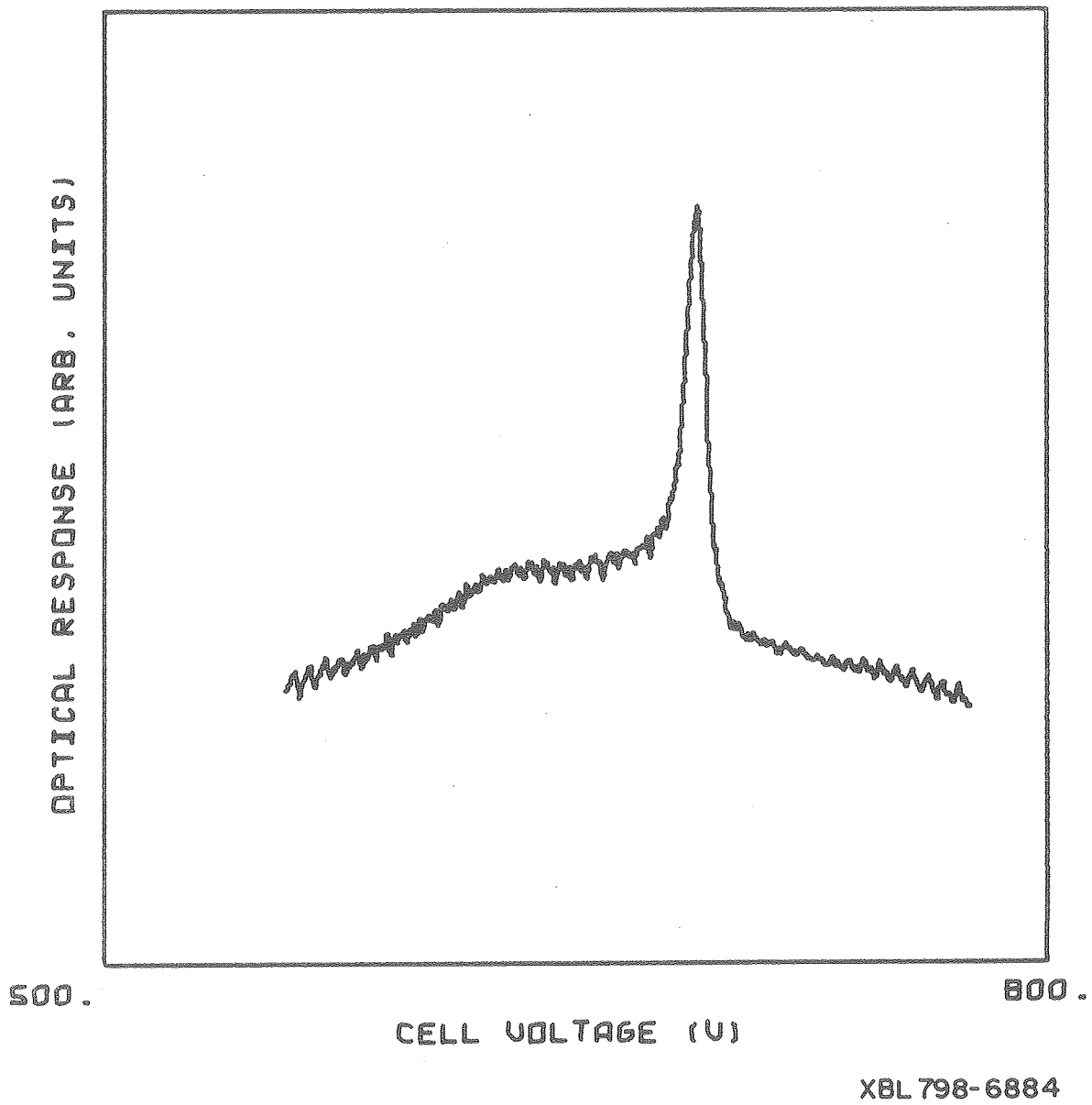

Fig. 24

GSS file SAWIT/E127/R12

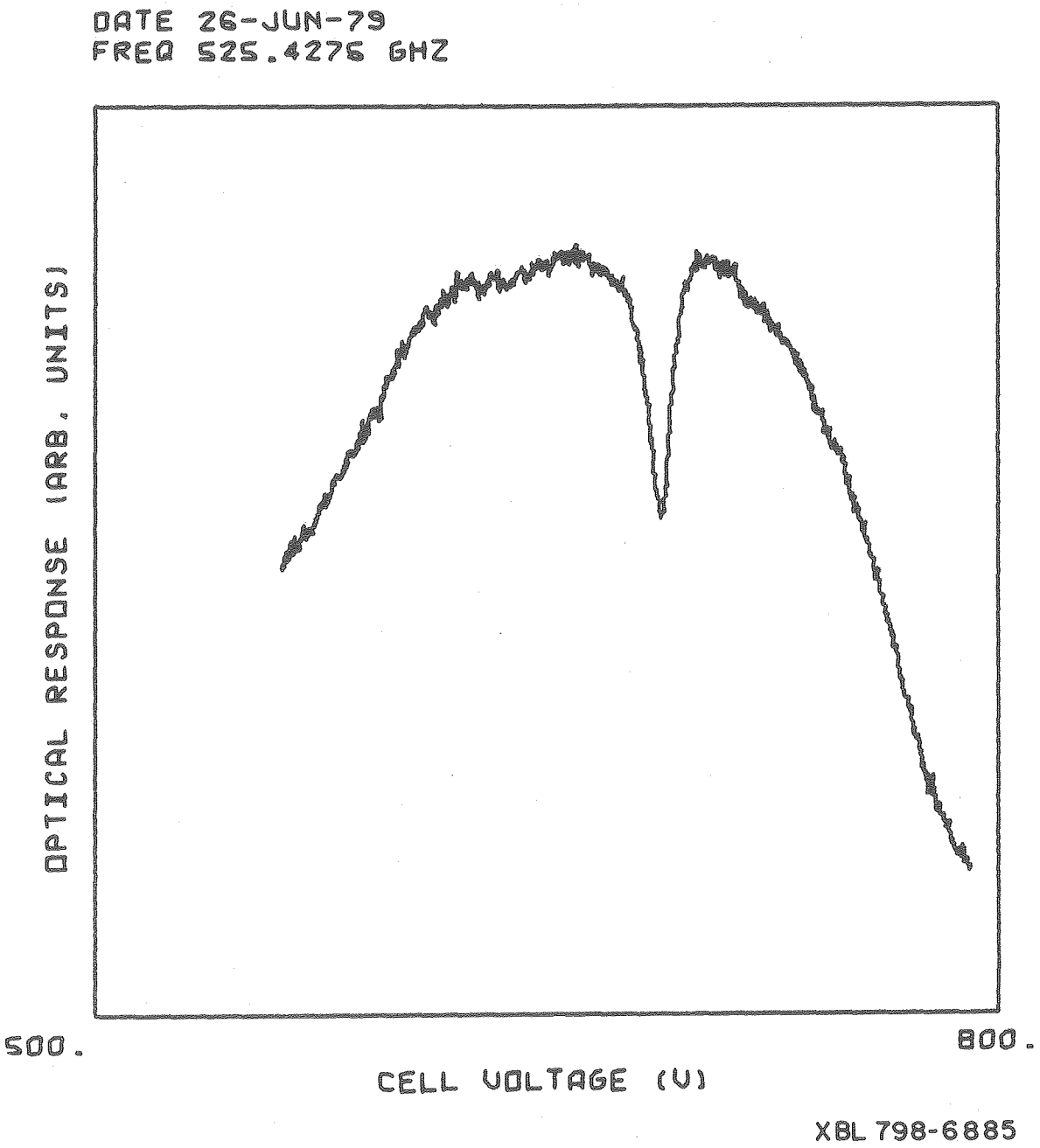

Fig. 25

GSS file SAWIT/E626/R10

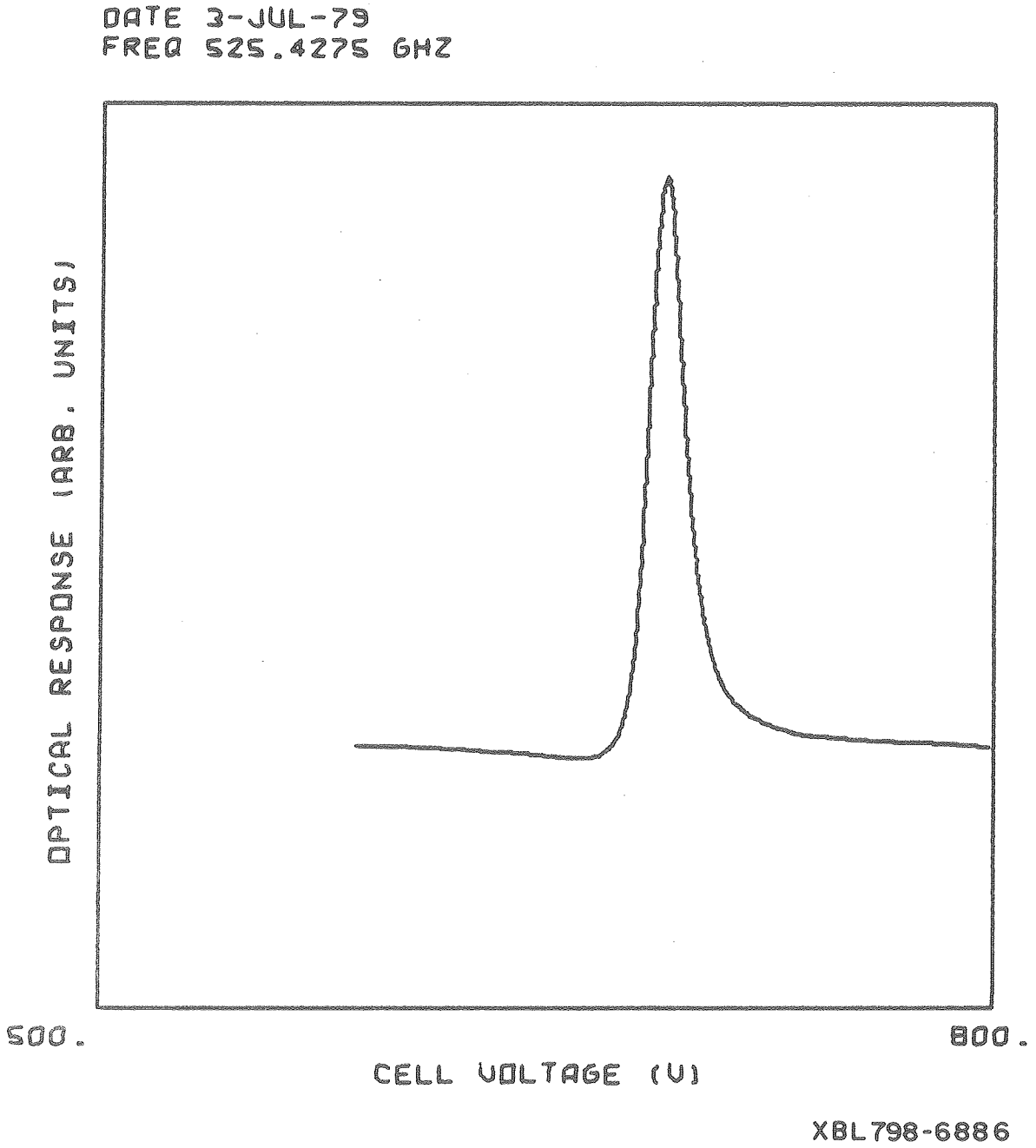

Fig. 26

GSS file SAWIT/E703/R7

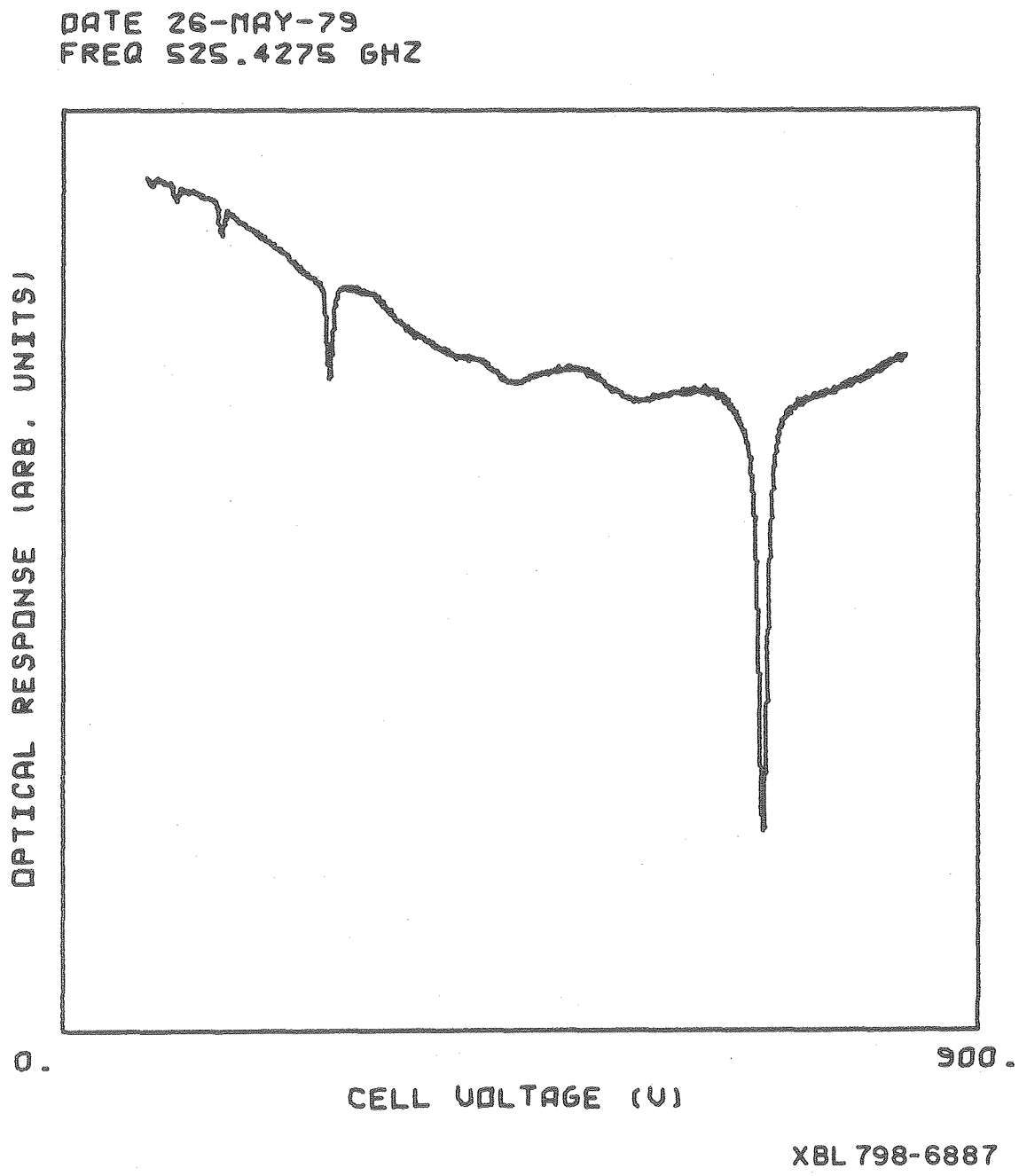

Fig. 27

GSS file SAWIT/E526/R7

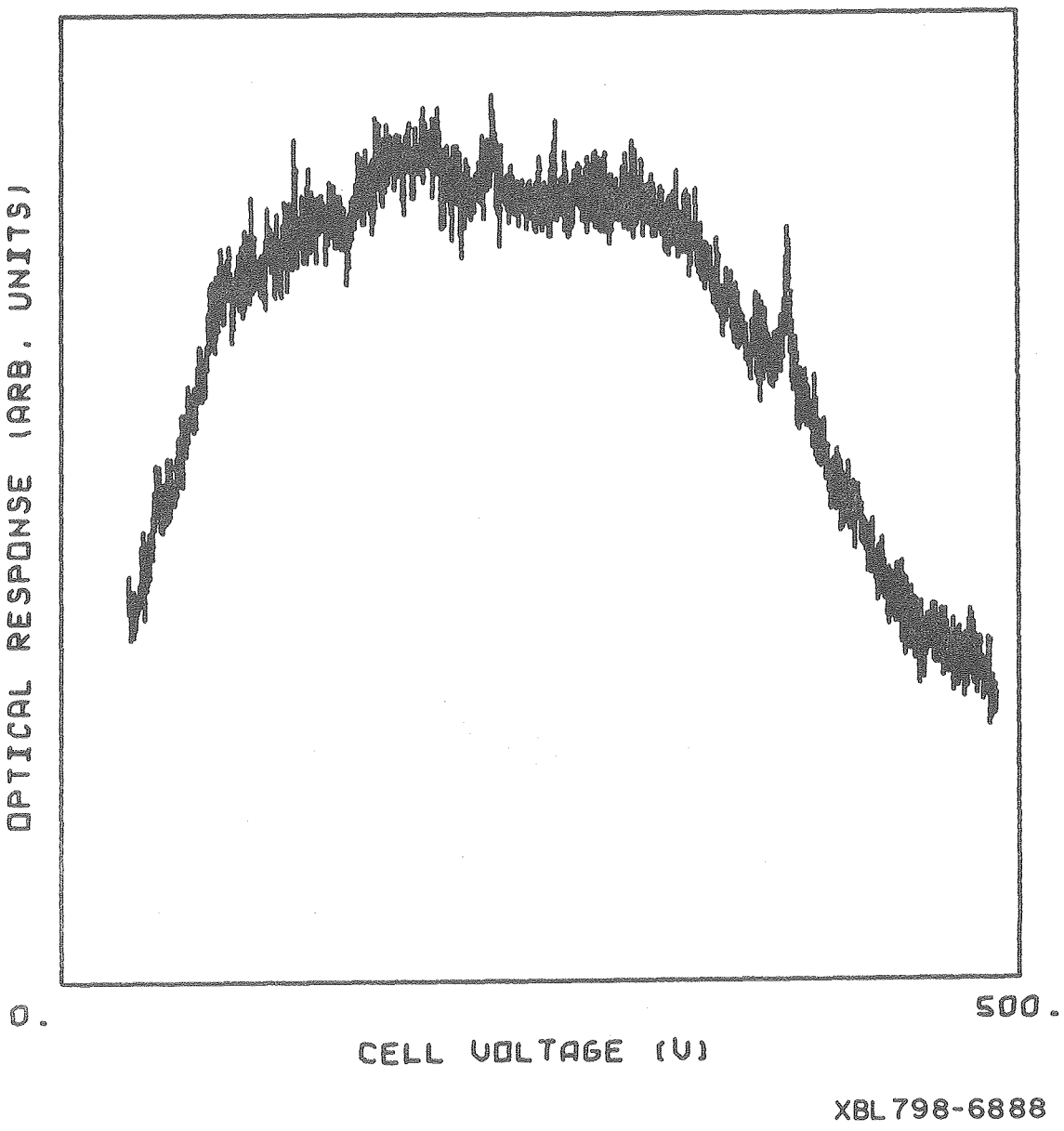

Fig. 28

GSS file SAWIT/E127/R1

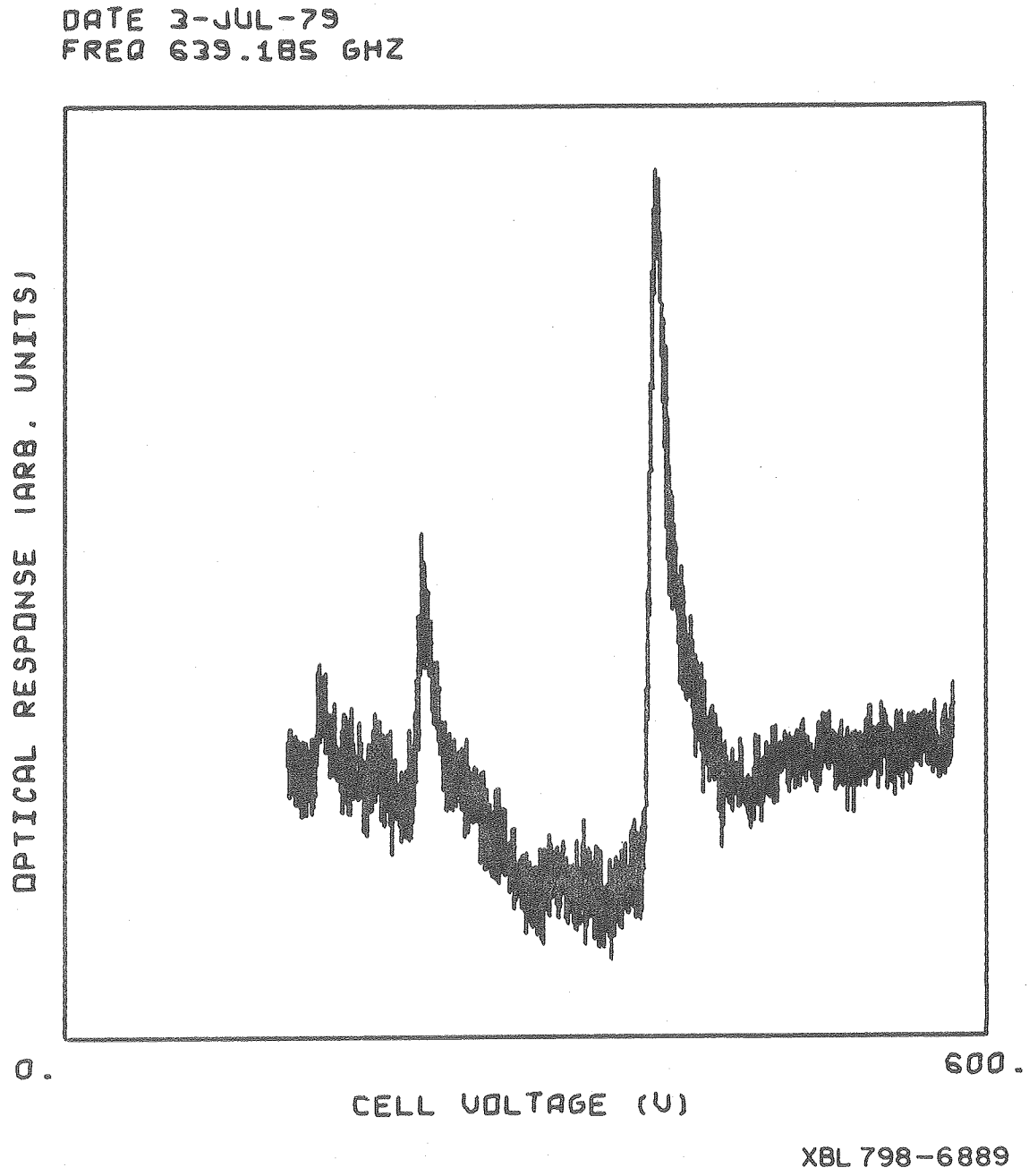

Fig. 29

GSS file SAWIT/E703/R1

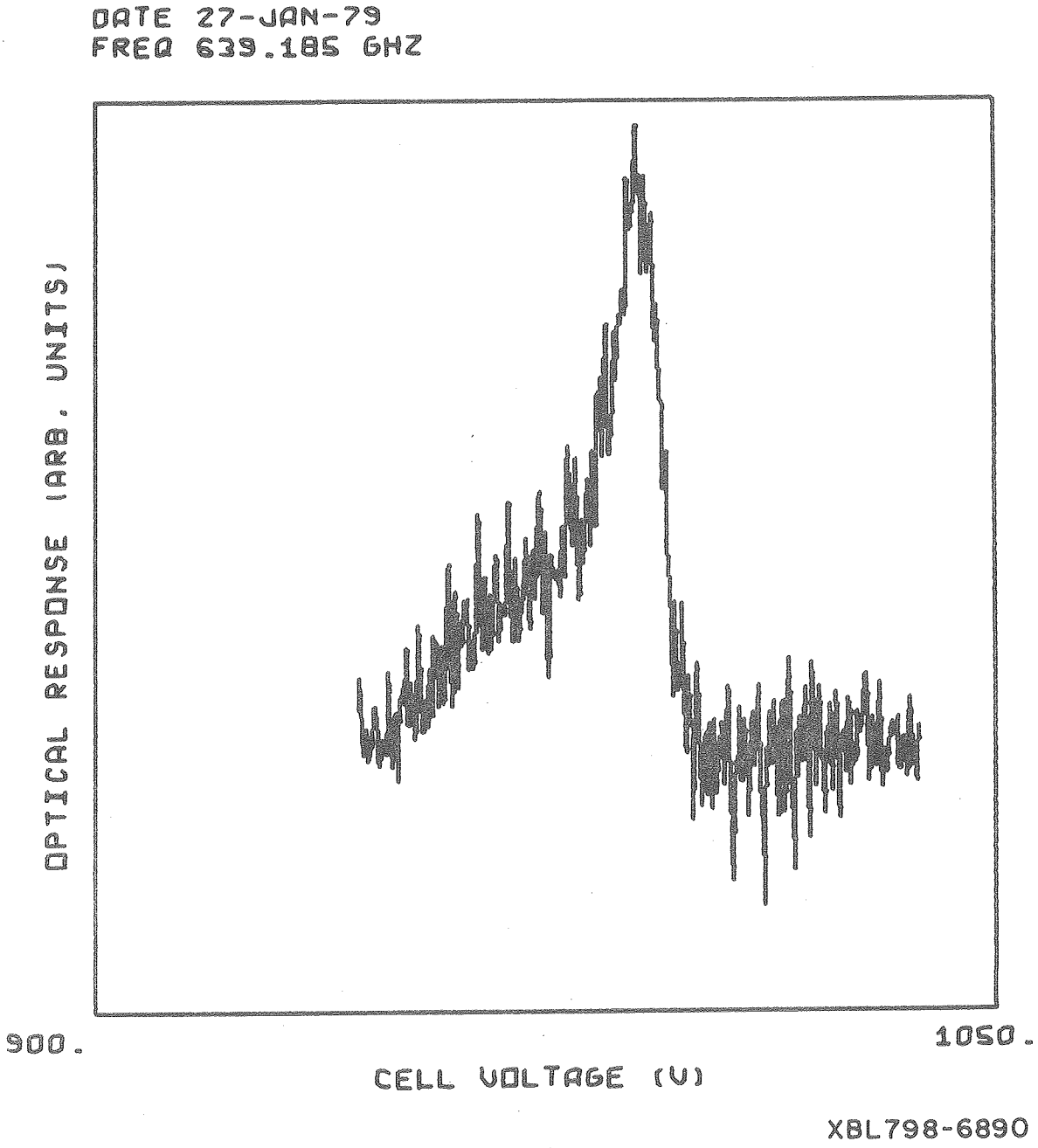

Fig. 30

GSS file SAWIT/E127/R3

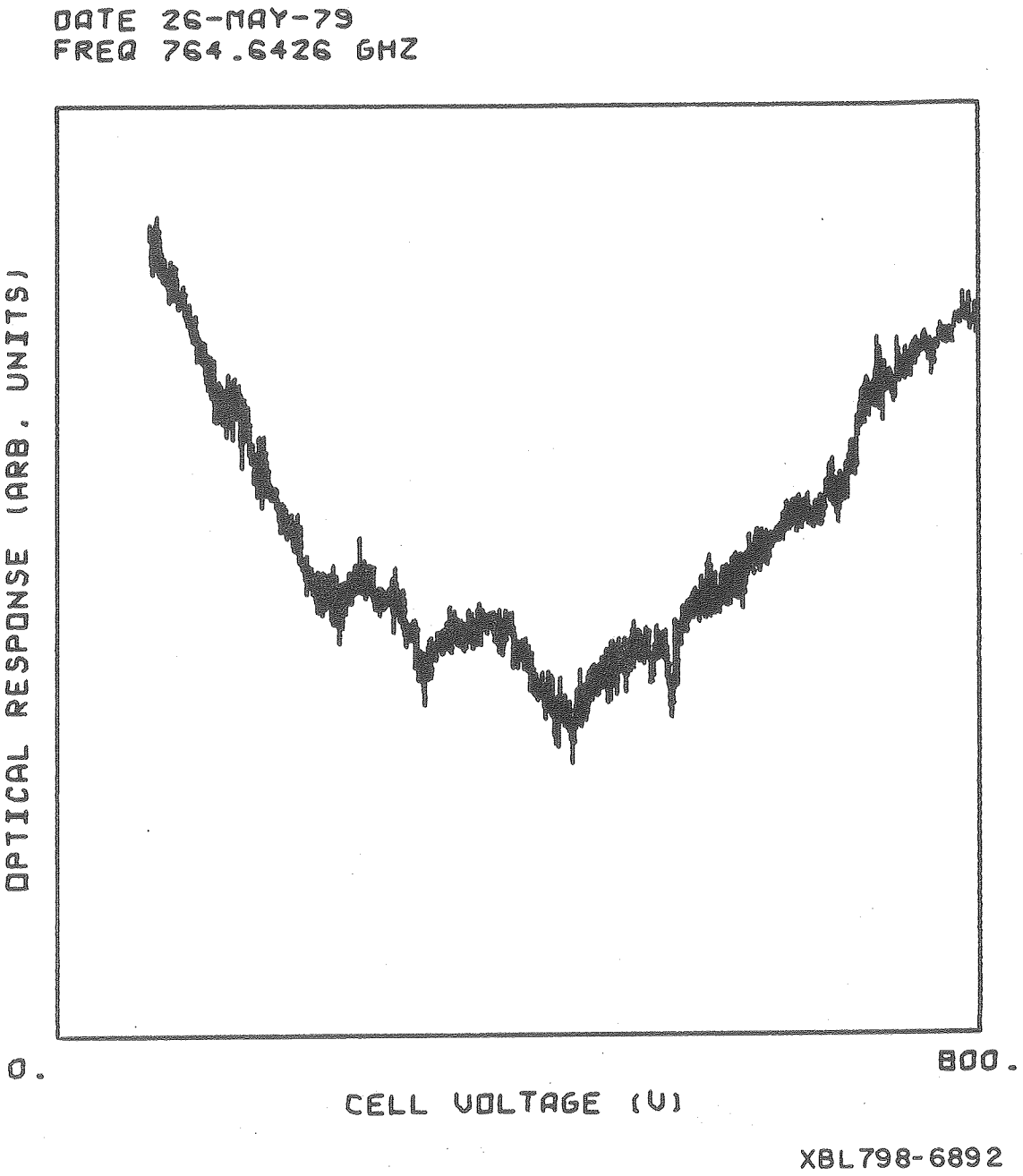

Fig. 32

GSS file SAWIT/E526/R3

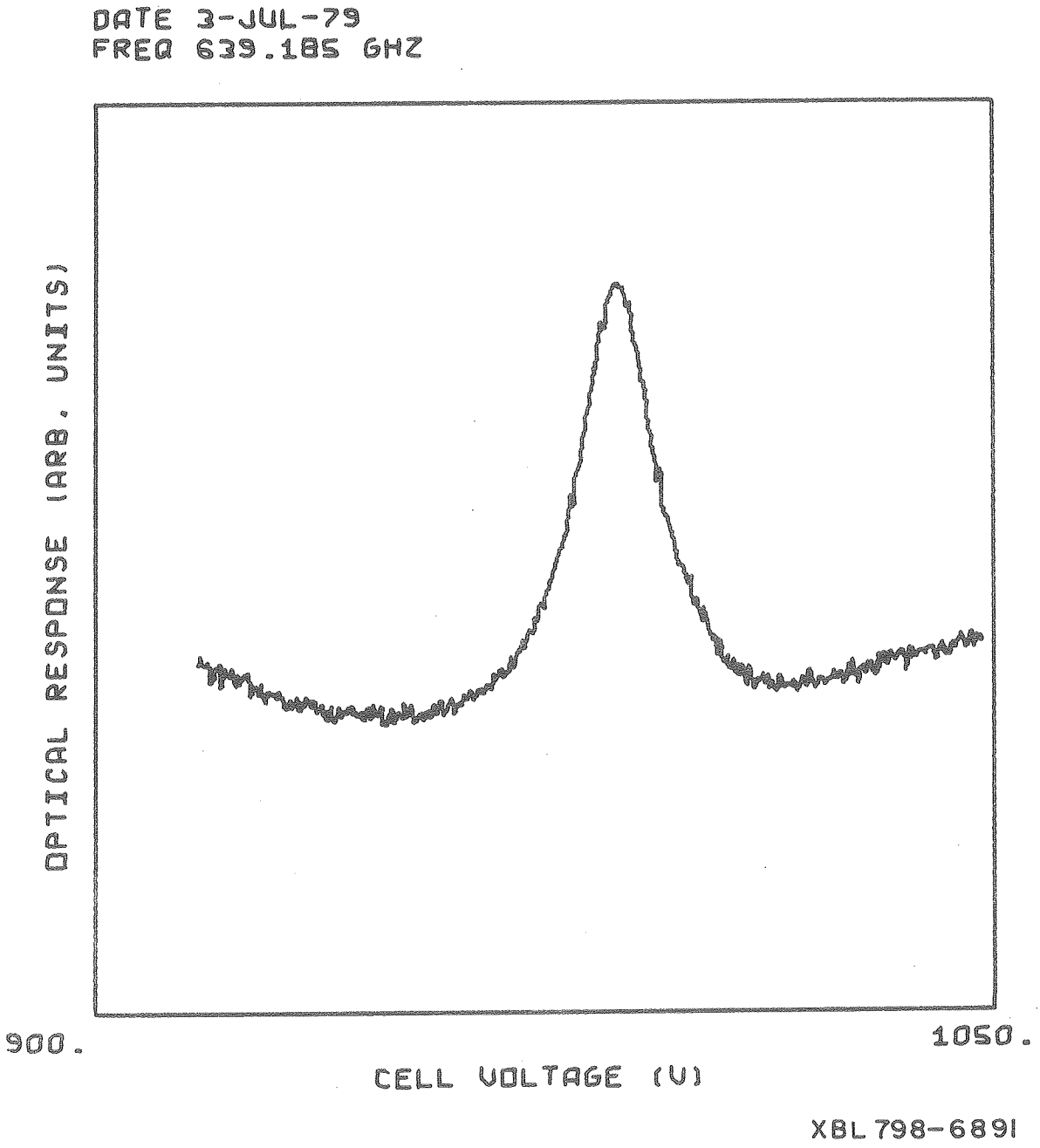

Fig. 31

GSS file SAWIT/E703/R4

TECHNICAL INFORMATION DEPARTMENT
LAWRENCE BERKELEY LABORATORY
UNIVERSITY OF CALIFORNIA
BERKELEY, CALIFORNIA 94720